Chapter 2
Early Cretaceous Volcanism in Central Argentina

Abstract The main exposed site of Early Cretaceous volcanism in central Argentina is located in Sierra Chica of Córdoba Province (SCC), within the Central Rift System. Also to the south, in Levalle basin, a thick Early Cretaceous volcanic pile lies buried in the subsurface. Other localities where volcanism is exposed are Sierra de las Quijadas and Cerrillada de las Cabras of San Luis Province. In SCC, as in the other mentioned localities, a volcanic–sedimentary complex was developed under rifting tectonics. Lava flows are frequently associated with scoria fall, pyroclastic and phreatomagmatic breccias within a strombolian-type volcanism. A new $^{40}Ar/^{39}Ar$ dating performed on sanidine phenocrysts of a trachyte from Almafuerte locality indicated an age of 129 ± 1 Ma. Diverse groups of rocks, mainly of potassic character, were distinguished: (1) alkali basalt—trachyte suite, (2) transitional basalt—latibasalt suite, (3) basanite—phonolite suite and (4) ankaratrites. Magma evolution must have taken place at crustal level(s) from distinct parental melts, mainly through fractional crystallization in an open-system magma chamber. Mantle source composition supports residual garnet and phlogopite, it does not exhibit features related to slab-derived metasomatism despite its location over Pampean mobile belt, and bears a lithospheric nature. SCC volcanism is of high Ti, display similarities with potassic Brazilian localities around Paraná basin as Alto Paranaíba and Goias, pointing out analogies in their mantle sources.

Keywords Early Cretaceous · Sierra Chica · Córdoba · Alkali basalts · Transitional basalts · Basanites · Ankaratrites · Lithospheric mantle

2.1 Early Cretaceous Volcanism in Córdoba Province

2.1.1 Volcanism of the Sierra Chica of Córdoba Province

2.1.1.1 Geological Setting

Córdoba ranges are essentially integrated by three mountain belts called Sierra Norte, Sierra Grande and Sierra Chica (Fig. 2.1), in the geological context of the

S.L. Lagorio et al., *Early Cretaceous Volcanism in Central and Eastern Argentina During Gondwana Break-Up*, SpringerBriefs in Earth System Sciences, DOI 10.1007/978-3-319-29593-0_2

eastern Sierras Pampeanas. Early Cretaceous alkaline volcanism is located in Sierra Chica. By contrast, Late Cretaceous, very small volcanic outcrops appear in Sierra Grande (Estancia Guasta and Ciénaga Grande) and to the south, in the locality of Chaján (Fig. 2.1).

Córdoba ranges are mainly composed of igneous–metamorphic basement of Precambrian–Early Carboniferous age, formed essentially by biotite gneisses, schists, cordierite migmatites, granitic bodies, pegmatites and aplites, with minor participation of amphibolites, ultramafic rocks and marbles (e.g. Gordillo and Lencinas 1980; Martino et al. 1995; Kraemer et al. 1995; Geuna et al. 2008; Lira and Sfragulla 2014).

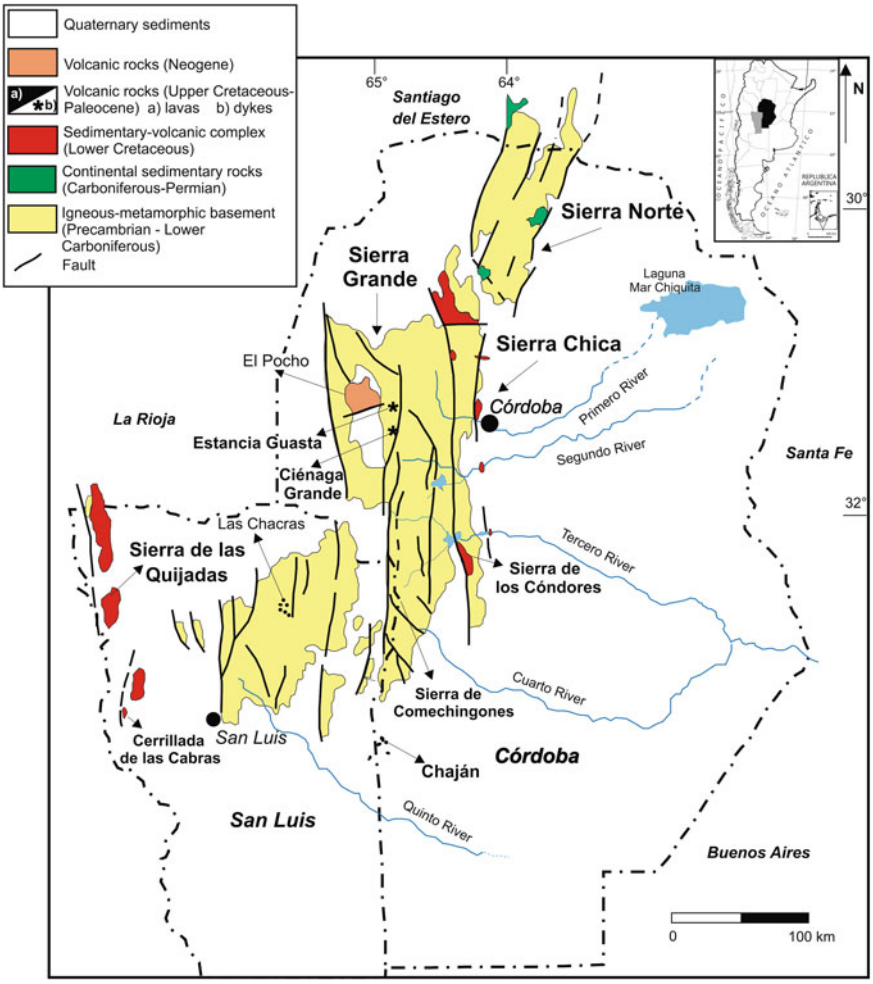

Fig. 2.1 Geological map of the provinces of Córdoba and San Luis, adapted from Lucero Michaut et al. (1995) and Caminos and González (1996)

Over the basement, the Early Cretaceous volcanic–sedimentary complex lies, generated as a consequence of extensional conditions (Uliana et al. 1990), within the Central Rift System (Rossello and Mozetic 1999; Ramos 1999; Fig. 2.2a). The structural style was mainly controlled by the Punilla and La Calera faults, with a dominant NNW direction (Fig. 2.2b). These structures were developed in zones of crustal weakness (Schmidt et al. 1995; Martino et al. 2014), as the suture represented by the eastern ophiolite belt of Kraemer et al. (1995) between the para-autochthonous Córdoba terrane and the Río de la Plata craton. Therefore, the rift could have been developed in the hanging wall of the suture between amalgamated terranes (Kay and Ramos 1996, Ramos et al. 2000). Andean tectonics in the area that belongs to the Nazca flat slab, provoked the lifting of Sierra Chica, exposing the Cretaceous complex through reverse faults that were previously normal faults (Sisto et al. 1993; Schmidt et al. 1995; Kay and Ramos 1996; Martino et al. 2014).

Outcrops of the Lower Cretaceous volcanic rocks in Sierra Chica are represented by remnants of a volcanic–sedimentary complex unconformably overlying its basement. This complex is composed of continental red beds and alkaline basic lavas (Gordillo and Lencinas 1980) that belong to syn-rift deposits of basins located from the south of Sierra Chica to Sierras de Guasayán (in Santiago del Estero Province, to the north of Córdoba Province) in a transtensional context (Schmidt et al. 1995). The kinematics of the associated strike-slip faults has been mentioned in different papers. Several authors indicate sinistral lateral displacements (Sisto and Cortés 1992; Sisto et al. 1993, 1995; Sánchez et al. 1995; Kay and Ramos 1996), whereas others consider dextral movements (Schmidt et al. 1995; Martino et al. 2014). These latter authors have pointed out that a dextral rifting would have determined the formation of depocenters as isolated pull-apart basins during the Early Cretaceous. This is consistent with the interpretation of the strike-slip faults in Paraná and Colorado basins pointed out by Uliana et al. (1990) and Tankard et al. (1995). The filling of the Lower Cretaceous basins of Sierra Chica would have taken place in restricted half-grabens. The sediments belong to alluvial fans, braided rivers and ephemeral lake deposits (e.g. Poiré et al. 1989; Sánchez et al. 1990; Astini et al. 1993; Piovano 1996). The climate must have been of a semi-arid and oxidizing environment, because there are no fossil records available. Four sedimentary depocenters were identified, three of them with considerable thicknesses. They remained as remnants after intense Tertiary erosion. The largest deponcenters are located in the following: (1) Sierra de Masa, Sierra de Copacabana and Sierra del Pajarillo, (2) the Saldán locality and (3) Sierra de los Cóndores (southern portion of Sierra Chica), whereas the smaller one is located in a zone known as El Pungo (4) (Fig. 2.2b, c). An updated and detailed sedimentological and stratigraphical study of the deposits that filled these depocenters has been recently presented by Astini and Oviedo (2014).

The sedimentary beds are interbedded with lava flows in the mountains of Sierra de los Cóndores and El Pungo; in the Saldán locality, only conglomerates with clasts of basalts and hydrothermal minerals have been recognized (Piovano 1996). Schmidt et al. (1995) considered two megasequences of Cretaceous deposits in Sierra Chica (Fig. 2.2c). The lower one reaches the largest thickness in Sierra de Copacabana and

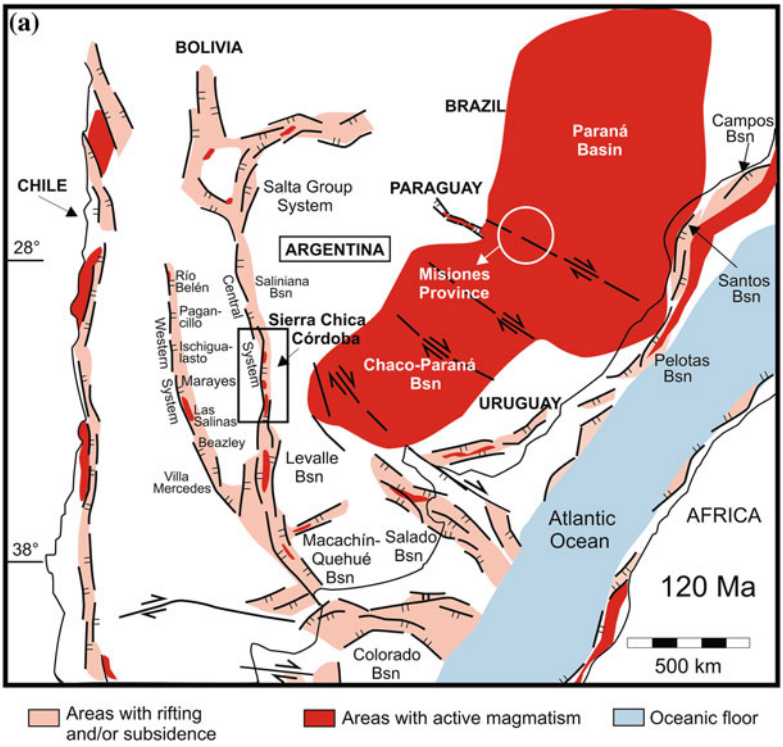

Fig. 2.2 **a** Extensional tectonics during Early Cretaceous (taken from Uliana et al. 1990), showing Sierra Chica of Córdoba as part of the Central Rift System (Rossello and Mozetic 1999; Ramos 1999). **b** Geological map of the Sierra Chica, based on Gordillo and Lencinas (1980), Schmidt et al. (1995) and Kay and Ramos (1996), as presented by Lagorio (2008). **c** Synthetic scheme of the main Cretaceous successions in the area of Sierra Chica, taken from Schmidt et al. (1995); division in megasequences proposed by these authors based on the presence of volcanism, with later modifications introduced by Minudri and Sánchez (1994) and Piovano (1996)

Sierra del Pajarillo, and there are no lava flows interbedded with the sedimentary deposits. The volcanic levels outcrop in El Pungo, Sierra de los Cóndores and around the localities of Almafuerte and Despeñaderos localities (Fig. 2.2b); in the area of Los Molinos dam, only several basaltic dykes that could belong to the Early Cretaceous volcanic event are recorded intruding the crystalline basement.

2.1.1.2 Volcanism in different localities of Sierra Chica

Sierra de los Cóndores

This range belongs to the southern end of Sierra Chica (Fig. 2.2b). It is composed of a volcanic–sedimentary complex that reaches over than 250 m unconformably overlying crystalline basement rocks.

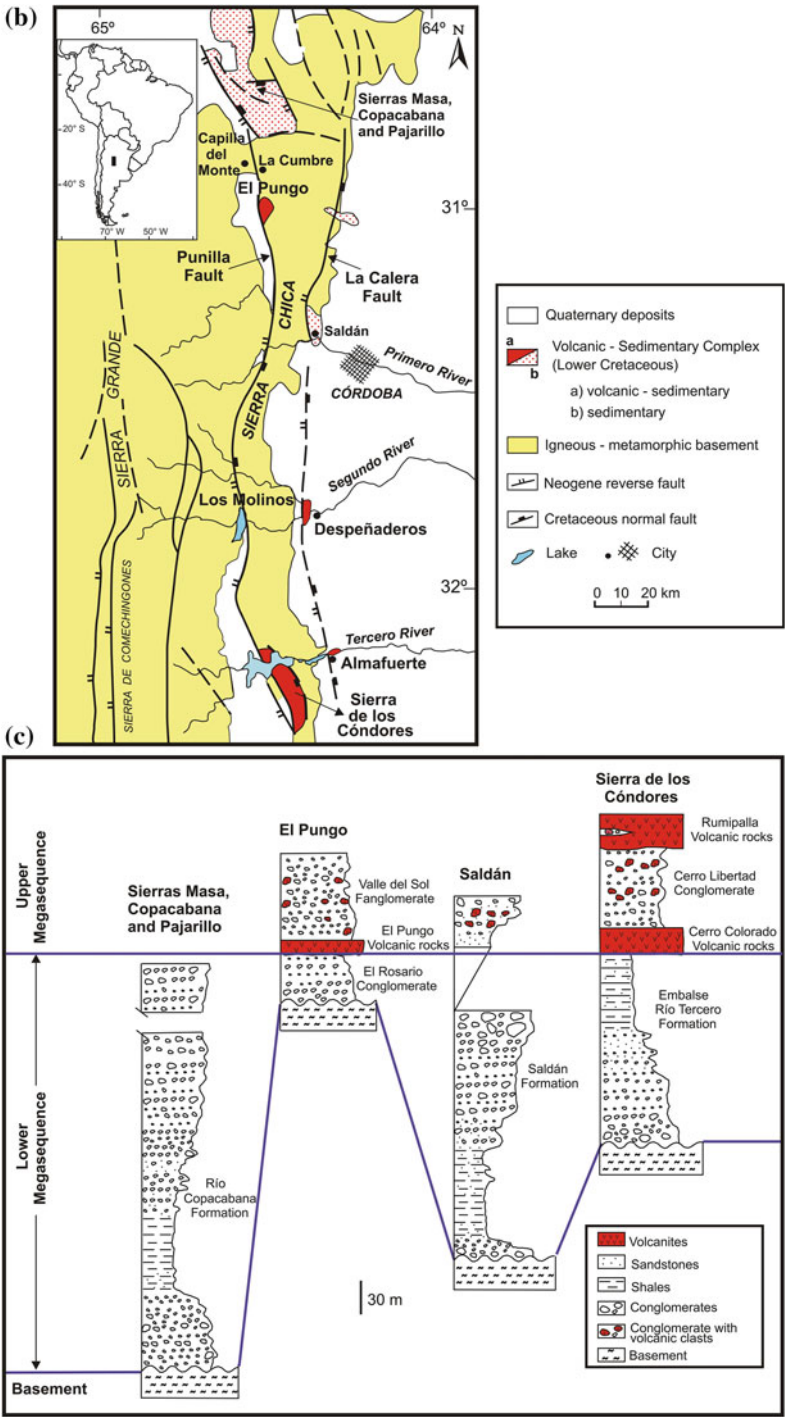

Fig. 2.2 (continued)

The volcanic rocks of this range were previously described by Tannhauser (1906), Bodenbender (1907) and Pastore (1930). Gordillo and Lencinas (1967a) defined in the northern section of this range the Sierra de los Cóndores Group, composed of a basal sedimentary unit (Embalse Río Tercero Formation) which is followed by two volcanic cycles (Cerro Colorado and Rumipalla Volcanic rocks, respectively) separated by a sedimentary unit (Cerro Libertad Conglomerate).

Gordillo and Lencinas (1967a) considered that a non-foidic trachybasalt rich in sanidine was the dominant rock type of the area; other varieties (picritic basalts, calc-alkaline and alkaline trachytes, rhombic porphyries) were subordinate and restricted to local lava flows. The rocks form a series of moderate alkaline character, relatively enriched in potassium.

Although radiometric dating coincides throughout the entire range (Table 2.1), Poiré et al. (1989), Sánchez et al. (1990) and Ferreira Pittau et al. (2008) considered that the volcanism must have begun in the southern area, whereas in the northern sector, there was an intense sedimentation. In the southern sector, the volcanic activity was characterized by a significant pyroclastic component, within a context

Table 2.1 Previous radiometric ages for volcanic rocks from Sierra Chica de Córdoba (SCC)

Locality	Rock type/mineral phase	K/Ar Age (Ma)	Corrected K/Ar Age (Ma)	Ref.
Sierra de los Cóndores				
Cerro Colorado	Trachybasalt	120	120	1
Cerro Colorado	Trachybasalt	117	117	1
Cerro Colorado	Trachybasalt	120 ± 5	123 ± 5	2
Cerro Colorado (mean age)	Trachybasalt	116 ± 5	119 ± 5	2
Cerro Colorado (mean age)	Trachybasalt	118.5 ± 6	121.5 ± 6	3
Cerro Libertad	Trachyte	128 ± 5	128 ± 5	1
Cerro Quebracho	Trachybasalt	116 ± 6	119 ± 6	3
Gianna quarry (Berrotarán)	Sanidine	112 ± 6	115 ± 6	1
Berrotarán	Sanidine	120 ± 2	123 ± 2	4
Berrotarán	Sanidine	130 ± 6	133 ± 6	4
El Quebracho quarry	Alkaline basalt	117 ± 5	120 ± 5	6
Almafuerte				
Middle section	Trachybasalt	122 ± 3	125 ± 3	4
Middle section	Trachybasalt	129 ± 8	132 ± 8	4
Upper section	Andesite	119 ± 10	122 ± 10	5
Upper section	Basalt	121 ± 5	124 ± 5	5
Dyke	Trachyte	120 ± 2	123 ± 2	4
Close to Río Tercero	Basalt	123 ± 4	126 ± 4	7
Two km to the N of Almafuerte	Trachybasalt	124 ± 5	127 ± 5	1
Close to Almafuerte locality	Porphyry	114 ± 5	117 ± 5	5

(continued)

Table 2.1 (continued)

Locality	Rock type/mineral phase	K/Ar Age (Ma)	Corrected K/Ar Age (Ma)	Ref.
Los Molinos dam				
Dyke N° 8 (mean age)	Trachybasalt	150 ± 10	154 ± 10	8
Dyke N° 5 (mean age)	Trachybasalt	140 ± 10	143 ± 10	8
Dyke N° 10 (mean age)	Trachybasalt	138 ± 10	141 ± 10	8
Dyke N° 9 (mean age)	Trachybasalt	131 ± 10	134 ± 10	8
Dyke N° 12 (mean age)	Trachybasalt	129 ± 10	132 ± 10	8
Dyke N° 4 (mean age)	Trachybasalt	68 ± 5	70 ± 5	8
Dyke N° 13 (mean age)	Trachybasalt	65 ± 5	67 ± 5	8
Dyke N° 14 (mean age)	Trachybasalt	63 ± 5	65 ± 5	8
Dyke N° 14	Trachybasalt	60.2 ± 3	61.7 ± 3	9
El Pungo				
El Pungo-La Cumbre	Basalt	119 ± 5	122 ± 5	4
El Pungo-La Cumbre	Basalt	119	119	10
Despeñaderos				
Saldán Formation	Basalt	122.9 ± 1.3	122.9 ± 1.3	11
Saldán Formation	Basalt	136.3 ± 1.5	136.3 ± 1.5	11
Saldán Formation	Basalt	130.7 ± 1.4	130.7 ± 1.4	11
Saldán Formation	Basalt	130.4 ± 1.4	130.4 ± 1.4	11
Saldán Formation	Basalt	128.5 ± 1.5	128.5 ± 1.5	11

Data source (1) Gordillo and Lencinas (1967a); (2) Stipanicic and Linares (1969); (3) Valencio (1972); (4) González and Kawashita (1972); (5) Linares and González (1990); (6) Cortelezzi et al. (1981); (7) Valencio and Vilas (1972); (8) Linares and Valencio (1974); (9) Gordillo and Lencinas (1969); (10) Lencinas (1971); (11) Cejudo Ruiz et al. (2006). A correction coefficient of 1.025 was applied to datings perfomed prior to 1978 (INGEIS 1977)

of strombolian-type volcanism, with scoriaceous and cinder cones together with the eruption of lava flows (Ferreira et al. 1999).

Towards the southern sector, the thickness of the volcanic rocks notably increases (Bodenbender 1929; Pensa 1957; Ferreira et al. 1999), and there are frequent volcanic dykes as feeders of lava flows with thickness that reach about 100 m (Sánchez and Bermúdez 1997). Escayola et al. (1998) described the roots of a volcanic neck that must have been an important centre of eruption lava and pyroclastic material in the southern part of this mountain chain. Sánchez and Bermúdez (1997) presented a map of the whole range, also distinguishing the units Cerro Colorado and Rumipalla Volcanic rocks. They noted three volcanic cycles, the last two integrating the Rumipalla Volcanic rocks.

Geuna (1997, 1998), Lagorio et al. (1997) and Lagorio (2003) performed sampling at different sections in order to complement previous studies of Gordillo and Lencinas in Sierra de Los Cóndores, carrying out an integrated palaeomagnetic and petrological–geochemical study. Figures 2.3 and 2.4 show some of the typically plateau-shaped hills, where several samplings have been performed. In these

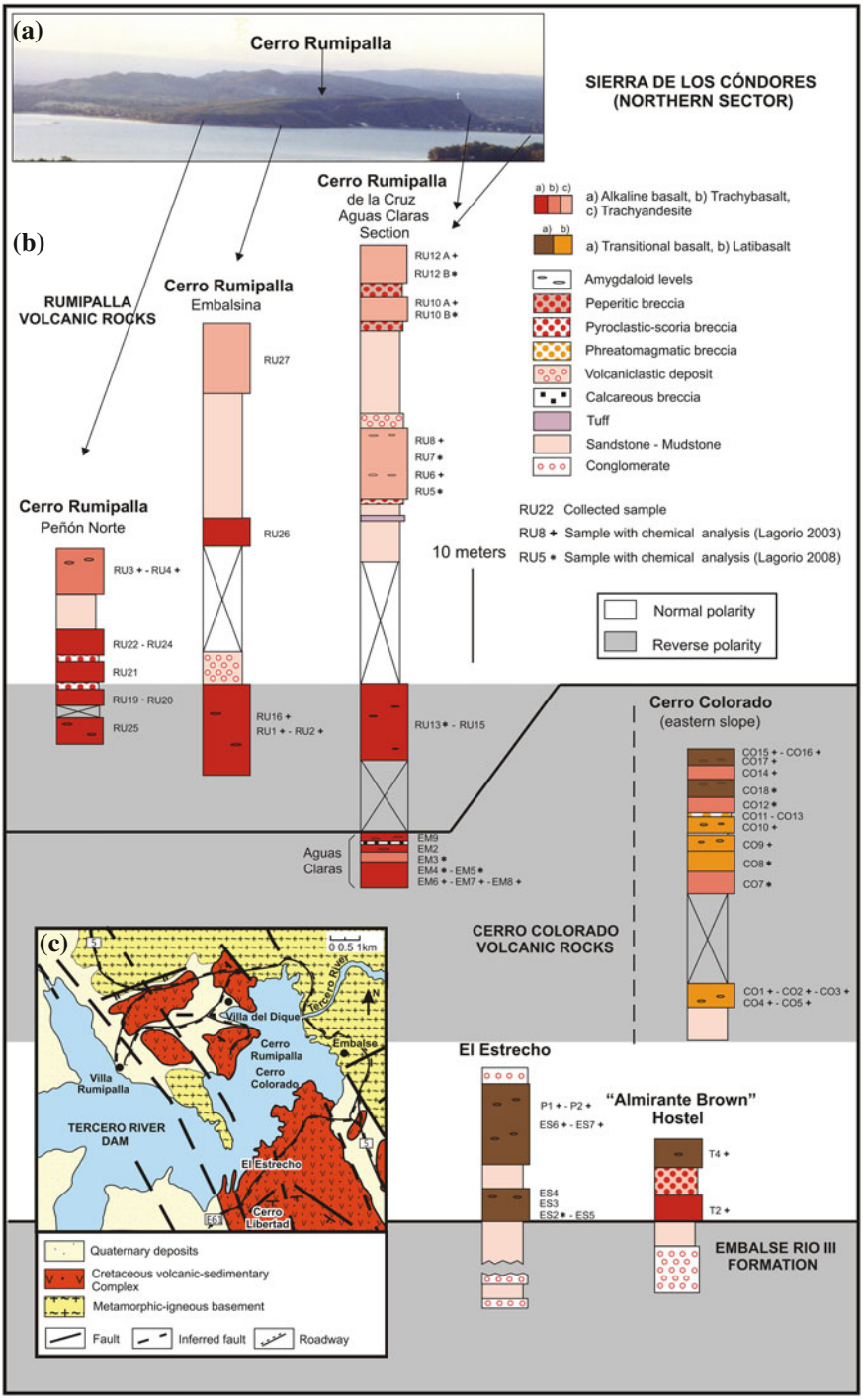
(a)
Cerro Rumipalla
SIERRA DE LOS CÓNDORES
(NORTHERN SECTOR)
(b)
Cerro Rumipalla
de la Cruz
Aguas Claras
Section
RUMIPALLA
VOLCANIC ROCKS
Cerro Rumipalla
Embalsina
Cerro Rumipalla
Peñón Norte
RU12 A +
RU12 B ●
RU10 A +
RU10 B ●
RU27
RU26
RU8 +
RU7 ●
RU6 +
RU5 ●
RU3 + - RU4 +
RU22 - RU24
RU21
RU19 - RU20
RU25
RU16 +
RU1 + - RU2 +
RU13 ● - RU15
EM9
EM2
EM3 ●
EM4 ● - EM5 ●
EM6 + - EM7 + - EM8 +
Aguas
Claras
a) b) c)
a) Alkaline basalt, b) Trachybasalt,
c) Trachyandesite
a) b)
a) Transitional basalt, b) Latibasalt
Amygdaloid levels
Peperitic breccia
Pyroclastic-scoria breccia
Phreatomagmatic breccia
Volcaniclastic deposit
Calcareous breccia
Tuff
Sandstone - Mudstone
Conglomerate
RU22 Collected sample
RU8 + Sample with chemical analysis (Lagorio 2003)
RU5 ● Sample with chemical analysis (Lagorio 2008)
10 meters
Normal polarity
Reverse polarity
Cerro Colorado
(eastern slope)
CO15 + - CO16 +
CO17 +
CO14 +
CO18 ●
CO12 ●
CO11 - CO13
CO10 +
CO9 +
CO8 ●
CO7 ●
CO1 + - CO2 + - CO3 +
CO4 + - CO5 +
CERRO COLORADO
VOLCANIC ROCKS
(c)
0 0.5 1km
Tercero River
Villa del Dique
Embalse
Cerro
Rumipalla
Cerro
Colorado
Villa
Rumipalla
TERCERO RIVER
DAM
El Estrecho
Cerro
Libertad
Quaternary deposits
Cretaceous volcanic-sedimentary
Complex
Metamorphic-igneous basement
Fault
Inferred fault
Roadway
El Estrecho
P1 + - P2 +
ES6 + - ES7 +
ES4
ES3
ES2 ● - ES5
"Almirante Brown"
Hostel
T4 +
T2 +
EMBALSE RIO III
FORMATION

◀ **Fig. 2.3** Sierra de los Cóndores (northern sector). **a** Panoramic view of Cerro Rumipalla from El Estrecho, as shown in Lagorio (2003) and Lagorio et al. (2014). **b** Stratigraphic sections around the Tercero River dam, with a stratigraphic proposal according to the recorded magnetic polarities (Geuna 1998), including the lithological types; volcanic rocks classified according to their chemistry. The subdivision in units defined by Gordillo and Lencinas (1967) for Sierra de los Cóndores Group is also indicated. **c** Schematic geological map based on Sánchez et al. (1990)

profiles, the diverse lithological types were also identified (Figs. 2.3b and 2.4b, d), according to the geochemical classification and the petrographic features, as will be described in the following item.

The sampled levels of volcanic rocks are massive, black to dark brown, with auburn lava flows that bear amygdales of granular zeolites and carbonate reflecting a deuterism sometimes intense.

Sedimentary and volcanic strata are very frequently interbedded in the northern sector, which indicates the simultaneity between both processes.

In some outcrops, the overlapping of lava flows produced marked thermal effects. In other cases, however, peperitic breccias were generated; these are characterized by fragments often with crenulated edges, invaded by the fine sandy matrix. Although the term breccia is used here, subrounded fragments predominate, which characterizes the globular, fluidal or pillowy peperites (Busby-Spera and White 1987). The genesis of deposits with peperitic texture can be due to lava flowing on wet unconsolidated sediments or due to the falling of pyroclasts in a plastic state (e.g. glassy shards) on a material with those characteristics. This is consistent with the presence of cord and pillow lavas on the southern shore of the lake formed by the Tercero River dam, mentioned by Sánchez and Bermúdez (1997), who interpreted this as an evidence of a possible subaqueous eruption. Furthermore, levels corresponding to gravitational flows, debris flow type, produced by remobilization of volcanic material are also observed. Outcrops corresponding to scoria fall and pyroclastic breccia deposits are particularly abundant in the southern sector of the range (Fig. 2.4d), which constitute typical products of strombolian activity, characterized by moderate explosiveness.

Volcanic breccias are constituted by fragments of vesicular lava generally with sharp edges, contained in a lapilli or tuffaceous matrix; sometimes, the fragments are cemented by carbonate or analcime (Fig. 2.4f). Volcanic bombs are also observed in these deposits, particularly in the southern area as pointed out by Ferreira et al. (1999). It should be noted that also some phreatomagmatic episodes must have also taken place locally. For example, a lapilli-bearing level mostly composed of angular fragments from the basement along with subordinate juvenile fragments has been observed in the northern sector (Cerro Colorado, Fig. 2.3b; "hybrid volcanic rock" of Gordillo and Lencinas 1967a).

On the other hand, also in the northern zone (the Aguas Claras area) a level of a calcrete, partially bearing a texture of a breccia, has been recognized, with similarities to the lithology described by Piovano (1994) in the locality of Saldán zone. This latter author attributes its genesis to thermal groundwater, inherent to the volcanic process, in an arid context with high evaporation and low biological activity.

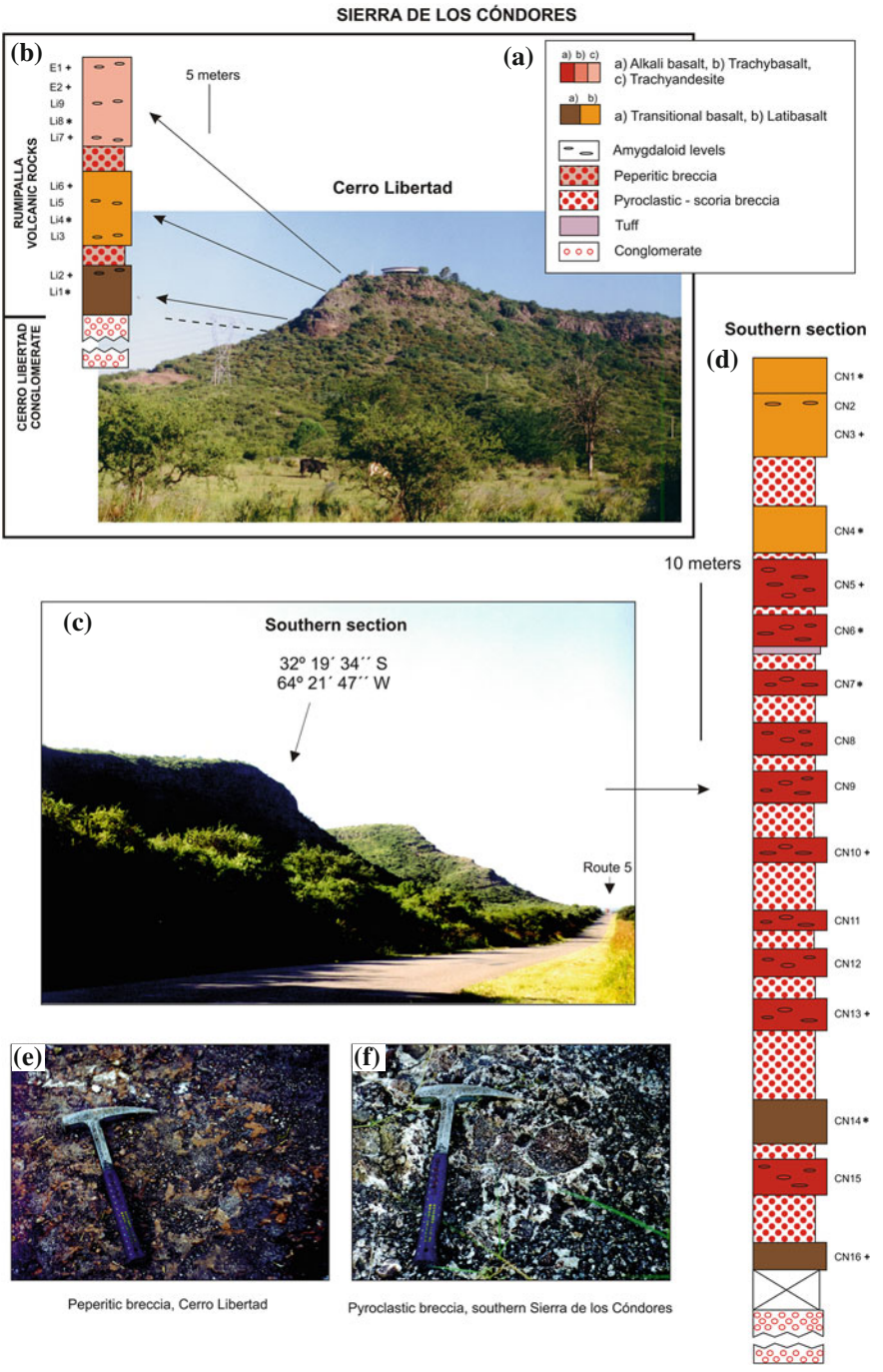
SIERRA DE LOS CÓNDORES
(b)
(a)
E1 +
E2 +
Li9
Li8 •
Li7 +
Li6 +
Li5
Li4 •
Li3
Li2 +
Li1 •
RUMIPALLA VOLCANIC ROCKS
CERRO LIBERTAD CONGLOMERATE
5 meters
Cerro Libertad
a) b) c)
a) Alkali basalt, b) Trachybasalt, c) Trachyandesite
a) b)
a) Transitional basalt, b) Latibasalt
Amygdaloid levels
Peperitic breccia
Pyroclastic - scoria breccia
Tuff
Conglomerate
Southern section
(d)
CN1 •
CN2
CN3 +
CN4 •
CN5 +
CN6 •
CN7 •
CN8
CN9
CN10 +
CN11
CN12
CN13 +
CN14 •
CN15
CN16 +
10 meters
(c)
Southern section
32° 19´ 34´´ S
64° 21´ 47´´ W
Route 5
(e)
(f)
Peperitic breccia, Cerro Libertad
Pyroclastic breccia, southern Sierra de los Cóndores

◀ **Fig. 2.4** Sierra de los Cóndores (southern section, south of the dam), as shown in Lagorio (2003) and Lagorio et al. (2014). **a** View of Cerro Libertad from El Estrecho. **b** Stratigraphic section in this hill, including different lithological types according to their chemistry; the subdivision of Sierra de los Cóndores Group defined by Gordillo and Lencinas (1967) is also indicated. **c** View of the outcrops in the southern sector of Sierra de los Cóndores. **d** Stratigraphic section including the different lithological types depending on their chemistry. Note that from Cerro Libertad to the south, all lavas were extruded in a normal magnetic polarity, different from what is recorded in the northern sector (area of the Tercero River dam). Pensa (1957) suggested that Cerro Libertad was the boundary between the northern and southern areas of Sierra de los Cóndores. **e** Detail of peperitic breccia in Cerro Libertad. **f** Detail of pyroclastic breccia in southern Sierra de los Cóndores

Petrological–geochemical and palaeomagnetic studies allowed establishing a stratigraphic proposal for the northern sector of the range (Fig. 2.3b). For this area, the lava flows are distributed throughout the whole sequence, diachronically and with lateral variations between different localities. According to the recorded magnetic polarities (Geuna 1998), the time span covering the volcanic event does not exceed 3 million years (Geuna 1997; Lagorio 2003). In this context, the distinction between two different volcanic cycles which can be mapped seems to be extremely difficult.

If the lava flows of the Libertad hill and those of the southern section are compared, it appears that both sites complete their evolution in one chron of normal polarity (Fig. 2.4) which is different to what happens in the northern sector (Geuna 1998). From the Libertad hill to the south, all the lava flows were extruded during a normal polarity chron. Previously, Pensa (1957) placed in this hill the boundary between the southern and northern areas of this range. Anyway, it is not possible to determine in which of the two normal polarity intervals recorded in the northern sector were extruded the lavas in the southern area, and if they poured out synchronously.

The locality of Almafuerte

The volcanic–sedimentary complex is exposed to about 3 km from the town of this name, near the Piedras Moras dam on the Tercero River, approximately 15 km to the east of Sierra de los Cóndores (Figs. 2.2b and 2.5). This succession is composed of lava flows interbedded with sandstones and breccias that are cut by dykes; it has has a thickness of 160 m, tilts 25°–30° to the SSE (Schröder 1967; Mendía 1978) and was entirely observed prior to the building of the dam. Presently, only the upper part of the section is outcropping.

Gordillo and Lencinas (1980) considered that these outcrops belong to the Sierra de los Cóndores Group, whereas Piovano (1996) includes this sequence, like others located to the east of the La Calera fault, in the Saldán Formation.

Geuna (1997) and Lagorio (2003) described the sequence close to Route 36, north of the bridge over the Tercero River (Fig. 2.5a, b). This is a sequence formed by several lava flows, with maximum thickness of 4 m, interbedded with breccia and sandstone levels of minor thickness, cut by basic dykes (Fig. 2.5c–e). Breccia levels are of different types.

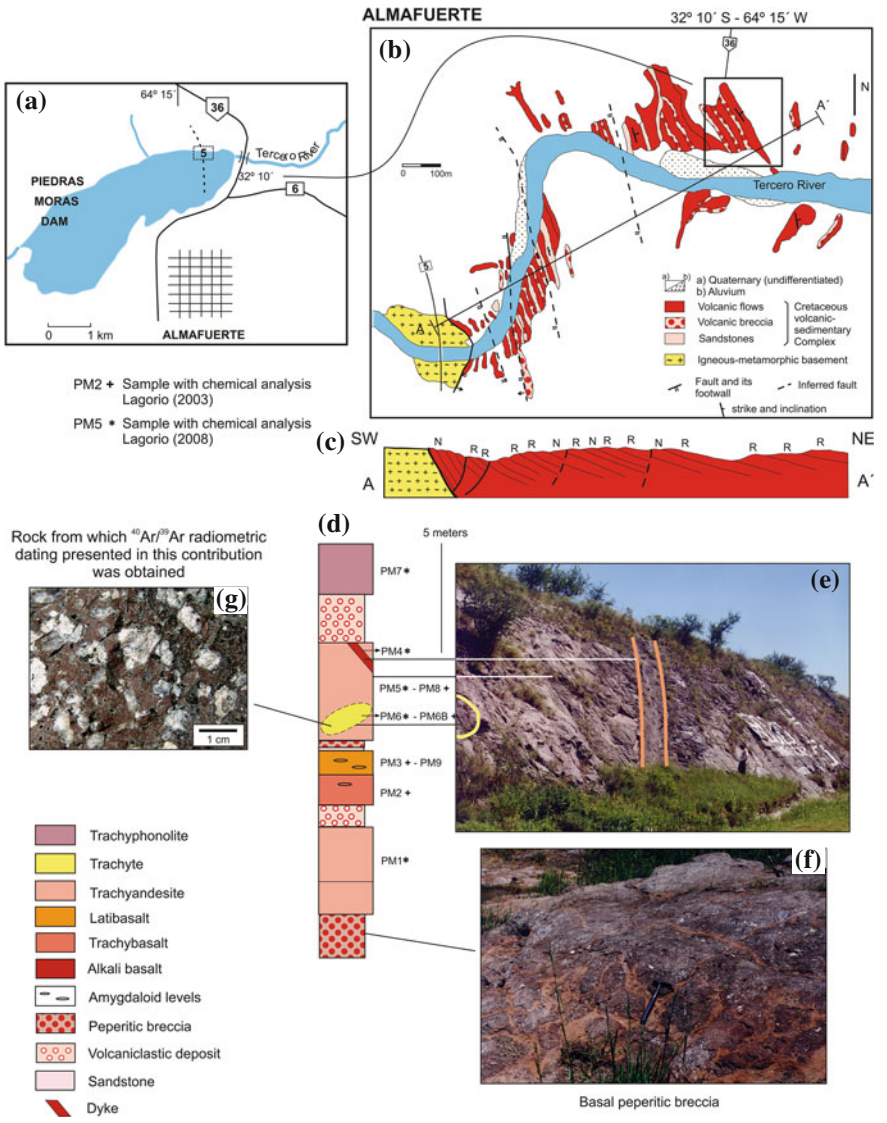

A peperitic-type breccia is located in the lower part of the section, characterized by large fragments of volcanic rocks with marked crenulations and interpenetrations of a matrix composed of reddish fine sandstone (Fig. 2.5f). It is noteworthy that Pensa (1957) pointed out a very frequent interaction between lava flows and sediments in this area, assigning special importance to the type of wetting affecting the sands, as a significant factor to determine the final texture of rocks. In fact, the degree of saturation in water, the consolidation and permeability of the sediments must have strongly conditioned the lithological features of the deposits. Other

◀ **Fig. 2.5** Locality of Almafuerte, as shown in Lagorio (2003) and Lagorio et al. (2014). **a** Location map of this area with the former track of Route 5 (now submerged). **b** Geological map of the area for times prior to the dam construction (based on Schröder 1967 and Mendía 1978); the area of the stratigraphic section is indicated (see track of Route 5 for reference). **c** Schematic section showing the magnetic polarity, as determined by Mendía (1978) and reinterpreted by Geuna (1997); note that at most three alternate polarities are present at each structural block. **d** Stratigraphic section of the currently outcropping levels close to the Piedras Moras dam, including the lithological types according to their chemistry. The magnetic polarity of this section is reverse, while basaltic dyke PM4 is of normal polarity. **e** Photograph of the lava flows (trachyandesite) intruded by a basaltic dyke (sample PM4); this lava flow presents also sectors of trachytic composition (sample PM6). f) Photograph of basal peperitic breccias. **g** Photograph of the trachyte (PM6) composed of macrophenocrysts and abundant phenocrysts of feldspar; the study under the microscope allowed the identification of anorthoclase with a thick rim of sanidine constituting the macrophenocrysts, whereas phenocrysts are essentially of sanidine. The $^{40}Ar/^{39}Ar$ of 129.6 ± 1 Ma dating was obtained in these phenocrysts

breccia levels unconformable overlain lava flows, indicating a brief erosive pre-depositional stage; they show subangular fragments without any interpenetration by thin sandstone matrix. They are interpreted as the result of debris flows. Schröder (1967) assigned this genesis to all of the breccia levels of this area.

A macroporphyritic trachyte-bearing sanidine crystals (Fig. 2.5g) was selected for dating through $^{40}Ar/^{39}Ar$ techniques, as it will be explained below. According to palaeomagnetic data from the entire sequence, including levels studied by Mendía (1978) before the water reservoir was filled, Geuna (1997) pointed out that most of the lava flows would have extruded during three chrones of alternate polarity (R–N–R, Fig. 2.5c). Meanwhile, the dykes must have intruded the section during a second period of normal polarity. Then, volcanic eruptions in the Almafuerte locality and northern Sierra de los Cóndores (area of the Tercero River dam) show a similar pace and are probably coeval.

The locality of Despeñaderos

The Cretaceous volcanic–sedimentary complex outcrops in parts of the margins of the Segundo River, near the Despeñaderos locality (Fig. 2.2b). It constitutes isolated outcrops in some canyons of the river, as they were observed by Bain Larrahona (1940), Kull and Methol (1979), and Gordillo and Lencinas (1980) who included them in the Sierra de Los Cóndores Group; on the other hand, Piovano (1996) included these outcrops in the Saldán Formation.

Geuna (1997) and Lagorio (2003) described the outcrops located west of the intersection with Route 36, about 300 m from the bridge over the Segundo River, on its right margin. Outcrops consist of lava flows interbedded with breccia levels making up a sequence of about 25 m, subhorizontal, originated during only one chron of normal polarity (Fig. 2.6a, b).

Previously, Gordillo and Lencinas (1969) analysed the petrography and chemistry of a sample from the left margin of the Segundo River, here also included in the classification diagrams.

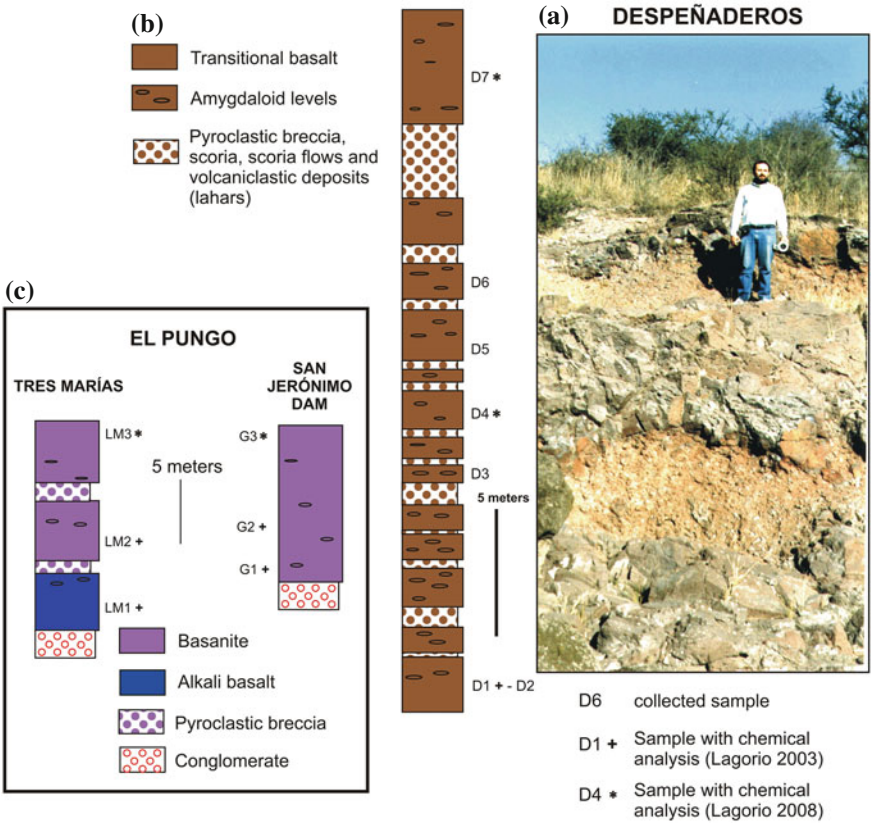

Fig. 2.6 **a** Partial view of the outcrops close to Despeñaderos locality, on the right margin of Segundo River, and to the west of the intersection with Route 36. Note the alternation of lava flows and breccia levels that form the sequence. **b** Stratigraphic section pointing out the lithological types according to their chemistry. **c** Stratigraphic section in El Pungo locality, note the lithological types according to their chemistry. Modified from Lagorio et al. (2014)

The sampled basaltic levels have thicknesses of up to 5 m, reddish-brown colour and are markedly amygdaloidal, denoting an intense deuterism under highly oxidizing conditions. The breccia levels have thicknesses between 0.20 and 3 m (Fig. 2.6b). Pyroclastic breccias, scoria fall deposits as well as dense gravitational flows (debris flows) of laharic type are also recorded, suggesting an origin related to a volcanic area with high and, therefore, unstable slopes.

An arid to semi-arid climate context with torrential rains and low vegetation must have favoured the formation of debris flows, as described by Piovano and Astini (1990) for basal conglomeratic facies of the Saldán Formation that integrate thick alluvial fan deposits, approximately at 60 km to the north of the Despeñaderos locality.

The locality of Los Molinos

In this area, basic dykes that intrude the crystalline basement are outcropping (Figs. 2.2b). Gordillo and Lencinas (1969) described 35 dykes, with thicknesses between 0.5 and 1.5 m, length of the order of a hundred metres, subvertical and generally NNW trending.

They were discriminated by Gordillo and Lencinas (1969) as unaltered dykes (olivine trachydiabases) and hydrothermalized (analcimites and potassium trachydiabases). These authors stated that despite having obtained a K–Ar age of 60.2 ± 3 Ma, the intrusive phases of Los Molinos must belong to the Early Cretaceous magmatic event, considering the mineralogical and chemical similarity to the lavas of Sierra de los Cóndores.

While later radiometric dating obtained by Linares and Valencio (1974) suggested two groups of contrasting ages (150 ± 10 Ma–129 ± 10 Ma and 68 ± 5 Ma–63 ± 5 Ma), Geuna (1997) and Geuna and Vizán (1998) determined that their palaeomagnetic directions are all reversed and similar to those of the lavas of Sierra de los Cóndores, which reinforces the hypothesis of a single intrusive event taking place during the Early Cretaceous.

Lagorio (2003) collected samples from several dykes in the proximity of the dam to characterize them from a petrological and geochemical point of view. While Lagorio (2008) presented complete chemical data for samples of dykes 4 and 14 (olivine trachydiabases of Gordillo and Lencinas 1969), Lagorio (2003) also reported chemical analyses of samples of dykes 8 and 9 (olivine analcimites of Gordillo and Lencinas 1969), characterized by high loss on ignition values conferred by the presence of analcime. For this contribution, the chemistry of the two varieties was considered. Also, an analysis of the potassic trachydiabase of Gordillo and Lencinas (1969) was even included in the classification diagrams presented below.

El Pungo—La Cumbre localities

In the northern sector of Sierra Chica, close to the towns of La Cumbre and Capilla del Monte (Fig. 2.2b), the outcrops of the Cretaceous volcanic–sedimentary complex have been defined as El Pungo Group by Gordillo and Lencinas (1967b). These authors described this group as formed by a thick basal conglomerate (El Rosario Conglomerate) on which successively lay a nephelinic basalt (El Pungo Volcanic) and sedimentary deposits (Valle del Sol Fanglomerate).

Later, Delpino et al. (1999), Sánchez et al. (1999, 2001) and Sánchez (2001a, b) defined the formational units El Rosario, El Saucecito and Peñón Blanco, as members of the El Pungo Group, excluding the Valle del Sol Fanglomerate. El Saucecito Formation is the volcanic unit that includes the lava flows described by Gordillo and Lencinas (1967b) and also the volcaniclastic deposits. The latter are more abundant than the volcanic rocks and related to hydroclastic and strombolian

eruptions (Delpino et al. 1999; Sánchez et al. 2001, 2002). The volcanic flows were studied also by Ancheta et al. (2002).

Geuna (1997) and Lagorio (2003) performed studies in three sites: (1) San Jerónimo dam, (2) Tres Marías town and (3) Estancia El Rosario area. The volcanic sequence has a thickness of less than 20 m. The lava flows are covering conglomerates (Fig. 2.6c); usually they are massive, only in some sectors they have carbonate amygdales, and seem to have been erupted through two chrones of normal and reverse polarity. In the area of Tres Marías, the lava flows are between 3 and 5 m thick and are interbedded by thin breccia/lapillitic levels that usually do not exceed 2 m in thickness (Fig. 2.6c). These levels have subangular and angular fragments of basalt, of various sizes, that belong to both lapilli and blocks. They were interpreted as fall deposits in a volcanic strombolian context, relatively close to the centre of eruption. Close to this area, Delpino et al. (1999) studied thick pyroclastic rocks that Sánchez et al. (2001) and Ancheta et al. (2002) characterized as hydromagmatic types and considered that they were formed in the initial periods of the volcanic activity in this region.

More recently, Oviedo and Astini (2014) presented a detailed study along Road El Cuadrado, across the Sierra Chica, that allowed the identification and characterization of a volcaniclastic unit that seems equivalent to that described by Delpino et al. (1999) and Sánchez et al. (1999) in El Pungo region. Oviedo and Astini (2014) better considered to preserve the original nomenclature of Gordillo and Lencinas (1967b), though amending it, in order to include in El Pungo Formation other materials. These comprise primary fall deposits, possible surge ones, gravity flows as well as reworked deposits, along with basaltic flows. Those authors consider that those deposits represent relicts of a syneruptive strombolian and phreatomagmatic activity close to a basaltic monogenic system conforming the synrift filling of the Cretaceous depocenters.

2.1.1.3 Age of this Volcanism

This volcanism has been intensively dated, mainly several decades ago, through the K/Ar method with ages ranging from 154 ± 10 Ma to 61.7 ± 3 Ma (Table 2.1). The latest K/Ar whole-rock dating on rocks from the Despeñaderos locality ranges from 136.3 to 122.9 Ma (Cejudo Ruiz et al. 2006).

The vast majority of dating was performed on whole-rock samples, so that frequent partially crystallized glassy groundmass, subtle deuteric alteration and weathering, as well as a possible insufficient outgassing during the volcanic event, could have determined the large age variability. Nevertheless, a slight diachronism considering the whole Sierra Chica de Córdoba cannot be ruled out. It should be noted, however, that no more than three periods of alternate magnetic polarity were recorded in every section according to the Early Cretaceous reversal rate that would mean a maximum time of 3 million years (My) in continuous records. Also, the

presence of magnetic reversals reinforces the fact that the volcanic event in SCC occurred mostly before 124 Ma (the onset of the Cretaceous Normal SuperChron).

We made a detailed microscopic analysis of several rock types from different localities of SCC, previously to the selection of samples. $^{40}Ar/^{39}Ar$ dating was then performed on a sample collected at the Almafuerte locality (32° 10′S; 64° 14′W), as it bears numerous sanidine phenocrysts. This sample corresponds to a trachyte with 8.62 wt% K_2O which was measured at Actlabs (Canada), through step-heating analysis. It should be noted that biotite (though scarce) only appears in this sample of SCC, while phlogopite was not even reported in any rock. The sample wrapped in Al foil was loaded in evacuated and sealed quartz vial with K and Ca salts and packets of LP-6 biotite used as a flux monitor. It was irradiated in the nuclear reactor for 48 h. After the flux monitors were run, J values were then calculated for the sample, using the measured flux gradient. LP-6 biotite has an assumed age of 128.1 Ma. The neutron gradient did not exceed 0.5 % on sample size. The Ar isotope composition was measured in a Micromass 5400 static mass spectrometer. 1200 °C blank of ^{40}Ar did not exceed $n \times 10^{-10}$ cc STP.

The sample yielded an age spectrum with six steps plateau characterized by 89 % of ^{39}Ar. Therefore, an age value of 129.6 ± 1.0 Ma was obtained, as it is shown in Fig. 2.7a.

On the Inverse Isochrone Plot Plateau points form a linear trend characterized by age value of 128.4 ± 1.5 Ma, with a mean square weighted deviation (MSWD) = 1.6 and $(^{40}Ar/^{36}Ar)_0 = 348 \pm 27$ (Fig. 2.7b). Inverse isochrone age (IIA) is concordant with weighted mean plateau age (WMPA) in the frame of error. Thus, WMPA, as more precise, should correspond to the age of formation or closing of isotope system of the sanidine.

2.1.1.4 Classification and Petrography

The first detailed studies on the petrography, mineralogy and geochemistry of Cretaceous volcanic rocks in Sierra Chica were made by Gordillo and Lencinas (1967a, b, 1969). Subsequently several authors conducted studies in different areas of Sierra Chica: Cortelezzi et al. (1981), Kay and Ramos (1996), Bermúdez and Sánchez (1997), Lagorio et al. (1997), Lagorio (1998), Escayola et al. (1998, 1999), Lucassen et al. (2002) and Ancheta et al. (2002). Lagorio (2003, 2008) carried out a petrological and geochemical study on these volcanic rocks throughout the Sierra Chica, including mineralogical analyses using electron microprobe.

The results are summarized below, considering also samples analysed by other authors. The classification was performed based on the chemistry of the major elements. The samples analysed in this study present a continuous variation from basalt to trachyte in the diagram alkalis versus silica (TAS, Le Bas et al. 1986; Fig. 2.8a) including trachybasalts, basaltic trachyandesites and trachyandesites. A few number of samples were classified in the fields of basanite and basaltic andesite.

The diagram of classification R1-R2 (De la Roche et al. 1980; Bellieni et al. 1981; Fig. 2.8b) allows the recognition of two volcanic suites: (1) alkali basalt–

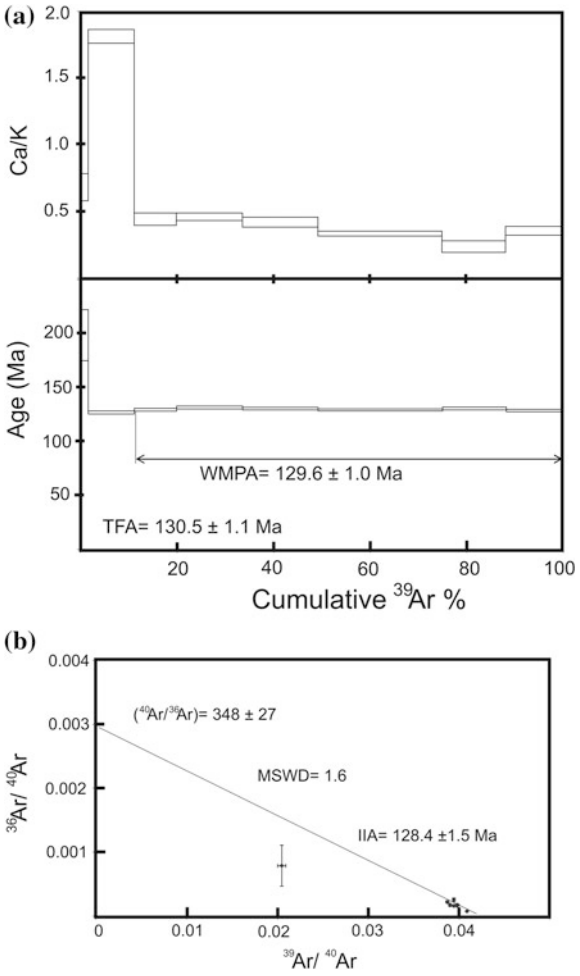

Fig. 2.7 **a** $^{40}Ar/^{39}Ar$ age and Ca/K spectra for sanidine phenocrysts of a trachyte of Sierra Chica of Córdoba (SCC). The sample yielded age spectrum with six steps plateau characterized by 89 % of ^{39}Ar, age value of 129 ± 1.0 Ma (WMPA). **b** On the Inverse Isochrone Plot Plateau points form a linear trend characterized by the age value of 128.4 ± 1.5 Ma, MSWD = 1.6 and $(^{40}Ar/^{36}Ar)_0$ = 348 ± 27. *WMPA* weighted mean plateau age; *MSWD* mean square weighted deviation; *TFA* total fusion age; *IIA* inverse isocrone age

trachybasalt–trachyandesite–trachyphonolite–trachyte (AkB-Tc), and (2) transitional basalt–latibasalt (TrB-Lb), as well as two groups of rocks: basanites (Bsn) and ankaratrites (Akr). The latter present samples with elevated loss on ignition (>5 %), determined by abundant analcime that characterizes these rocks (analcimites of Gordillo and Lencinas 1969). However, classification based on immobile trace element ratios (e.g. Floyd and Winchester 1978) of the few samples with high loss on ignition included here confirm classification through major elements. It should be noted that, considering that the diagram R1-R2 allows a more complete discrimination of these rocks, it was thus adopted for the nomenclature.

The basanites and part of the rocks of the alkaline suite are CIPW-normative nepheline (Ne); meanwhile, the transitional suite is characterized, instead, for being hypersthene normative (Hy). Furthermore, the nomenclature employed by Gordillo and Lencinas (1967a) for some samples of Sierra de los Cóndores (e.g. calc-alkaline

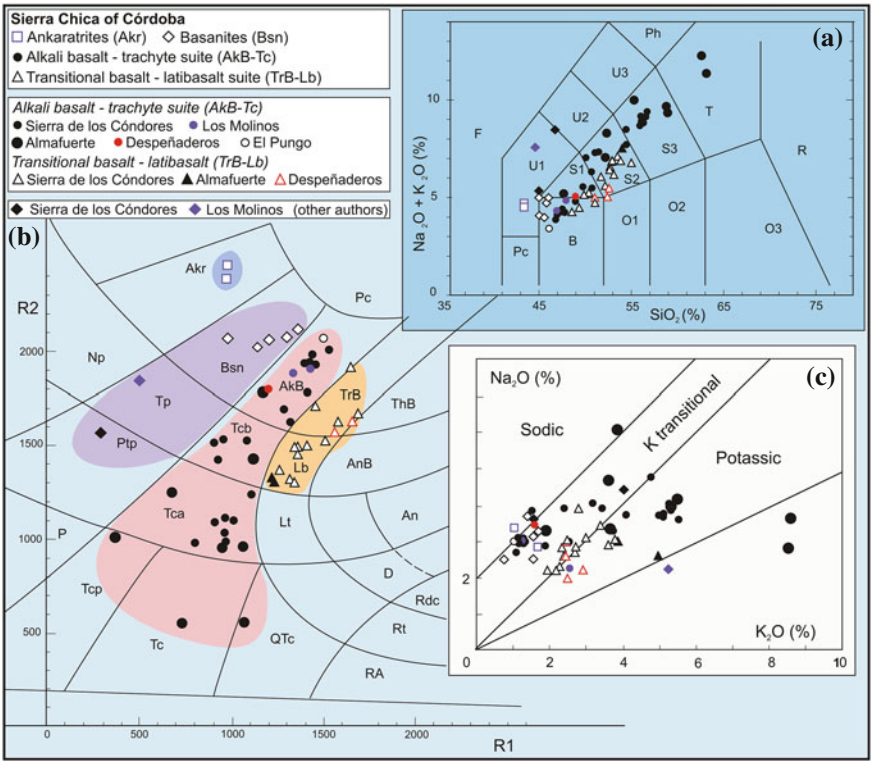

Fig. 2.8 Classification diagrams of volcanic rocks of Sierra Chica, adapted from Lagorio (2008) and Lagorio et al. (2014). The following data are also included: potassic trachydiabase of Los Molinos and alkali basalt of Despeñaderos according to analysis presented by Gordillo and Lencinas (1969); basanite and phonotephrite from the southern sector of Sierra de Los Cóndores provided by Cortelezzi et al. (1981) and Escayola et al. (1998). **a** Alkalis versus silica diagram (TAS, Le Bas et al. 1986); *B* basalt, *S1* trachybasalt, *S2* basaltic trachyandesite, *S3* trachyandesite, *T* trachyte, *F* foidite, *U1* basanite/tephrite, *U2* phonotephrite, *U3* tephriphonolite, *Ph* phonolite, *O1* basaltic andesite. **b** R1-R2 diagram (from De la Roche et al. 1980; Bellieni et al. 1981); R1 = 4Si − 11 (Na + K) − 2 (Fe + Ti), R2 = 6Ca + 2Mg + Al; *Pc* picrite, *Akr* ankaratrite, *Bsn* basanite, *AkB* alkali basalt, *TrB* transitional basalt, *ThB* tholeiitic basalt, *Np* nephelinite, *Tp* tephrite, *Tcb* trachybasalt, *Lb* latibasalt, *AnB* andesi-basalt, *Ptp* phonotephrite, *Tca* trachyandesite, *Lt* latite, *P* phonolite, *Tph* trachyphonolite, *T* trachyte, *QTc* quartz trachyte, *Lan* latiandesite, *An* andesite, *QLc* quartz latite, *D* dacite, *Rd* rhyodacite, *R* rhyolite, *AR* alkaline rhyolite. **c** Na_2O versus K_2O diagram with fields according to Comin-Chiaramonti et al. (1997)

trachytes, equivalents of latibasalts in the classification used here) let infer a transitional character that reinforces the distinction between two suites.

According to the criteria of alkalinity of Comin-Chiaramonti et al. (1997), the analysed rocks have essentially a potassic ($1 < K_2O/Na_2O \leq 2$) and transitional to potassic ($Na_2O - 2 < K_2O$ and $K_2O/Na_2O \leq 1$) character; only few examples typify as high potassic rocks ($K_2O/Na_2O > 2$) or as sodic lithological types ($Na_2O - 2 \geq K_2O$), as it is shown in Fig. 2.8c.

Alkaline Suite (BA-T)

Alkali basalts outcrop in Sierra de los Cóndores (there, they are comparable to the picritic basalts and partially to the brown andesinic trachybasalts of Gordillo and Lencinas 1967a), Almafuerte and Los Molinos (olivine trachydiabases of Gordillo and Lencinas 1969). They present a porphyritic texture, with phenocrysts and microphenocrysts of olivine (Fo_{90-83}) and clinopyroxene ($Wo_{53-46}En_{46-35}Fs_{15-5}$); the glassy groundmass consists of clinopyroxene ($Wo_{51-49}En_{43-41}Fs_{8-6}$), olivine ($Fo_{87-79}$), Ti-magnetite (ulvöspinel = 63–48 %) ± ilmenite (R_2O_3 = 7 %), alkali feldspar (Or_{62-12} $Ab_{69-37}An_{26-1}$) and plagioclase (An_{30-26}). Apatite and Ti-biotite occur as accessory minerals. The most primitive rocks usually have small ultramafic xenoliths (lherzolitic, dunitic, harzburgitic, Fig. 2.9a).

On the other hand, some samples of Los Molinos dykes exhibit quartz xenocrysts with rims of reaction formed by clinopyroxene; they also have granitic basement xenoliths.

There are frequent ocellar-type textures, particularly in Sierra de los Cóndores, defining ellipsoidal patches that consist of sanidine and/or nepheline, egirinic clinopyroxene ± Ti-biotite ± apatite (Fig. 2.9b).

In relation to dykes from Los Molinos locality, according to their chemical composition, they classify as alkaline basalts and based on petrographic features they were considered as lamprophyres by Gordillo and Lencinas (1969). Particularly, they typify as hyalomonchiquites (IUGS nomenclature: Le Maitre 1989; Le Bas and Streckeisen 1991). However, the absence of biotite and/or amphibole phenocrysts does not allow, in fact, considering them as classical lamprophyres. These phases appear only in the groundmass in small proportions and could have even been formed by devitrification.

The sample collected by Gordillo and Lencinas (1969) near the Despeñaderos locality, also included in the classification diagrams, typifies as alkali basalt (Fig. 2.8b), and the petrographic features described by those authors are similar to those described here for this lithotype.

Trachybasalts outcrop in Sierra de los Cóndores (equivalent to black andesinic trachybasalts of Gordillo and Lencinas 1967a) and the Almafuerte locality. Two varieties, one porphyritic and other aphyric, are recognized. The first consists of phenocrysts and/or microphenocrysts of clinopyroxene ($Wo_{48}En_{46-45}Fs_{8-6}$), olivine ($Fo_{86-72}$) ± plagioclase ± Ti-magnetite immersed in a hypocrystalline basis formed by alkali feldspar ($Or_{58-39}Ab_{47-34}An_{14-8}$), plagioclase ($An_{46}$), clinopyroxene ($Wo_{46}En_{47}Fs_7$), olivine ($Fo_{72}$), Ti-magnetite (Ulv. = 59 %) ± ilmenite (R_2O_3 = 7 %), apatite and Ti-biotite. Occasionally, few xenocrysts of plagioclase and quartz with reaction rims and schist xenoliths are observed. Ocellar-type textures are frequent, defining ellipsoidal patches composed of sanidine and/or nepheline, aegirinic clinopyroxene ± Ti-biotite ± apatite. The aphyric trachybasalts (Sierra de los Cóndores, Fig. 2.9c) consist of clinopyroxene crystals ($Wo_{49-46}En_{46-41}Fs_{10-6}$), olivine ($Fo_{77}$), alkali feldspar ($Or_{67-42}Ab_{49-30}An_{9-3}$) and plagioclase ($An_{45}$); feldspars are characterized by including small crystals of

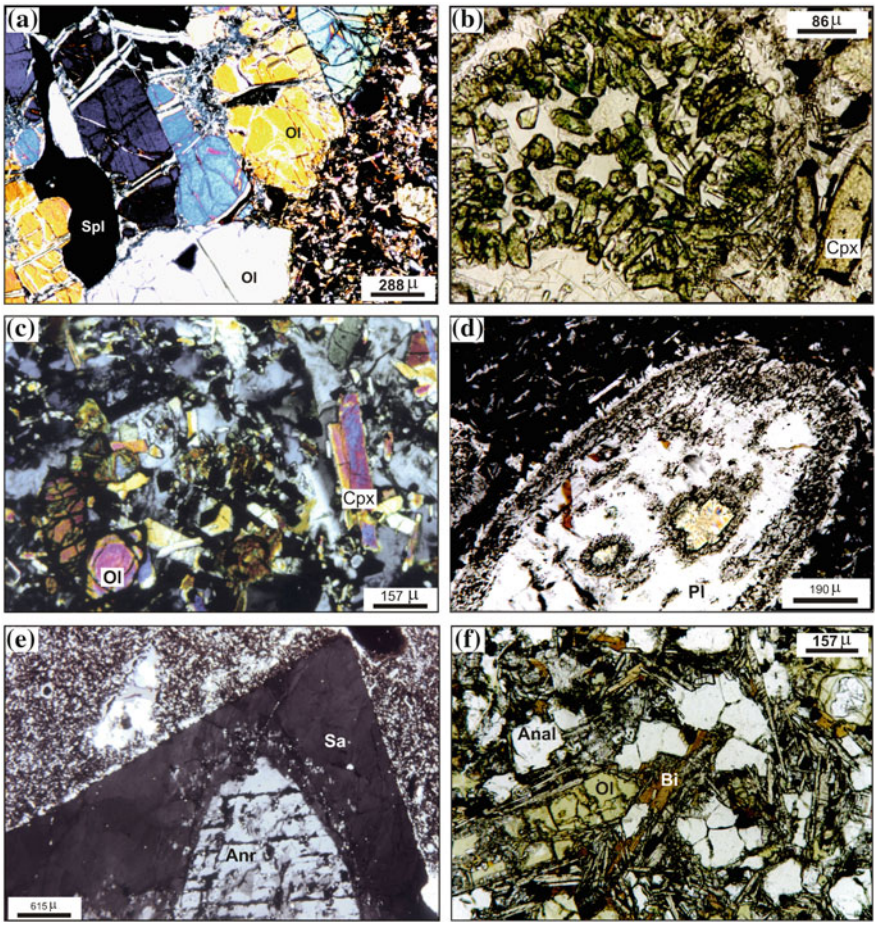

Fig. 2.9 Photomicrographs, taken from Lagorio (2003) and Lagorio et al. (2014). **a** Olivine crystals (Ol_{89}) showing straight contacts and interstitial spinel section (Spl) (picotite variety) forming lherzolitic xenolith in alkali basalt (picritic variety of Gordillo and Lencinas 1967a) from Aguas Claras (northern Sierra de los Cóndores), crossed nicols, 3.5X. **b** Ocellar structure in alkali basalt from the north of Sierra de los Cóndores) formed by egirinic clinopyroxene and alkali feldspar; note the compositional contrast with the microphenocrysts located in the lower right corner (*chestnut colour*), parallel nicols, 20X. **c** Trachybasalt from the north of Sierra de los Cóndores; crystals of olivine (Ol), clinopyroxene (Cpx), and opaque minerals are observed encompassed by feldspar sections, crossed nicols, 10X. **d** Sieve texture in macrophenocrysts of plagioclase (Pl) of a trachyandesite from the northern sector of Sierra de los Cóndores (rhombic porphyry of Gordillo and Lencinas 1967a), crossed nicols, 10X. **e** Macrophenocryst of anorthoclase (Anr) with large euhedral rim of sanidine (Sa) immersed in fine bostonitic groundmass, belonging to the trachyte of Almafuerte locality, crossed nicols, 2.5X. **f** Crystals of olivine (Ol) replaced by bowlingite, analcime (Anl), biotite (Bt), clinopyroxene and of opaque minerals along with interstitial glass forming an analcimite (ankaratrite), corresponding to one of the dykes of Los Molinos, parallel nicols, 10X

clinopyroxene, altered olivine and Ti-magnetite (Ulv. = 50 %) ± ilmenite (R_2O_3 = 6 %).

Trachyandesites outcrop in Sierra de los Cóndores (alkali trachytes of Gordillo and Lencinas 1967a) and the Almafuerte locality. Whereas in the first locality, they are Hy-normative, in the second one, Ne- and quartz-normative varieties occur. They show from microporphyritic to macroporphyritic textures characterized by phenocrysts and/or microphenocrysts of clinopyroxene ($Wo_{50-44}En_{48-40}Fs_{14-6}$), iddingsitized olivine ± Ti-magnetite and feldspar (as long as 1 cm). In macroporphyritic rocks, there are plagioclase crystals (An_{51-46}) as well as anorthoclase ($Or_{28-23}Ab_{48-45}An_{29-27}$) ones, in both Hy-normative (e.g. rhombic porphyry of Gordillo and Lencinas 1967a from Sierra de los Cóndores) and Q-normative (the rocks of the Almafuerte locality) varieties. In the latter, anorthoclase crystals are covered by a coat of sanidine, and also biotite and kaersutite phenocrysts as well as apatite microphenocrysts occur. In all of these varieties, crystals of feldspar and clinopyroxene show disequilibrium textures (Fig. 2.9d) with frequent resorption, strong corrosion and sieve texture. Groundmass is composed of alkali feldspar ($Or_{59-25}Ab_{52-39}An_{27-2}$), plagioclase ($An_{52-31}$), clinopyroxene ($Wo_{48-43}En_{48-42}Fs_{10-8}$), iddingsitized olivine, titanomagnetite (Ulv. = 84–4 %) ± ilmenite (R_2O_3 = 8–7 %), with apatite and biotite as accessory phases.

Trachytes outcrops in Almafuerte are Q-normative and have macroporphyritic texture (Fig. 2.5g). They are composed of crystals of 15 mm of anorthoclase ($Or_{22}Ab_{63}An_{15}$) covered by a thick edge of sanidine ($Or_{47}Ab_{47}An_6$) (Fig. 2.9e), phenocrysts and microphenocrysts of sanidine ($Or_{53-49}Ab_{43}An_4$), plagioclase (An_{54-53}), biotite and clinopyroxene ($Wo_{50-48}En_{45-43}Fs_{8-6}$), with microphenocrysts of Ti-magnetite and apatite. Groundmass is composed of sodic sanidine ($Or_{62}Ab_{36}An_2$), clinopyroxene ($Wo_{48}En_{44}Fs_8$), biotite, Ti-magnetite (Ulv. = 52 %), apatite and ± quartz in sparse fine veinlets and microamygdales.

Trachyphonolites also outcrop in the locality of Almafuerte. They are Ne-normative and have macroporphyritic texture. They are characterized by having plagioclase crystals (An_{52-45}) up to 10 mm long, microphenocrysts and phenocrysts of clinopyroxene ($Wo_{48-47}En_{43-42}Fs_{11-9}$) along with microphenocrysts of olivine altered to iddingsite, Ti-magnetites and apatite, immersed in a fine-grained matrix. The latter is made up of plagioclase, clinopyroxene, Ti-magnetite (Ulv. = 78 %), iddingsitized olivine, biotite and apatite. Plagioclase and clinopyroxene crystals show strong corrosion and sieve textures.

Some rocks of the suite bear vesicles filled by an intermediate term of the series analcime-wairakite (Lagorio and Montenegro 1996) along with calcite and smectites.

It should be noted that alkali basalts, trachybasalts, trachyphonolites and some trachyandesites are Ne-normative (Ne up to 7.30 % in trachyphonolites). Most trachyandesites are Hy-normative (Hy between 2.90 and 12.31 %) and a few Q-normative (Q ∼ 1 %); on the other hand, the latter feature is dominant in trachytes (Q upto 7.88 %).

Transitional Suite

Transitional basalts outcrop in Sierra de los Cóndores (equivalent to the brown and black andesinic trachybasalts of Gordillo and Lencinas 1967a) and in the locality of Despeñaderos. They have both porphyritic and aphyric textures. The first consists of phenocrysts and microphenocrysts of olivine altered to iddingsite together with clinopyroxene microphenocrysts ($Wo_{50\text{-}48}En_{46\text{-}41}Fs_{10\text{-}7}$). The glassy groundmass contains clinopyroxene ($Wo_{49}En_{45}Fs_6$), iddingsitized olivine, plagioclase ($An_{29\text{-}26}$), alkaline feldspar and Ti-magnetite (Ulv. = 81 %); accessory phases such as apatite and biotite are common. The aphyric variety consists of olivine crystals altered to iddingsite, plagioclase (An_{43}), alkali feldspar ($Or_{36\text{-}16}Ab_{69\text{-}55}An_{14\text{-}9}$) and clinopyroxene; feldspars enclose smaller crystals of clinopyroxene ($Wo_{45}En_{47}Fs_8$), iddingsitized olivine, Ti-magnetite and apatite.

Latibasalts are rocks from Sierra de los Cóndores (calc-alkaline trachytes of Gordillo and Lencinas 1967a) and the locality of Almafuerte. They have porphyritic texture defined by phenocrysts of iddingsitized olivine and clinopyroxene ($Wo_{49\text{-}41}En_{51\text{-}42}Fs_{10\text{-}5}$), together with occasional plagioclase phenocrysts and microphenocrysts of Ti-magnetite. The crystals of clinopyroxene and plagioclase often show sieve texture. The mesostasis consists of clinopyroxene ($Wo_{50\text{-}42}En_{50\text{-}43}Fs_{8\text{-}7}$), olivine altered to iddingsite, Ti-magnetite (Ulv. = 70–59 %), plagioclase ($An_{48\text{-}28}$), alkali feldspar ($Or_{47\text{-}33}Ab_{63\text{-}52}An_{4\text{-}1}$), apatite and occasional biotite. Some xenocrysts of quartz with reactions rims formed by small crystals of clinopyroxene are sporadically observed.

Rocks of the transitional suite are Hy-normative (Hy up to 15.75 %).

Basanites

Basanites outcrop in El Pungo locality; they have porphyritic texture composed of phenocrysts and microphenocrysts of olivine (Fo_{87}) and clinopyroxene ($Wo_{52}En_{44\text{-}42}Fs_{6\text{-}5}$). The glassy groundmass is made up of clinopyroxene ($Wo_{51}En_{44}Fs_5$), olivine (Fo_{87}), Ti-magnetite (Ulv. = 86 %) and sodic anorthoclase ($Or_{11}Ab_{76}An_{13}$), together with apatite and Ti-biotite as accessory phases. Dunitic xenoliths and glomeroporphyritic clusters of olivine sparsely occur. They possess high content of Ne-normative (Ne between 8.20 and 14.48 %).

Studies performed by Cortelezzi et al. (1981) and Escayola et al. (1998) in the southern section of Sierra de los Cóndores revealed the presence of a basanitic–tephritic to tephriphonolitic lavas in Basalto and Quebracho quarries. In the first site, Cortelezzi et al. (1981) recognized a monzodioritic diabase, whereas in the second locality, a nephelinitic basanite. Subsequently, rocks of the latter type were described by Escayola et al. (1998) also in Basalto quarry, as part of the exposed roots of a volcanic neck bearing numerous mantle xenoliths that represents an important centre of effusion of lavas in the southern part of the range. According to the description presented by those authors, the rocks have porphyritic texture with phenocrysts of olivine and clinopyroxene, immersed in a groundmass made up of

nepheline and augite microlites, Ti-magnetite and scarce biotite, involving also sanidine which is not associated with nepheline and shows an irregular arrangement. Rocks bear numerous xenocrysts of olivines as well of xenoliths of garnet and spinel lherzolites, dunites and alkali feldspar syenites. There are also abundant pegmatoid segregations of alkali gabbroid composition. Xenoliths of garnet lherzolite are the first ones reported from all the alkaline Cretaceous lithological types of the central–south-western area of South America (Escayola et al. 1998). According to chemical data presented by the aforementioned authors, samples of the Basalto and Quebracho quarries plot in the fields U1 (basanite/tephrite) and U2 (phonotephrite) in TAS diagram, whereas in the diagram R1-R2, they typify as basanite and phonotephrite, respectively (Fig. 2.8a, b). Lucassen et al. (2002) presented several samples classifying in those fields also from that zone. More recently, Ferreira Pittau et al. (2008) defined an eruptive cycle of basanite–phonolite composition in the southern sector of Sierra de los Cóndores.

The sample from Los Molinos locality characterized as a potassic trachydiabase by Gordillo and Lencinas (1969) classify as tephrite in both TAS and R1-R2 diagrams (Fig. 2.8a, b). It was described by those authors as a porphyritic rock with olivine phenocrysts altered to antigorite and/or calcite, phenocrysts of diopsidic augite and Ti-biotite, set in a groundmass rich in sanidine including microlites of plagioclase and Ti-magnetite, bearing calcite nodules and veins of analcime.

Ankaratrites

These rocks belong to the dykes that outcrop in the locality of Los Molinos locality that were considered by Gordillo and Lencinas (1969) as olivinic analcimites. Microscopic studies show that they are composed of clinopyroxene, analcime, olivine altered to saponite, Ti-biotite, kaersutite, opaque minerals, carbonate, apatite, interstitial glass replaced by clays of the group of smectites, little alkali feldspar and small sections of euhedral sphene, which form a compact texture (Fig. 2.9f). These rocks were considered as lamprophyres by Gordillo and Lencinas (1969) and typified as analcimic monchiquites on the basis of the classification proposed by the IUGS. However, they have not the porphyritic texture characteristic of this type of rocks.

2.1.1.5 Mineralogy

Lagorio (2003, 2008) presented microprobe analyses that were carried out by a Cameca–Camebax operating at 15 kV and 15 nA at the Dipartimento di Mineralogia e Petrologia of Padova University (Italy). The PAP-Cameca program has been used to convert X-ray counts into weight percentage of the corresponding oxides. Results are considered accurate within 2–3 % for major elements and 9 % for minor elements. Selected analyses of mineral phases are given in different

tables, expanded from those presented in Lagorio (2008), while the complete set of data is reported in Lagorio (2003).

Clinopyroxene

Selected clinopyroxene compositions of SCC volcanic rocks are given in Table 2.2. They plot as diopside and augite (Fig. 2.10a) in the Ca–Mg–Fe* (Fe^{2+} + Fe^{3+} + Mn) diagram of Morimoto et al. (1988).

Clinopyroxenes show high values of Mg, so that a clear trend towards Fe* is not defined, as in other alkaline provinces (Fig. 2.10a).

Clinopyroxenes of basanites show the highest Ca content (up to 50.64 %), whereas those from the transitional suite reach the lowest Ca values (Table 2.2; Fig. 2.10b). It is also noteworthy the slight core to rim increase in Ca in some phenocryst and/or microphenocrysts, and especially the slight but generalized Mg increase from crystal rims towards groundmass microlites (Table 2.2; Fig. 2.10c).

TiO_2 is variable (0.14–4.71 wt%), usually lower than 3 % (mean 1.63 ± 0.74 %) so that SCC clinopyroxenes are not titaniferous according to Deer et al. (1992), except some late-crystallized ones from Los Molinos (MO1) and Almafuerte (PM4) AkB dykes. Ti/Al ratios of all the SCC clinopyroxenes range from 0.2 to 0.5, as expected for moderately alkaline rocks, as it should be taken into account that Ti/Al ratios > 0.5 are typical of strongly alkaline to peralkaline rocks (Cundari and Ferguson 1982).

Early-crystallized clinopyroxenes display Al^{VI} ranging from 0.018 to 0.091 a.f.u. (mean 0.038 ± 0.024 a.f.u.), pointing out, in general, low-pressure crystallization (Nimis 1995; Nimis and Ulmer 1998). The highest crystallization pressures have been found (Nimis and Ulmer 1998) for the Cpx phenocryst of the alkali basalt PM4 (Table 2.2), i.e. core = 4.7 and rim = 5.7 kbar, given the relatively high Al^{VI} content (0.091 and 0.098, respectively).

Olivine

Selected olivine compositions of SCC volcanic rocks are given in Table 2.3. The forsterite (Fo) content of olivine pheno- and microphenocrysts of basanites and alkali basalts ranges from 90–84 % (core) to 89–83 % (rim), and from 87 to 79 % for groundmass olivine (microlites). Similarly, the olivine of trachybasalts spans from Fo 86–75 % (core) to 85–71 % (rim) and 72 % (microlites).

Comparison between mg# [Mg/(Mg + Fe^{2+})] values of olivines and those [Mg/(Mg + Fe^{2+}); Fe_2O_3/FeO = 0.18] of host rocks shows that some early-crystallized olivines may have mg# values quite lower than those expected, suggesting crystallization from Mg poorer melts.

Table 2.2 Clinopyroxene microprobe compositions from selected rocks of Sierra Chica de Córdoba, expanded from Lagorio (2008)

Sample	G3			MO1			EM5		EM3		
Suite/group	Bsn			AkB-Tc			AkB-Tc		AkB-Tc		
Rock type	Bsn			AkB			AkB		Tcb		
Locality	El Pungo			Los Molinos			Cóndores		Cóndores		
	mp/c	mp/r	gm	mp/c	mp/r	gm	gm	gm	mp/c	mp/r	gm
SiO_2	50.50	49.80	50.79	51.95	44.93	48.92	51.79	48.78	51.42	51.23	51.33
TiO_2	2.06	2.29	1.81	1.35	4.71	2.66	1.88	2.61	1.15	1.48	0.95
Al_2O_3	4.07	5.01	3.31	2.04	6.74	4.07	2.76	4.88	2.34	2.48	1.98
FeO_{total}	5.49	5.24	4.76	5.15	9.63	6.43	5.78	6.14	5.36	6.28	4.77
MnO	0.13	0.00	0.16	0.19	0.13	0.09	0.13	0.11	0.09	0.17	0.07
MgO	14.82	14.02	15.02	15.9	10.98	14.27	15.14	13.78	15.83	15.51	15.98
CaO	24.33	24.19	24.66	22.76	22.15	22.85	23.84	23.73	22.72	22.97	21.90
Na_2O	0.44	0.44	0.30	0.37	0.69	0.41	0.41	0.48	0.39	0.35	0.34
Cr_2O_3	0.27	0.60	0.44	0.28	0.04	0.30	0.14	0.38	0.13	0.06	0.47
Sum	102.10	101.59	101.26	100.00	100.00	100.00	101.87	100.89	99.43	100.51	97.79
Fe_2O_3*	3.10	1.84	1.89	1.14	2.84	1.81	1.47	3.07	2.22	1.77	0.83
Si	1.825	1.812	1.851	1.910	1.696	1.815	1.878	1.791	1.898	1.883	1.924
Al (IV)	0.173	0.188	0.142	0.089	0.300	0.178	0.118	0.209	0.102	0.107	0.076
Sum	1.998	2.000	1.993	1.999	1.996	1.993	1.996	2.000	2.000	1.990	2.000
Al (VI)	0.000	0.027	0.000	0.000	0.000	0.000	0.000	0.002	0.000	0.000	0.011
Fe^{2+}	0.082	0.109	0.093	0.127	0.223	0.149	0.135	0.104	0.104	0.144	0.126
Fe^{3+}	0.084	0.050	0.052	0.032	0.081	0.005	0.040	0.085	0.062	0.049	0.023
Cr	0.008	0.017	0.013	0.008	0.001	0.009	0.004	0.011	0.004	0.002	0.014
Mg	0.798	0.760	0.816	0.871	0.618	0.789	0.818	0.754	0.871	0.850	0.893
Mn	0.004	0.000	0.005	0.006	0.004	0.003	0.004	0.003	0.003	0.005	0.002
Ti	0.056	0.063	0.050	0.037	0.134	0.074	0.051	0.072	0.032	0.041	0.027
Ca	0.942	0.943	0.963	0.896	0.896	0.908	0.926	0.934	0.898	0.904	0.879
Na	0.031	0.031	0.022	0.027	0.005	0.003	0.029	0.034	0.028	0.025	0.025
Sum	2.005	2.000	2.014	2.004	2.007	2.012	2.007	1.999	2.002	2.020	2.000
Ca	49.32	50.64	49.92	46.38	49.18	47.81	48.15	49.68	46.34	46.31	45.71

(continued)

Table 2.2 (continued)

Sample	G3			MO1			EM5		EM3		
Suite/group	Bsn			AkB-Tc			AkB-Tc		AkB-Tc		
Rock type	Bsn			AkB			AkB		Tcb		
Locality	El Pungo			Los Molinos			Cóndores		Cóndores		
	mp/c	mp/r	gm	mp/c	mp/r	gm	gm	gm	mp/c	mp/r	gm
Mg	41.78	40.82	42.30	45.08	33.92	41.55	42.54	40.11	44.94	43.55	46.44
Fe*	8.90	8.54	7.78	8.54	16.90	10.64	9.31	10.21	8.72	10.14	7.85

Sample	RU5					RU10B					
Suite/group	AkB-Tc					AkB-Tc					
Rock type	Tca					Tca					
Locality	Cóndores					Cóndores					
	p/c	p/r	mp/c	mp/r	gm	p/c	p/r	mp1/c	mp1/r	mp2/c	mp2/r
SiO_2	51.41	51.73	49.60	49.17	52.41	50.32	49.99	51.56	51.37	50.34	50.29
TiO_2	0.89	0.71	2.21	2.55	1.04	1.54	1.78	1.34	1.32	1.58	1.56
Al_2O_3	3.39	2.79	4.71	4.57	2.81	4.14	5.32	3.56	3.4	4.19	4.2
FeO_{total}	9.37	8.67	8.60	8.39	6.40	9.81	9.32	5.93	6.08	9.84	10.04
MnO	0.44	0.40	0.20	0.17	0.17	0.26	0.21	0.05	0.12	0.27	0.17
MgO	13.15	13.26	14.57	13.26	16.44	13.93	13.99	16.08	16.19	13.8	13.36
CaO	21.85	21.94	21.09	22.97	20.59	20.4	20.07	21.56	21.57	20.14	20.61
Na_2O	1.14	0.83	0.79	0.50	0.58	0.76	0.7	0.54	0.55	0.65	0.71
Cr_2O_3	0.00	0.00	0.08	0.00	0.68	0.02	0.08	0.57	0.76	0.00	0.00
Sum	101.65	100.34	101.84	101.58	101.13	101.19	101.47	101.19	101.34	100.81	100.96
Fe_2O_3*	4.73	2.40	4.62	3.17	1.49	3.32	2.28	2.13	2.91	2.12	2.47
Si	1.878	1.915	1.802	1.805	1.902	1.848	1.828	1.869	1.86	1.859	1.857
Al (IV)	0.122	0.085	0.198	0.195	0.098	0.152	0.172	0.131	0.140	0.141	0.143
Sum	2.000	2.000	2.000	2.000	2.000	2.000	2.000	2.000	2.000	2.000	2.000
Al (VI)	0.024	0.037	0.004	0.003	0.022	0.027	0.057	0.021	0.005	0.041	0.040
Fe^{2+}	0.156	0.202	0.135	0.170	0.154	0.209	0.222	0.122	0.105	0.245	0.242
Fe^{3+}	0.130	0.067	0.126	0.088	0.041	0.092	0.063	0.058	0.079	0.059	0.069
Cr	0.000	0.000	0.002	0.000	0.020	0.001	0.002	0.016	0.022	0.000	0.000

(continued)

Table 2.2 (continued)

Sample	RU5					RU10B					
Suite/group	AkB-Tc					AkB-Tc					
Rock type	Tca					Tca					
Locality	Cóndores					Cóndores					
	p/c	p/r	mp/c	mp/r	gm	p/c	p/r	mp1/c	mp1/r	mp2/c	mp2/r
Mg	0.716	0.732	0.789	0.726	0.889	0.763	0.763	0.869	0.874	0.759	0.735
Mn	0.014	0.012	0.006	0.005	0.005	0.008	0.007	0.002	0.004	0.009	0.005
Ti	0.024	0.020	0.060	0.070	0.028	0.043	0.049	0.036	0.036	0.044	0.043
Ca	0.855	0.870	0.821	0.903	0.801	0.803	0.787	0.838	0.837	0.797	0.815
Na	0.081	0.060	0.056	0.036	0.041	0.054	0.049	0.038	0.038	0.046	0.051
Sum	2.000	2.000	1.999	2.001	2.001	2.000	2.000	2.000	2.000	2.000	2.000
Ca	45.70	46.20	43.74	47.73	42.38	42.83	42.73	44.36	44.08	42.64	43.68
Mg	38.27	38.87	42.04	38.37	47.04	40.69	41.42	46.00	46.02	40.61	39.39
Fe*	16.03	14.92	14.22	13.90	10.58	16.48	15.85	9.63	9.90	16.75	16.93

Sample	PM4					PM1					PM6				
Suite/group	AkB-Tc					AkB-Tc					AkB-Tc				
Rock type	AkB					Tca					Tc				
Locality	Almafuerte					Almafuerte					Almafuerte				
	p/c	p/r	mp/c	mp/r	gm	p/c	p/r	mp/c	mp/r	gm	p/c	p/r	mp/c	mp/r	gm
SiO_2	50.21	50.6	53.76	44.96	48.57	50.86	50.13	49.8	50.33	49.63	48.91	48.59	48.73	48.76	49.75
TiO_2	1.16	1.31	0.14	4.16	3.01	1.75	2.06	2.18	1.85	1.83	2.19	2.17	2.22	2.00	1.98
Al_2O_3	5.21	5.35	0.9	7.08	4.64	3.57	3.66	4.34	3.32	4.35	5.36	5.79	5.33	5.54	4.77
FeO_{total}	8.55	8.37	9.58	7.79	7.09	8.65	7.85	8.72	8.19	8.63	7.7	7.89	7.73	8.17	7.75
MnO	0.23	0.19	0.47	0.05	0.14	0.18	0.15	0.21	0.17	0.18	0.18	0.09	0.10	0.20	0.11
MgO	11.56	11.75	13.23	11.89	13.48	13.9	13.44	13.38	13.77	13.66	14.28	13.91	14.20	13.90	14.42
CaO	20.88	20.59	21.64	22.65	23.79	21.39	22.6	22.06	22.56	21.64	21.67	22.15	21.84	21.53	21.74
Na_2O	1.86	2.02	0.77	0.62	0.47	0.69	0.53	0.72	0.50	0.72	0.70	0.67	0.61	0.62	0.60
Cr_2O_3	0.02	0.01	0.00	0.00	0.00	0.04	0.00	0.00	0.00	0.05	0.20	0.12	0.08	0.03	0.09
Sum	99.68	100.19	100.49	99.20	101.19	101.03	100.41	101.43	100.69	100.69	101.2	101.38	100.85	100.75	101.22
Fe_2O_3*	4.09	3.94	0.6	3.79	2.47	2.02	1.73	3.21	2.53	3.56	4.31	4.66	4.12	3.89	3.27

(continued)

Table 2.2 (continued)

Sample	PM4					PM1					PM6				
Suite/group	AkB-Tc					AkB-Tc					AkB-Tc				
Rock type	AkB					Tca					Tc				
Locality	Almafuerte					Almafuerte					Almafuerte				
	p/c	p/r	mp/c	mp/r	gm	p/c	p/r	mp/c	mp/r	gm	p/c	p/r	mp/c	mp/r	gm
Si	1.863	1.865	1.996	1.694	1.789	1.870	1.858	1.827	1.859	1.83	1.787	1.774	1.787	1.792	1.818
Al (IV)	0.137	0.135	0.004	0.306	0.202	0.13	0.142	0.173	0.141	0.17	0.213	0.226	0.213	0.208	0.182
Sum	2.000	2.000	2.000	2.000	1991	2.000	2.000	2.000	2.000	2.000	2.000	2.000	2.000	2.000	2.000
Al (VI)	0.091	0.098	0.035	0.008	0.000	0.025	0.018	0.015	0.004	0.019	0.018	0.023	0.017	0.032	0.023
Fe^{2+}	0.151	0.149	0.281	0.138	0.150	0.210	0.195	0.179	0.183	0.167	0.117	0.113	0.123	0.143	0.147
Fe^{3+}	0.114	0.109	0.017	0.107	0.069	0.056	0.048	0.089	0.07	0.099	0.118	0.128	0.114	0.108	0.090
Cr	0.001	0.000	0.000	0.000	0.000	0.001	0.000	0.000	0.000	0.001	0.006	0.004	0.002	0.001	0.003
Mg	0.639	0.645	0.732	0.668	0.740	0.762	0.743	0.732	0.758	0.751	0.778	0.757	0.776	0.762	0.786
Mn	0.007	0.006	0.015	0.002	0.005	0.006	0.005	0.007	0.005	0.006	0.006	0.003	0.003	0.006	0.003
Ti	0.032	0.036	0.004	0.118	0.083	0.048	0.057	0.06	0.051	0.051	0.06	0.06	0.061	0.055	0.055
Ca	0.830	0.813	0.861	0.914	0.939	0.843	0.897	0.867	0.893	0.855	0.848	0.866	0.858	0.848	0.851
Na	0.134	0.144	0.056	0.045	0.034	0.049	0.038	0.051	0.036	0.051	0.049	0.047	0.044	0.044	0.043
Sum	1.999	2.000	2.001	2.000	2.020	2.000	2.001	1.998	1.999	2.001	2.000	2.001	1.998	1.999	2.001
Ca	47.67	47.21	45.17	49.97	49.34	44.91	47.51	46.26	46.78	45.53	45.42	46.38	45.78	45.42	45.34
Mg	36.70	37.46	38.41	36.52	38.89	40.6	39.35	39.06	39.71	39.99	41.67	40.55	41.41	40.81	41.88
Fe*	15.62	15.33	16.42	13.50	11.77	14.49	13.14	14.67	13.51	14.48	12.91	13.07	12.81	13.77	12.79

Sample	Li1					Li4				
Suite/group	TrB-Lb					TrB-Lb				
Rock type	TrB					Lb				
Locality	Cóndores					Cóndores				
	p/c	p/r	mp/c	mp/r	gm	p/c	p/r	mp/c	mp/r	gm
SiO_2	51.10	50.98	53.08	50.29	51.99	50.60	49.97	50.75	50.71	48.89
TiO_2	0.65	0.75	1.30	1.91	1.24	1.51	1.63	0.73	1.77	2.06
Al_2O_3	4.57	5.18	2.01	2.93	2.83	4.13	4.45	3.05	3.53	4.27
FeO_{total}	7.38	7.36	4.46	6.53	3.95	6.59	6.78	9.08	5.96	7.00

(continued)

Table 2.2 (continued)

Sample	Li1					Li4				
Suite/group	TrB-Lb					TrB-Lb				
Rock type	TrB					Lb				
Locality	Cóndores					Cóndores				
	p/c	p/r	mp/c	mp/r	gm	p/c	p/r	mp/c	mp/r	gm
MnO	0.27	0.24	0.03	0.06	0.09	0.1	0.07	0.45	0.09	0.09
MgO	13.50	13.29	16.26	14.52	15.65	15.25	15.23	13.43	15.06	13.82
CaO	22.76	22.41	23.65	23.25	23.41	20.85	21.26	21.09	22.90	22.77
Na_2O	0.55	0.63	0.24	0.32	0.31	0.71	0.87	0.90	0.46	0.49
Cr_2O_3	0.04	0.04	0.44	0.08	1.23	0.15	0.23	0.00	0.57	0.08
Sum	100.83	100.87	101.47	99.89	100.70	99.89	100.49	99.46	101.05	99.47
Fe_2O_3*	1.95	1.41	0.29	1.51	0.09	2.22	4.50	3.66	2.36	3.19
Si	1.875	1.870	1.920	1.866	1.897	1.861	1.825	1.894	1.851	1.821
Al (IV)	0.125	0.130	0.080	0.128	0.103	0.139	0.175	0.106	0.149	0.179
Sum	2.000	2.000	2.000	1.994	2.000	2.000	2.000	2.000	2.000	2.000
Al (VI)	0.073	0.094	0.006	0.000	0.019	0.040	0.016	0.028	0.003	0.008
Fe^{2+}	0.173	0.187	0.127	0.160	0.118	0.141	0.084	0.181	0.117	0.129
Fe^{3+}	0.054	0.039	0.008	0.042	0.003	0.062	0.124	0.103	0.065	0.089
Cr	0.001	0.001	0.013	0.002	0.036	0.004	0.007	0.000	0.016	0.002
Mg	0.739	0.727	0.877	0.803	0.851	0.836	0.829	0.747	0.819	0.767
Mn	0.009	0.008	0.001	0.002	0.003	0.003	0.002	0.014	0.003	0.003
Ti	0.018	0.021	0.035	0.053	0.034	0.042	0.045	0.020	0.049	0.058
Ca	0.895	0.880	0.916	0.924	0.915	0.822	0.832	0.843	0.895	0.908
Na	0.039	0.045	0.017	0.023	0.022	0.050	0.062	0.065	0.032	0.036
Sum	0.000	0.000	0.000	0.000	0.000	2.000	2.001	2.001	1.999	2.000
Ca	47.86	47.80	47.49	47.85	48.41	44.10	44.47	44.65	47.13	47.89
Mg	39.520	39.490	45.46	41.58	45.03	44.85	44.31	39.57	43.13	40.45
Fe*	12.620	12.710	7.05	10.56	6.56	11.05	11.22	15.78	9.74	11.66

Bsn basanite, *AkB* alkali basalt, *Tcb* trachybasalt, *Tca* trachyandesite, *TrB* transitional basalt, *Cóndores* Sierra de los Cóndores, *p* phenocryst, *mp* microphenocryst, *gm* microlite, *c* core, *r* rim
Fe_2O_3* calculated according Papike et al. (1974); Fe* = Fe^{2+} + Fe^{3+} + Mn. Structural formulae on the basis of 4 cations and 6 oxygens

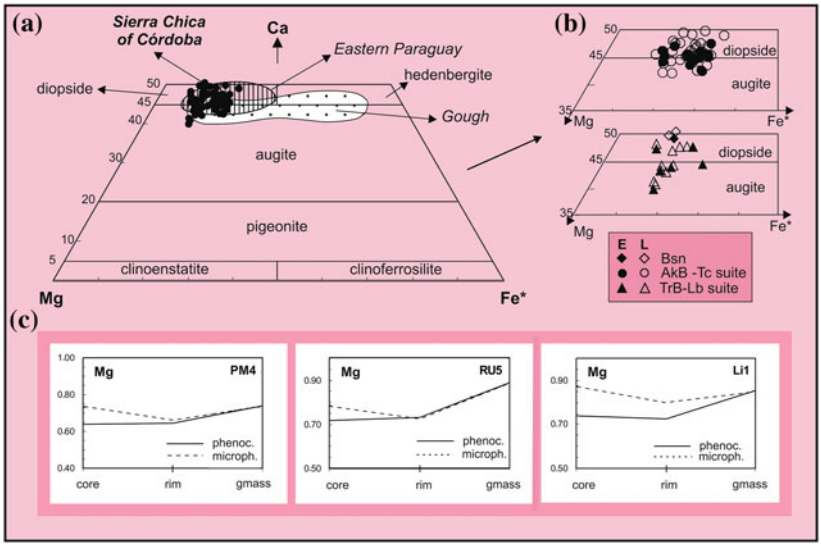

Fig. 2.10 **a** Ca–Mg–Fe* (Fe^{2+} + Mn + Fe^{3+}) plot for clinopyroxene of rocks of Sierra Chica of Córdoba, according to the classification of Morimoto (1988), in comparison with those from other alkaline provinces: eastern Paraguay (Cundari and Comin-Chiaramonti 1996) and Gough (le Roex 1985). **b** Ca–Mg–Fe* plots for clinopyroxenes of alkali basalt—trachyte suite (AkB-Tc) and transitional basalt—latibasalt suite (TrB-Lb) and the group of basanites (Bsn) shown in Lagorio (2008). *E* early clinopyroxenes (phenocrysts and microphenocryst cores), *L* late clinopyroxenes (phenocryst and microphenocrys rims and microlites of the groundmass). **c** Clinopyroxene diagrams showing Mg (a.f.u.) variation from core to rim of phenocryst and/or microphenocryst and the microlites of the groundmass (gmass)

Feldspar

Selected feldspar compositions of the SCC volcanic rocks are given in Table 2.4. Feldspars span from calcic andesine to sanidine in the An–Ab–Or diagram (Fig. 2.11). Macro-, pheno- and microphenocrysts of feldspars are characteristic of the salic rocks, while scarce or absent in the more basic ones. They correspond to plagioclase (An_{54-40}) ± anorthoclase ($An_{27-15}Ab_{45-63}Or_{28-22}$) and ± sanidine ($An_4Ab_{45}Or_{51}$). Groundmass of the different lithological types is generally characterized by the presence of plagioclase (An_{52-27}) and alkali feldspar ($Or_{67-15}Ab_{68-30}An_{27-1}$); nevertheless, in basanites, it is only composed of sodic anorthoclase ($Or_{11}Ab_{76}An_{13}$) as shown in Fig. 2.11.

Fe–Ti Oxides

Selected samples of homogeneous Fe–Ti oxides of the SCC volcanic rocks are presented in Table 2.5. They are common in the groundmass, scarce as

Table 2.3 Olivine microprobe compositions from selected rocks of Sierra Chica de Córdoba expanded from Lagorio (2008)

Sample	G3					EM5					CO7			
Suite/group	Bsn					AkB-Tc					AkB-Tc			
Rock type	Bsn					AkB					Tcb			
Locality	El Pungo					Cóndores					Cóndores			
	p/c	p/r	mp/c	mp/r	gm	p/c	p/r	mp/c	mp/r	gm	mp/c1	mp/r1	mp/c2	mp/r2
SiO_2	40.47	40.60	40.59	40.52	40.42	41.14	39.89	40.14	39.27	39.23	40.11	38.57	38.98	37.64
Al_2O_3	0.02	0.00	0.03	0.05	0.04	0.02	0.03	0.05	0.04	0.00	0.04	0.00	0.02	0.04
FeO_{total}	12.55	12.55	12.55	12.37	12.76	9.48	16.01	15.43	15.63	19.68	17.90	22.40	19.43	25.99
MnO	0.18	0.28	0.17	0.23	0.19	0.15	0.3	0.24	0.20	0.32	0.16	0.26	0.27	0.45
MgO	46.66	46.70	47.32	47.03	46.22	49.46	43.99	45.31	44.50	41.14	43.36	39.00	41.06	36.22
CaO	0.19	0.34	0.17	0.25	0.35	0.05	0.31	0.13	0.20	0.41	0.21	0.26	0.23	0.30
Sum	0.00	0.00	0.00	0.00	0.00	0.00	0.00	0.00	0.00	0.00	0.00	0.00	0.00	0.00
Si	1.003	1.002	0.998	1.000	1.004	1.002	1.001	0.996	0.992	0.999	1.000	0.998	0.999	0.992
Al (IV)	0.001	0.000	0.001	0.001	0.001	0.000	0.001	0.001	0.001	0.000	0.001	0.000	0.001	0.001
Sum	1.004	1.002	0.999	1.001	1.005	1.002	1.002	0.997	0.993	0.999	1.001	0.998	1.000	0.993
Fe^{2+}	0.260	0.259	0.258	0.255	0.265	0.193	0.336	0.320	0.330	0.419	0.373	0.485	0.417	0.573
Mn	0.004	0.006	0.004	0.005	0.004	0.003	0.006	0.005	0.004	0.007	0.003	0.006	0.006	0.010
Mg	1.724	1.719	1.735	1.730	1.712	1.797	1.646	1.676	1.675	1.562	1.612	1.504	1.569	1.422
Ca	0.005	0.009	0.005	0.007	0.009	0.001	0.008	0.003	0.005	0.011	0.006	0.007	0.006	0.009
Sum	1.993	1.993	2.002	1.997	1.990	1.994	1.996	2.004	2.014	1.999	1.994	2.002	1.998	2.014
Fo	86.72	86.64	86.89	86.92	86.42	90.16	82.78	83.75	83.36	78.56	81.06	75.42	78.78	70.94
Fa	13.09	13.06	12.93	12.83	13.38	9.69	16.90	16.00	16.43	21.09	18.77	24.3	20.92	28.56
Tph	0.19	0.29	0.18	0.25	0.20	0.16	0.32	0.25	0.21	0.35	0.17	0.28	0.30	0.50

Sample	EM3					MO1				
Suite/group	AkB-Tc					AkB-Tc				
Rock type	Tcb					AkB				
Locality	Cóndores					Los Molinos				
	p/c	p/r	mp/c	mp/r	gm	p/c	p/r	mp/c	mp/r	gm
SiO_2	40.39	41.08	37.97	37.99	37.90	40.69	40.61	40.1	40.12	40.25

(continued)

Table 2.3 (continued)

Sample	EM3					MO1				
Suite/group	AkB-Tc					AkB-Tc				
Rock type	Tcb					AkB				
Locality	Cóndores					Los Molinos				
	p/c	p/r	mp/c	mp/r	gm	p/c	p/r	mp/c	mp/r	gm
Al_2O_3	0.00	0.03	0.01	0.13	0.00	0.00	0.00	0.00	0.00	0.02
FeO_{total}	13.12	14.11	22.58	24.84	24.19	10.29	10.23	12.49	12.72	12.20
MnO	0.17	0.24	0.4	0.67	0.73	0.17	0.10	0.14	0.24	0.12
MgO	47.37	46.88	38.02	36.85	36.77	48.76	48.98	47.04	46.53	47.15
CaO	0.25	0.27	0.33	0.31	0.27	0.10	0.08	0.23	0.39	0.26
Sum	0.00	0.00	0.00	0.00	0.00	100.00	100.00	100.00	100.00	100.00
Si	0.992	1.000	0.998	0.994	0.998	0.999	0.996	0.995	0.997	0.996
Al (IV)	0.000	0.001	0.000	0.004	0.000	0.000	0.000	0.000	0.000	0.001
Sum	0.992	1.001	0.998	0.998	0.998	0.999	0.996	0.995	0.997	0.997
Fe^{2+}	0.269	0.287	0.496	0.544	0.533	0.211	0.210	0.259	0.264	0.252
Mn	0.003	0.005	0.009	0.015	0.016	0.003	0.002	0.003	0.005	0.003
Mg	1.734	1.700	1.489	1.438	1.444	1.784	1.792	1.740	1.724	1.739
Ca	0.006	0.007	0.009	0.009	0.008	0.002	0.002	0.006	0.010	0.007
Sum	2.012	1.999	2.003	2.006	2.001	2.000	2.006	2.008	2.003	2.001
Fo	86.41	85.34	74.67	72.02	72.45	89.26	89.42	86.91	86.48	87.21
Fa	13.42	14.41	24.88	27.23	26.74	10.57	10.48	12.95	13.26	12.66
Tph	0.17	0.25	0.45	0.74	0.81	0.17	0.10	0.14	0.25	0.13

Abbreviations as in Table 2.2. *Fo* forsterite, *Fa* fayalite, *Tph* tephroite

Table 2.4 Feldspar microprobe compositions from selected rocks of Sierra Chica de Córdoba expanded from Lagorio (2008)

Sample	G3	EM5				CO7			EM3		
Suite/Group	Bsn	AkB-Tc				AkB-Tc			AkB-Tc		
Rock type	Bsn	AkB				Tcb			Tcb		
Locality	Pungo	Cóndores				Cóndores			Cóndores		
	gm	gm1	gm2	gm3	gm4	gm1	gm2	gm3	gm1	gm2	gm3
SiO_2	64.56	62.94	60.79	62.58	58.92	63.93	64.56	56.83	56.85	64.32	63.07
TiO_2	0.05	0.21	0.25	0.29	5.61	0.22	0.28	0.21	0.20	0.19	0.22
Al_2O_3	21.49	22.00	23.90	22.30	16.83	20.2	18.94	26.68	26.88	20.08	21.17
FeO_{total}	0.35	0.46	0.35	0.31	5.13	0.33	0.30	0.61	0.61	0.27	0.27
CaO	2.66	3.46	5.53	3.79	0.13	1.75	0.56	8.76	8.76	1.56	2.74
Na_2O	8.94	7.96	7.70	8.08	3.89	5.69	3.56	6.27	6.27	4.08	5.51
K_2O	1.80	2.42	1.09	1.96	9.42	7.08	11.15	0.42	0.42	9.74	6.58
Sum	99.85	99.45	99.61	99.31	99.93	99.20	99.35	99.78	99.99	100.24	99.56
Or (wt%)	10.66	14.46	6.50	11.73	62.39	42.41	66.70	2.53	3.20	57.64	39.23
Ab (wt%)	76.05	68.17	65.78	69.23	36.89	48.82	30.49	53.59	52.33	34.62	47.04
An (wt%)	13.29	17.37	27.72	19.04	0.72	8.77	2.81	43.88	44.47	7.74	13.74

Sample	RU10B								PM4		PM1				
Suite/group	AkB-Tc								AkB-Tc		AkB-Tc				
Rock type	Tca								AkB		Tca				
Locality	Cóndores								Almafuerte		Almafuerte				
	Mp/c	Mp/r	p/c	p/r	mp/c	mp/r	gm1	gm2	gm1	gm2	p/c	p/r	mp/c	mp/r	gm
SiO_2	57.74	58.13	60.36	59.82	57.61	56.96	60.25	55.97	60.78	60.33	56.29	56.88	55.85	56.15	65.19
TiO_2	0.13	0.14	0.18	0.10	0.12	0.12	0.14	0.15	0.37	0.38	0.14	0.16	0.14	0.12	0.27

(continued)

Table 2.4 (continued)

Sample	RU10B								PM4		PM1				
Suite/group	AkB-Tc								AkB-Tc		AkB-Tc				
Rock type	Tca								AkB		Tca				
Locality	Cóndores								Almafuerte		Almafuerte				
	Mp/c	Mp/r	p/c	p/r	mp/c	mp/r	gm1	gm2	gm1	gm2	p/c	p/r	mp/c	mp/r	gm
Al_2O_3	26.07	26.16	23.65	24.00	26.26	27.06	23.62	27.36	23.53	24.76	27.28	26.42	26.99	27.45	19.54
FeO_{total}	0.42	0.47	0.29	0.30	0.44	0.49	0.39	0.54	0.32	0.39	0.46	0.33	0.40	0.40	0.27
CaO	8.04	8.02	5.43	5.84	8.22	9.03	5.43	9.52	5.23	6.35	9.38	8.53	9.23	9.54	0.91
Na_2O	5.50	5.67	5.33	5.58	5.71	5.38	5.60	5.23	6.88	6.65	5.34	5.67	5.27	5.43	6.07
K_2O	2.23	2.09	4.64	3.89	1.78	1.66	4.20	1.35	2.51	2.11	1.35	1.48	1.43	1.09	7.31
Sum	100.13	100.68	99.88	99.53	100.14	100.70	99.63	100.12	99.62	100.97	100.24	99.31	99.31	100.18	99.56
Or (wt%)	13.23	12.34	27.58	23.18	10.58	9.80	25.04	8.03	15.01	12.44	7.99	8.86	8.53	6.46	43.59
Ab (wt%)	46.74	47.92	45.33	47.60	48.49	45.46	47.79	44.50	58.78	56.13	45.35	48.42	45.11	46.04	51.86
An (wt%)	40.04	39.75	27.09	29.22	40.94	44.75	27.17	47.47	26.21	31.43	46.67	42.72	46.36	47.50	4.55

Sample	PM6							PM7					
Suite/group	AkB-Tc							AkB-Tc					
Rock type	Tc							Tcp					
Locality	Almafuerte							Almafuerte					
	Mp/c	Mp/r	p/c	p/r	mp/c	mp/r	gm	Mp/c	Mp/r	p/c	p/r	mp/c	mp/r
SiO_2	63.51	64.76	65.43	65.71	55.42	55.49	65.58	56.62	56.09	58.72	57.96	57.17	56.56
TiO_2	0.05	0.07	0.03	0.08	0.03	0.05	0.16	0.16	0.15	0.08	0.14	0.15	0.11
Al_2O_3	21.51	19.59	19.54	19.45	28.22	27.97	18.95	27.09	27.57	25.22	26.26	26.70	26.71
FeO_{total}	0.21	0.27	0.13	0.21	0.50	0.45	0.48	0.34	0.37	0.55	0.39	0.40	0.41

(continued)

Table 2.4 (continued)

Sample	PM6							PM7					
Suite/group	AkB-Tc							AkB-Tc					
Rock type	Tc							Tcp					
Locality	Almafuerte							Almafuerte					
	Mp/c	Mp/r	p/c	p/r	mp/c	mp/r	gm	Mp/c	Mp/r	p/c	p/r	mp/c	mp/r
CaO	2.92	1.05	0.85	0.71	10.35	10.13	0.33	9.14	9.66	7.10	8.14	8.69	8.84
Na_2O	7.36	5.54	5.50	5.12	5.13	5.21	4.25	5.36	5.28	6.34	5.88	5.62	5.56
K_2O	3.78	7.92	8.27	9.00	0.90	0.92	10.50	1.54	1.23	1.75	1.66	1.54	1.39
Sum	99.34	99.20	99.75	100.28	100.55	100.22	100.25	100.25	100.35	99.76	100.43	100.27	99.58
Or (wt%)	22.52	47.32	49.06	53.17	5.32	5.47	62.27	9.12	7.28	10.04	9.82	9.12	8.29
Ab (wt%)	62.85	47.40	46.71	43.30	43.37	44.17	36.08	45.44	44.73	54.07	49.79	47.66	47.46
An (wt%)	14.63	5.27	4.23	3.52	51.31	50.37	1.64	45.44	47.99	35.54	40.40	43.22	44.25

Sample	Li1			ES2					Li4			
Suite/group	TrB-Lb			TrB-Lb					TrB-Lb			
Rock type	TrB			TrB					Lb			
Locality	Cóndores			Cóndores					Cóndores			
	gm1	gm2	gm3	gm1	gm2	gm3	gm4	gm5	mp/c	mp/r	gm1	gm2
SiO_2	60.66	61.62	62.16	64.02	57.54	64.56	64.79	57.58	59.62	59.68	61.42	56.07
TiO_2	0.32	0.28	0.31	0.17	0.26	0.27	0.16	0.25	0.09	0.06	0.22	0.19
Al_2O_3	23.67	23.3	23.46	21.71	26.34	20.38	20.41	26.46	24.72	24.57	23.64	27.31
FeO_{total}	0.39	0.46	0.40	0.51	0.51	0.31	0.28	0.63	0.3	0.34	0.34	0.46
CaO	5.37	4.85	4.85	2.97	8.30	1.75	1.72	8.39	6.48	6.35	5.17	9.45
Na_2O	7.56	7.76	7.98	8.12	6.42	6.43	6.82	6.59	6.54	6.66	7.87	5.92

(continued)

Table 2.4 (continued)

Sample	Li1			ES2					Li4			
Suite/group	TrB-Lb			TrB-Lb					TrB-Lb			
Rock type	TrB			TrB					Lb			
Locality	Cóndores			Cóndores					Cóndores			
	gm1	gm2	gm3	gm1	gm2	gm3	gm4	gm5	mp/c	mp/r	gm1	gm2
K_2O	1.36	1.60	1.41	2.73	0.64	6.12	5.61	0.34	2.02	1.93	1.2	0.37
Sum	99.33	99.87	100.57	100.23	100.01	99.82	99.79	100.24	99.77	99.59	99.86	99.77
Or (wt%)	8.15	9.52	8.32	16.20	3.81	36.44	33.35	2.04	12.01	11.47	7.16	2.23
Ab (wt%)	64.83	66.23	67.59	69.01	54.71	54.83	58.09	56.07	55.65	56.78	67.00	50.51
An (wt%)	27.02	24.24	24.10	14.79	41.48	8.73	8.57	41.89	32.34	31.75	25.84	47.26

Abbreviations as in Table 2.2. *Or* orthoclase, *Ab* albite, *An* anorthite, *Mp* macrophenocryst

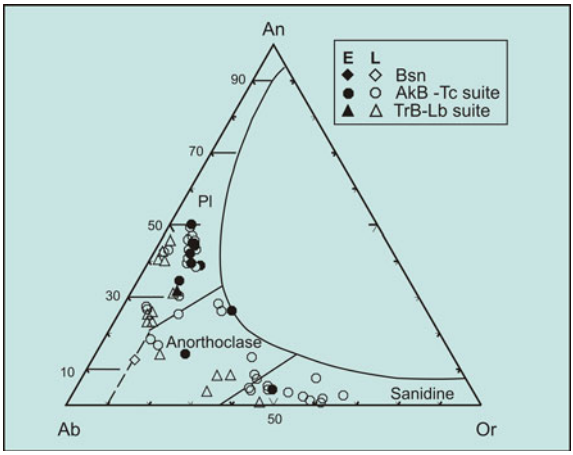

Fig. 2.11 Feldspar compositions in relation to the contents of Ab–An–Or, according to the limits proposed by Deer et al. (1992). *Pl* plagioclase, *E* early feldspar; *L* late feldspar. Based on Lagorio (2008)

microphenocrysts and compositionally correspond to Ti-magnetite (Mt) and ilmenite (Ilm). Ti-magnetite is the common oxide phase, while ilmenite coexists in few rocks.

Ti-magnetite compositions are mainly rich in ulvöspinel component (Ulv. = 85–48 %), with the exception of a few samples (Ulv. = 14–4 %). The R_2O_3 component of ilmenites ranges from 4 to 8 %.

Coexistence of Mt and Ilm yielded (Spencer and Lindsley 1981) temperatures ranging between 1190 and 845 °C, and fO_2 values that straddle FQM buffer (Fig. 2.12). Temperature decrease suggests different stages of post-eruptive re-equilibration. This re-equilibration was accompanied by maghemitization and haematite replacement, which both were interpreted as the cause for the acquisition of a stable magnetic remanence in SCC volcanic rocks (Geuna et al. 2015).

2.1.1.6 Geochemistry

Previous chemical data of major elements have been presented by Gordillo and Lencinas (1967a, b, 1969), as it was previously mentioned. Later, in the following decades, several authors carried out geochemical studies in different areas of Sierra Chica, as Cortelezzi et al. (1981), Kay and Ramos (1996), Sánchez and Bermúdez (1997), Lagorio et al. (1997), Lagorio (1998, 2003, 2008), Escayola et al. (1998, 1999), Lucassen et al. (2002) and Ancheta et al. (2002), most of them including also the study of trace elements. Major and trace element contents provided by Lagorio (2003, 2008) were determined at the Dipartimento di Scienze della Terra, University of Trieste, by using a PW-1404 XRF spectrometer and the procedures of Philips (1994) for the correction of matrix effects. Major element abundance was

Table 2.5 Magnetite and ilmenite microprobe compositions from selected rocks of Sierra Chica de Córdoba expanded from Lagorio (2008)

Sample	G3	MO1	EM5	CO7	EM3	RU5	Li8	RU10B	PM4	PM1	PM6	PM7	Li1	ES2	Li4	CN1
Suite/group	Bsn	AkB-Tc	AkB-Tc	AkB-Tc	AkB-Tc	AkB-Tc	AkB-Tc	AkB-Tc	AkB-Tc	AkB-Tc	AkB-Tc	AkB-Tc	TrB-Lb	TrB-Lb	TrB-Lb	TrB-Lb
Rock type	Bsn	AkB	AkB	Tcb	Tcb	Tca	Tca	Tca	AkB	Tca	Tc	Tcp	TrB	TrB	TrB	TrB
Locality	Pungo	Molinos	Cónd.	Cónd.	Cónd.	Cónd.	Cónd.	Cónd.	Almaf.	Almaf.	Almaf.	Almaf.	Cónd.	Cónd.	Cónd.	Cónd.
	gm	gm	gm	gm	gm	gm	gm	gm	gm	gm	gm	gm	gm	gm	gm	gm
Magnetite																
SiO_2	0.23	0.13	0.04	0.26	0.27	0.24	0.27	0.24	0.27	0.11	0.14	0.28	0.28	0.24	0.05	0.28
TiO_2	30.00	17.06	22.21	17.70	20.87	1.22	23.11	4.82	29.99	29.36	18.28	27.97	30.25	2.40	21.28	25.05
Al_2O_3	0.31	2.86	2.52	0.68	1.67	4.00	0.28	3.54	0.34	1.33	1.13	1.45	0.72	0.94	1.45	0.47
FeO_{total}	65.45	74.35	71.41	77.77	74.32	83.86	73.47	82.99	65.45	65.24	75.71	66.26	65.46	90.3	72.69	70.91
MnO	1.68	0.79	1.10	2.21	1.02	1.17	0.29	0.43	1.35	2.13	0.85	1.45	0.68	0.10	0.38	0.29
MgO	0.08	2.28	0.60	0.08	0.17	3.61	0.29	1.63	0.28	0.03	1.11	0.92	1.37	1.00	2.11	1.77
CaO	0.29	0.00	0.10	0.11	0.41	1.10	0.35	1.85	1.03	0.09	0.07	0.27	0.36	0.12	0.04	0.55
Cr_2O_3	0.05	0.06	0.21	0.00	0.01	0.00	0.15	0.00	0.08	0.13	0.02	0.00	0.07	0.00	0.49	0.00
Total	98.09	97.53	98.19	98.81	98.74	95.20	98.21	95.50	98.79	98.42	97.31	98.60	99.19	95.10	98.49	99.32
FeO	56.84	43.56	50.21	46.20	49.75	25.67	51.97	31.69	56.27	56.23	45.95	54.44	56.50	32.45	47.86	51.56
Fe_2O_3	9.57	34.21	23.55	35.07	27.29	64.66	23.89	57.00	10.20	10.01	33.06	13.14	9.96	64.28	27.59	21.50
Total	99.06	100.95	100.55	102.31	101.48	101.66	100.6	101.19	99.82	99.42	100.60	99.91	100.20	101.52	101.26	101.47
% Ulv.	85.92	48.03	62.82	50.19	59.35	4.28	65.88	14.48	85.10	83.69	51.85	79.43	85.05	7.70	59.17	69.78
Ilmenite																
SiO_2			0.24	0.01	0.06		0.15			0.03						
TiO_2			49.64	49.41	50.95		48.41			50.28						
Al_2O_3			0.79	0.00	0.04		0.2			0.25						
FeO_{total}			43.32	45.57	42.82		48.32			41.68						
MnO			0.87	0.70	0.83		0.23			2.52						
MgO			3.47	2.11	3.32		1.07			3.99						
CaO			0.11	0.06	0.14		0.20			0.17						
Cr_2O_3			0.06	0.00	0.03		0.23			0.01						

(continued)

Table 2.5 (continued)

Sample	G3	MO1	EM5	CO7	EM3	RU5	Li8	RU10B	PM4	PM1	PM6	PM7	Li1	ES2	Li4	CN1
Suite/group	Bsn	AkB-Tc	AkB-Tc	AkB-Tc	AkB-Tc	AkB-Tc	AkB-Tc	AkB-Tc	AkB-Tc	AkB-Tc	AkB-Tc	AkB-Tc	TrB-Lb	TrB-Lb	TrB-Lb	TrB-Lb
Rock type	Bsn	AkB	AkB	Tcb	Tcb	Tca	Tca	Tca	AkB	Tca	Tc	Tcp	TrB	TrB	TrB	TrB
Locality	Pungo	Molinos	Cónd.	Cónd.	Cónd.	Cónd.	Cónd.	Cónd.	Almaf.	Almaf.	Almaf.	Almaf.	Cónd.	Cónd.	Cónd.	Cónd.
	gm	gm	gm	gm	gm	gm	gm	gm	gm	gm	gm	gm	gm	gm	gm	gm
Total			0.00	0.00	98.19		0.00			0.00						
FeO			37.73	39.89	38.94		41.31			35.37						
Fe_2O_3			6.21	6.31	4.31		7.79			7.01						
Total			99.12	98.49	98.63		99.58			99.63						
% R_2O_3			7.04	6.00	4.14		7.93			6.88						
T (°C)			980	845	848		1040			1190						
log fO_2			−11.5	−14.1	−14.2		−10.4			−8.7						

Abbreviations as in Table 2.2. FeO, Fe_2O_3, R_2O_3, and Ulvöspinel (Ulv.) calculated according to Carmichael (1967). Temperature and log fO_2 following Spencer and Lindsley (1981) for homogeneous magnetite–ilmenite pairs. *Cónd.* Sierra de los Cóndores, *Almaf.* Almafuerte

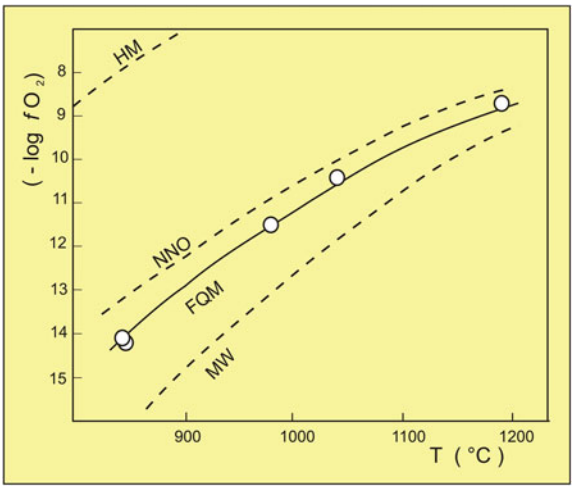

Fig. 2.12 Temperature (°C) versus $-\log fO_2$ (Spencer and Lindsley 1981) for homogeneous groundmass magnetite–ilmenite pairs of Sierra Chica. *HM* haematite–magnetite; *NNO* nickel–nickel oxide; *FQM* fayalite–quartz–magnetite; *MW* magnetite–wüstite. Based on Lagorio (2008)

recalculated to 100 % on a volatile-free basis; FeO was obtained by titration and loss on ignition (L.O.I.) corrected for FeO oxidation, gravimetrically. The analytical uncertainties are estimated at less than 5 and 10 % for major and trace elements, respectively. Rare earth elements (REE), Th, Ta, Hf, U and Ga of selected rocks were measured by inductively coupled mass spectrometry (ICP-MS) at Activation Laboratory (Canada).

Representative analyses are given in Table 2.6, whereas the complete set of data is in Lagorio (2003) and available on request. CIPW-normative parameters and mg# (at. $Mg/(Mg + Fe^{2+})$) values were calculated assuming $Fe_2O_3/FeO = 0.18$.

As it has been previously pointed out, major element composition allowed the distinction of the rocks in several groups: (1) alkali basalt—trachyte suite, (2) transitional basalt—latibasalt suite, (3) basanites and (4) ankaratrites (Fig. 2.8b). In these graphics, the samples presented by other authors whose compositions are complementary to those obtained by Lagorio (2003, 2008) have been included. It should be noted that a suite consisting of basanite–phonolite is depicted, as was defined by Ferreira Pittau et al. (2008) considering several samples from the southern sector of Sierra de los Cóndores provided by other authors.

Major element variation diagrams of samples presented by Lagorio (2003, 2008) show a strong overlap between alkaline and transitional suites, with slightly higher values of SiO_2 and subtle lower of CaO and P_2O_5 in the transitional suite (Fig. 2.13). Regarding trace elements, this suite has the lowest values of Nb (Fig. 2.14). Basanites display a slightly lower content of SiO_2 and TiO_2, as well as slightly higher FeO_t and CaO tenors, for the same MgO values regarding both alkaline and transitional suites. They are distinguished by having the lowest Zr content of all studied rocks, low tenors of LREE and high Nb and Sr values (Fig. 2.14). Ankaratrites are characterized by displaying the lowest percentages of SiO_2 and Al_2O_3, high contents of TiO_2 and the highest CaO, P_2O_5, Ba and LREE values (Figs. 2.13 and 2.14).

Table 2.6 Major and trace element compositions of representative volcanic rocks of Sierra Chica of Córdoba expanded from Lagorio (2008)

Sample	G3	LM3	G2	G1	MO1	MO19	EM4	EM5	RU13	CN7	CN6	EM3	CO7
Suite/group	Bsn	Bsn	Bsn	Bsn	AkB-Tc	AkB-Tc	AkB-Tc	AkB-Tc	AkB-Tc	AkB-Tc	AkB-Tc	AkB-Tc	AkB-Tc
Rock type	Bsn	Bsn	Bsn	Bsn	AkB	AkB	AkB	AkB	AkB	AkB	AkB	Tcb	Tcb
Locality	Pungo	Pungo	Pungo	Pungo	Molinos	Molinos	Cónd.	Cónd.	Cónd.	Cónd.	Cónd.	Cónd.	Cónd..
SiO_2 (wt%)	45.07	44.87	45.84	46.05	47.94	46.92	46.82	46.98	50.80	49.05	49.77	51.08	51.46
TiO_2	2.68	2.71	2.60	2.61	3.15	3.68	2.90	2.89	2.22	3.47	3.42	2.32	2.91
Al_2O_3	9.92	10.06	10.48	10.82	10.36	10.94	9.71	9.84	13.53	11.03	11.61	14.21	13.19
FeO_{total}	11.09	11.24	10.75	10.52	9.81	11.27	10.61	10.60	9.12	10.98	10.49	8.78	8.82
MnO	0.16	0.17	0.16	0.16	0.16	0.17	0.16	0.16	0.13	0.17	0.16	0.14	0.12
MgO	15.51	14.61	13.85	13.30	13.20	11.81	15.30	14.89	10.14	9.68	8.28	7.61	8.31
CaO	10.79	10.68	10.86	10.77	9.81	10.07	9.89	9.77	7.97	10.24	9.95	8.05	6.98
Na_2O	2.52	3.68	3.15	3.28	2.28	3.06	2.73	2.96	3.90	2.87	2.99	4.06	3.91
K_2O	1.57	1.41	1.57	1.72	2.59	1.28	1.13	1.18	1.55	1.91	2.57	3.23	3.43
P_2O_5	0.70	0.58	0.75	0.78	0.70	0.80	0.75	0.75	0.56	0.60	0.76	0.52	0.88
mg-no.	0.74	0.73	0.73	0.72	0.74	0.68	0.75	0.74	0.70	0.65	0.62	0.64	0.66
FeO (wt%)	5.36	5.30	6.08	6.42	n.m.	n.m.	6.25	6.58	n.m.	2.66	2.31	5.74	5.78
Fe_2O_3 (wt%)	6.33	6.57	5.16	4.52	n.m.	n.m.	4.81	4.43	n.m.	9.21	9.07	3.36	3.36
L.O.I. (wt%)	4.96	3.63	4.02	4.21	5.30	4.80	4.67	4.50	5.41	5.06	5.49	2.42	3.53
Q (CIPW)													
Ne (CIPW)	8.20	14.48	9.91	10.40	3.08	3.33	3.25	4.18	0.99	1.18	1.65	6.71	3.23
Hy (CIPW)													
Ol (CIPW)	25.93	23.19	22.34	21.25	21.04	19.81	26.03	25.24	19.39	15.09	12.52	13.13	15.10
Cr (ppm)	591	627	630	624	317	308	653	632	284	411	325	282	205
Ni	443	430	423	397	249	266	464	468	235	289	249	152	167
Rb	53	21	48	55	60	22	14	16	6	44	55	30	30
Ba	970	993	999	992	1071	1181	918	921	789	1077	963	745	702
Sr	1229	1139	1174	1207	2318	1840	994	903	961	1107	1120	1100	936
Nb	87	86	85	89	82	95	83	78	78	83	86	73	80

(continued)

Table 2.6 (continued)

Sample	G3	LM3	G2	G1	MO1	MO19	EM4	EM5	RU13	CN7	CN6	EM3	CO7
Suite/group	Bsn	Bsn	Bsn	Bsn	AkB-Tc	AkB-Tc	AkB-Tc	AkB-Tc	AkB-Tc	AkB-Tc	AkB-Tc	AkB-Tc	AkB-Tc
Rock type	Bsn	Bsn	Bsn	Bsn	AkB	AkB	AkB	AkB	AkB	AkB	AkB	Tcb	Tcb
Locality	Pungo	Pungo	Pungo	Pungo	Molinos	Molinos	Cónd.	Cónd.	Cónd.	Cónd.	Cónd.	Cónd.	Cónd..
Zr	194	198	204	195	409	468	287	298	422	313	399	376	544
Y	21	21	22	21	27	31	26	25	23	30	29	23	25
La	*58.5*	*58.2*	57	58	*98.8*	*91.3*	*65.3*	68	*73.3*	69	*62.7*	*71.9*	*74.4*
Ce	*109.0*	*110.0*	100	106	*166.0*	*164.0*	*121.0*	125	*128.0*	118	*121.0*	*135.1*	*148.0*
Pr	*11.49*	*11.84*			*16.97*	*17.39*	*13.66*		*14.9*		*14.06*	*14.6*	*16.01*
Nd	*49.9*	*49.9*	50	49	*66.2*	*66.6*	*56.1*	53	*56.5*	56	*60.7*	*53.9*	*65.6*
Sm	*9.93*	*10.10*			*12.20*	*13.20*	*10.90*		*9.52*		*12.10*	*8.87*	*11.60*
Eu	*3.00*	*3.05*			*3.29*	*3.89*	*3.30*		*2.96*		*3.74*	*2.91*	*3.34*
Gd	*7.75*	*7.78*			*8.50*	*10.10*	*8.42*		*8.12*		*9.45*	*7.09*	*8.43*
Tb	*1.10*	*1.14*			*1.23*	*1.45*	*1.24*		*1.11*		*1.37*	*1.01*	*1.16*
Dy	*5.24*	*5.32*			*5.96*	*7.03*	*6.20*		*5.35*		*6.58*	*4.96*	*5.45*
Ho	*0.87*	*0.89*			*0.95*	*1.17*	*1.02*		*0.91*		*1.07*	*0.85*	*0.94*
Er	*2.13*	*2.24*			*2.49*	*3.08*	*2.71*		*2.44*		*2.75*	*2.23*	*2.39*
Tm	*0.23*	*0.24*			*0.31*	*0.37*	*0.31*		*0.30*		*0.31*	*0.27*	*0.26*
Yb	*1.37*	*1.42*			*1.70*	*1.89*	*1.78*		*1.83*		*1.84*	*1.61*	*1.54*
Lu	*0.17*	*0.18*			*0.25*	*0.29*	*0.25*		*0.25*		*0.24*	*0.22*	*0.31*
Hf	*4.9*	*5.0*			*8.0*	*9.7*	*6.4*		*8.6*		*8.3*	*8.0*	*12.0*
Ta	*4.11*	*4.19*			*4.95*	*5.26*	*3.87*		*4.20*		*4.39*	*3.90*	*4.82*
Th	*7.82*	*7.36*			*10.30*	*9.57*	*6.60*		*8.04*		*11.40*	*9.03*	*7.99*
U	*1.66*	*1.36*			*1.91*	*1.80*	*1.12*		*1.43*		*1.33*	*1.72*	*1.71*
Ga	*19*	*19*			*20*	*22*	*19*		*25*		*22*	*21*	*19*
$(La/Yb)_{cn}$	28.79	27.63			39.18	32.57	24.73		27.00		22.79	30.11	32.31
$(Eu/Eu^*)_{cn}$	1.05	1.05			0.99	1.03	1.06		1.03		1.07	1.12	1.03

(continued)

Table 2.6 (continued)

Sample	CO12	RU5	RU7	Li8	RU10B	RU12B	PM4	PM2	PM1	PM5	PM7	PM6	PM6B
Suite/Group	AkB-Tc	AkB-Tc	AkB-Tc	AkB-Tc	AkB-Tc	AkB-Tc	AkB-Tc	AkB-Tc	AkB-Tc	AkB-Tc	AkB-Tc	AkB-Tc	AkB-Tc
Rock type	Tcb	Tca	Tca	Tca	Tca	Tca	AkB	Tcb	Tca	Tca	Tcp	Tc	QTc
Locality	Cónd.	Cónd.	Cónd.	Cónd.	Cónd.	Cónd.	Almaf.	Almaf.	Almaf.	Almaf.	Almaf.	Almaf.	Almaf.
Sample	CO12	RU5	RU7	Li8	RU10B	RU12B	PM4	PM2	PM1	PM5	PM7	PM6	PM6B
Suite/Group	AkB-Tc	AkB-Tc	AkB-Tc	AkB-Tc	AkB-Tc	AkB-Tc	AkB-Tc	AkB-Tc	AkB-Tc	AkB-Tc	AkB-Tc	AkB-Tc	AkB-Tc
Rock type	Tcb	Tca	Tca	Tca	Tca	Tca	AkB	Tcb	Tca	Tca	Tcp	Tc	QTc
Locality	Cónd.	Cónd.	Cónd.	Cónd.	Cónd.	Cónd.	Almaf.	Almaf.	Almaf.	Almaf.	Almaf.	Almaf.	Almaf.
SiO_2 (wt%)	50.08	56.31	56.07	56.04	56.69	56.72	47.67	52.14	52.36	58.94	55.28	62.62	63.15
TiO_2	3.10	2.04	2.15	2.18	1.78	1.76	3.12	2.66	2.59	1.57	2.05	0.94	1.04
Al_2O_3	12.95	15.09	14.97	14.81	17.38	17.48	11.13	15.14	15.47	16.14	17.59	17.55	17.31
FeO_{total}	9.31	6.51	6.74	6.92	6.51	6.25	11.03	8.62	8.30	5.58	6.49	3.67	4.01
MnO	0.13	0.10	0.13	0.11	0.09	0.10	0.16	0.12	0.11	0.12	0.10	0.10	0.08
MgO	8.48	5.58	5.13	5.01	3.12	2.89	11.63	5.96	5.95	3.38	3.12	1.12	1.47
CaO	8.02	4.92	5.31	5.21	4.59	4.62	9.27	7.67	6.20	4.53	4.76	1.46	1.32
Na_2O	3.33	3.70	3.77	3.64	3.77	4.63	3.31	3.35	4.70	4.01	6.13	3.65	2.83
K_2O	3.71	5.13	5.11	5.52	5.30	4.77	1.88	3.65	3.59	5.33	3.85	8.62	8.52
P_2O_5	0.89	0.61	0.61	0.56	0.77	0.78	0.80	0.69	0.72	0.41	0.62	0.25	0.27
mg-no.	0.65	0.64	0.61	0.60	0.50	0.49	0.69	0.59	0.60	0.56	0.50	0.39	0.43
FeO (wt%)	6.56	1.24	1.9	1.23	0.99	0.80	2.78	1.45	1.71	1.36	1.98	1.61	0.41
Fe_2O_3 (wt%)	3.03	5.84	5.37	6.31	6.12	6.04	9.14	7.94	7.31	4.68	5.00	2.28	3.99
L.O.I. (wt%)	3.15	2.75	2.95	3.11	3.43	2.60	4.89	4.99	3.71	2.92	2.66	1.33	2.60
Q (CIPW)										1.08		2.47	7.88
Ne (CIPW)	4.49						5.03	0.23	5.37		7.30		
Hy (CIPW)		6.98	3.95	7.28	12.31	2.90				10.35		6.80	7.91
Ol (CIPW)	14.60	6.43	7.24	8.53	0.70	6.32	20.33	11.66	12.10		7.15		
Cr (ppm)	227	89	88	99	20	12	357	107	81	50	20	16	26
Ni	173	77	70	65	14	12	311	78	73	33	10	5	12
Rb	46	94	92	109	139	107	42	49	51	143	92	225	199
Ba	740	825	738	765	1155	1494	1213	972	990	868	1109	736	684
Sr	1152	871	863	762	962	973	919	797	846	601	949	224	192

(continued)

Table 2.6 (continued)

Sample	CO12	RU5	RU7	Li8	RU10B	RU12B	PM4	PM2	PM1	PM5	PM7	PM6	PM6B
Suite/Group	AkB-Tc	AkB-Tc	AkB-Tc	AkB-Tc	AkB-Tc	AkB-Tc	AkB-Tc	AkB-Tc	AkB-Tc	AkB-Tc	AkB-Tc	AkB-Tc	AkB-Tc
Rock type	Tcb	Tca	Tca	Tca	Tca	Tca	AkB	Tcb	Tca	Tca	Tcp	Tc	QTc
Locality	Cónd.	Cónd.	Cónd.	Cónd.	Cónd.	Cónd.	Almaf.	Almaf.	Almaf.	Almaf.	Almaf.	Almaf.	Almaf.
Nb	86	84	86	88	94	93	91	91	91	82	86	111	111
Zr	510	667	670	715	649	645	387	536	543	568	539	743	775
Y	27	27	28	30	35	35	26	28	27	34	28	43	44
La	80	100	*84.0*	*91.9*	*95.0*	107	*70.3*	87	*80.6*	*81.1*	*89.4*	*98.1*	94
Ce	157	176	*161.0*	*169.3*	*181.0*	188	*130.0*	157	*144.7*	*146.6*	*158.0*	*178.0*	171
Pr			*15.94*	*17.80*	*18.04*		*14.05*		*15.30*	*15.30*	*16.05*	*17.47*	
Nd	65	66	*60.3*	*62.4*	*67.6*	74	*58.5*	61	*56.3*	*54.0*	*61.3*	*61.4*	62
Sm			*10.10*	*9.77*	*11.40*		*10.60*		*8.98*	*8.95*	*10.00*	*10.50*	
Eu			*2.74*	*2.94*	*2.94*		*3.26*		*2.75*	*2.63*	*2.98*	*2.14*	
Gd			*7.31*	*7.47*	*8.03*		*8.44*		*7.24*	*7.20*	*7.04*	*7.44*	
Tb			*1.05*	*1.04*	*1.22*		*1.19*		*1.05*	*1.09*	*1.10*	*1.25*	
Dy			*5.06*	*5.24*	*5.90*		*5.93*		*5.19*	*5.71*	*5.58*	*6.40*	
Ho			*0.89*	*0.89*	*1.06*		*0.98*		*0.89*	*1.03*	*0.96*	*1.19*	
Er			*2.37*	*2.39*	*2.93*		*2.50*		*2.41*	*2.93*	*2.72*	*3.50*	
Tm			*0.29*	*0.30*	*0.36*		*0.29*		*0.31*	*0.39*	*0.33*	*0.50*	
Yb			*1.72*	*1.82*	*2.26*		*1.57*		*1.78*	*2.39*	*1.99*	*3.15*	
Lu			*0.24*	*0.25*	*0.31*		*0.22*		*0.25*	*0.33*	*0.29*	*0.44*	
Hf			*13.0*	*12.6*	*12.0*		*8.0*		*9.4*	*10.5*	*11.0*	*14.0*	
Ta			*4.54*	*4.70*	*4.82*		*4.30*		*5.00*	*4.60*	*4.77*	*6.46*	
Th			*14.50*	*15.00*	*19.50*		*9.05*		*13.20*	*15.50*	*14.80*	*24.70*	
U			*1.75*	*1.92*	*2.07*		*1.70*		*2.20*	*2.49*	*2.84*	*3.08*	
Ga			*25*	*26*	*28*		*21*		*25*	*22*	*28*	*26*	
$(La/Yb)_{cn}$			32.93	33.77	28.34		29.94		30.28	22.69	30.04	20.83	
$(Eu/Eu^*)_{cn}$			0.98	1.05	0.94		1.05		1.04	1.00	1.09	0.74	

(continued)

Table 2.6 (continued)

Sample	Li1	ES2	CO18	CN14	CO8	Li4	CN4	CN1	PM3	D4	D7	MO5	MO6
Suite/Group	TrB-Lb	TrB-Lb	TrB-Lb	TrB-Lb	TrB-Lb	TrB-Lb	TrB-Lb	TrB-Lb	TrB-Lb	TrB-Lb	TrB-Lb	Akt	Akt
Rock type	TrB	TrB	TrB	TrB	Lb	Lb	Lb	Lb	Lb	TrB	TrB	Akt	Akt
Locality	Cónd.	Cónd.	Cónd.	Cónd.	Cónd.	Cónd.	Cónd.	Cónd.	Almaf.	Despeñ.	Despeñ.	Molinos	Molinos
Sample	Li1	ES2	CO18	CN14	CO8	Li4	CN4	CN1	PM3	D4	D7	MO5	MO6
Suite/Group	TrB-Lb	TrB-Lb	TrB-Lb	TrB-Lb	TrB-Lb	TrB-Lb	TrB-Lb	TrB-Lb	TrB-Lb	TrB-Lb	TrB-Lb	Akt	Akt
Rock type	TrB	TrB	TrB	TrB	Lb	Lb	Lb	Lb	Lb	TrB	TrB	Akt	Akt
Locality	Cónd.	Cónd.	Cónd.	Cónd.	Cónd.	Cónd.	Cónd.	Cónd.	Almaf.	Despeñ.	Despeñ.	Molinos	Molinos
SiO_2 (wt%)	48.57	51.03	49.34	49.87	53.85	52.70	53.11	55.00	53.01	52.31	52.71	43.11	43.09
TiO_2	2.77	2.89	3.97	2.76	2.39	2.31	2.46	2.12	2.70	2.51	2.45	3.80	4.27
Al_2O_3	10.38	11.47	10.73	11.22	14.23	13.45	12.69	13.85	15.24	11.03	11.82	8.56	8.72
FeO_{total}	9.85	9.05	10.76	9.70	7.34	7.91	8.99	8.14	8.43	9.50	9.19	11.12	10.69
MnO	0.15	0.14	0.17	0.14	0.09	0.14	0.13	0.12	0.12	0.10	0.11	0.19	0.17
MgO	13.87	12.50	12.37	12.35	9.18	8.98	8.19	7.08	5.91	11.13	10.02	13.45	10.88
CaO	9.60	7.63	7.49	8.22	5.42	7.25	7.81	6.30	7.00	7.96	7.84	14.44	16.51
Na_2O	2.23	2.32	2.18	2.76	3.41	2.91	3.13	3.90	3.08	2.62	2.97	3.36	2.79
K_2O	1.96	2.34	2.23	2.35	3.40	3.60	2.99	2.81	3.81	2.39	2.46	1.05	1.75
P_2O_5	0.62	0.63	0.75	0.63	0.68	0.75	0.52	0.67	0.69	0.46	0.42	0.92	1.13
mg-no.	0.74	0.74	0.70	0.73	0.72	0.70	0.65	0.64	0.59	0.71	0.69	0.71	0.68
FeO (wt%)	2.00	2.34	2.40	3.5	1.61	1.64	2.06	1.9	1.73	1.21	1.84	n.m.	n.m.
Fe_2O_3 (wt%)	8.7	7.43	9.27	6.87	6.36	6.94	7.68	6.92	7.43	9.19	8.14	n.m.	n.m.
L.O.I. (wt%)	5.03	2.21	4.61	4.33	4.64	4.67	4.16	3.24	5.27	7.78	5.75	10.56	9.80
Q (CIPW)													
Ne (CIPW)													
Hy (CIPW)	0.06	17.16	17.45	1.07	13.72	7.28	9.15	15.75	9.90	15.49	12.23		
Ol (CIPW)	23.29	10.79	11.00	21.36	9.03	11.56	8.15	3.32	5.38	8.85	9.18		
Cr (ppm)	492	322	349	457	176	270	286	189	104	446	433	553	417
Ni	366	250	291	314	157	151	198	178	81	298	316	325	301
Rb	11	37	43	48	41	28	72	61	50	61	60	13	18
Ba	1057	764	827	915	728	852	885	1083	951	665	668	1528	1677
Sr	974	1050	923	886	997	978	1017	1064	726	947	767	754	728

(continued)

Table 2.6 (continued)

Sample	Li1	ES2	CO18	CN14	CO8	Li4	CN4	CN1	PM3	D4	D7	MO5	MO6
Suite/Group	TrB-Lb	TrB-Lb	TrB-Lb	TrB-Lb	TrB-Lb	TrB-Lb	TrB-Lb	TrB-Lb	TrB-Lb	TrB-Lb	TrB-Lb	Akt	Akt
Rock type	TrB	TrB	TrB	TrB	Lb	Lb	Lb	Lb	Lb	TrB	TrB	Akt	Akt
Locality	Cónd.	Cónd.	Cónd.	Cónd.	Cónd.	Cónd.	Cónd.	Cónd.	Almaf.	Despeñ.	Despeñ.	Molinos	Molinos
Nb	79	60	65	69	72	88	59	52	90	60	52	92	99
Zr	436	253	432	279	484	538	271	227	508	251	244	609	577
Y	21	25	43	22	22	25	26	26	27	23	25	28	30
La	*91.6*	*63.9*	69	*71.4*	*77.6*	*93.4*	64	*76.8*	83	52	45	*120.0*	*144.0*
Ce	*165.0*	*123.0*	134	*134.0*	*147.0*	*174.0*	118	*134.0*	151	100	98	*214.0*	*245.0*
Pr	*16.63*	*13.45*		*14.90*	*16.00*	*17.58*		*15.12*				*22.01*	*26.22*
Nd	*62.6*	*56.8*	67	*59.9*	*60.3*	*66.0*	60	*61.8*	57	47	47	*79.6*	*98.6*
Sm	*10.10*	*11.40*		*11.00*	*9.85*	*11.20*		*11.40*				*13.30*	*16.10*
Eu	*2.96*	*3.32*		*3.30*	*3.12*	*3.10*		*3.41*				*3.65*	*4.11*
Gd	*7.43*	*8.51*		*8.06*	*7.62*	*7.82*		*8.40*				*10.50*	*12.20*
Tb	*1.05*	*1.26*		*1.20*	*1.00*	*1.16*		*1.20*				*1.37*	*1.60*
Dy	*5.15*	*5.90*		*5.84*	*4.96*	*5.49*		*5.73*				*6.22*	7.28
Ho	*0.87*	*1.02*		*0.95*	*0.81*	*0.95*		*0.91*				*1.01*	*1.12*
Er	*2.37*	*2.58*		*2.55*	*2.07*	*2.58*		*2.38*				*2.74*	*3.15*
Tm	*0.27*	*0.28*		*0.28*	*0.24*	*0.29*		*0.27*				*0.31*	*0.36*
Yb	*1.51*	*1.70*		*1.64*	*1.41*	*1.81*		*1.49*				*1.53*	*1.80*
Lu	*0.22*	*0.22*		*0.22*	*0.18*	*0.25*		*0.21*				*0.23*	*0.26*
Hf	*9.6*	*6.3*		*6.5*	*9.2*	*11.0*		*6.0*				*13.0*	*14.0*
Ta	*4.06*	*3.09*		*3.46*	*3.80*	*4.82*		*2.34*				*5.40*	*6.28*
Th	*8.76*	*8.37*		*7.14*	*8.93*	*12.10*		*9.24*				*10.10*	*11.20*
U	*0.96*	*1.29*		*1.29*	*1.52*	*2.02*		*0.84*				*1.97*	*1.87*
Ga	*20*	*22*		*21*	*23*	*24*		*24*				*19*	*20*
$(La/Yb)_{cn}$	40.56	25.13		29.11	36.80	34.51		34.47				52.88	53.94
$(Eu/Eu^*)_{cn}$	1.04	1.03		1.07	1.10	1.01		1.07				0.94	0.90

Major elements recalculated to 100 % on a volatile-free basis. *mg*-no = $Mg/(Mg + Fe^{2+})$ and CIPW-normative compositions assuming $Fe_2O_3/FeO = 0.18$. Q, Ne, Hy, and Ol = CIPW-normative quartz, nepheline, hypersthene, and olivine, respectively. Trace element contents in normal and italic styles indicate measurement by XRF and ICP-MS techniques, respectively. *Bsn* basanite, *AkB* alkali basalt, *Tcb* trachybasalt, *Tca* trachyandesite, *Tc* trachyte, *QTc* quartz trachyte, *Tcp* trachyphonolite, *TrB* transitional basalt, *Lb* latibasalt; *Pungo* El Pungo; *Molinos* Los Molinos; *Cónd.* Sierra de los Cóndores; *Almaf.* Almafuerte; *Despeñ.* Despeñaderos; *cn* chondrite normalized (Boynton 1984).

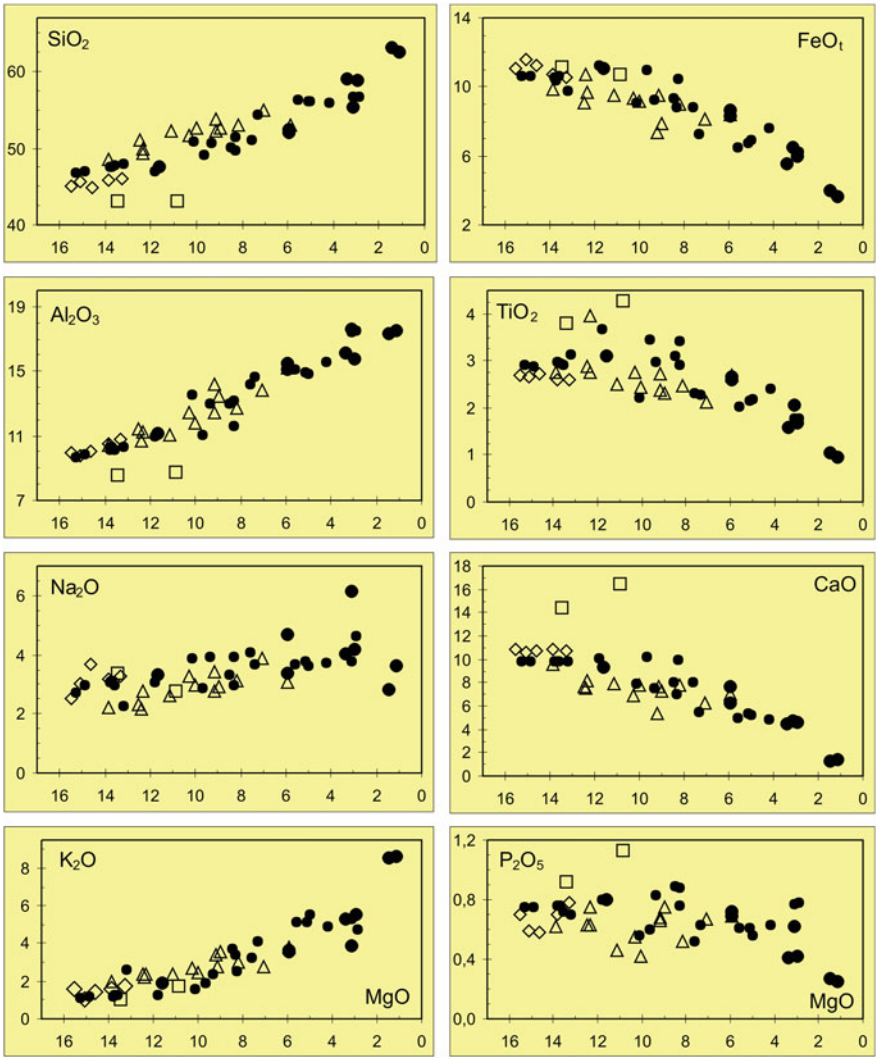

Fig. 2.13 Variation diagrams of the major elements in terms of MgO (wt%) for different groups of rocks in Sierra Chica, adapted from Lagorio (2008) incluiding also ankaratrites. Diamonds: basanites of El Pungo (Bsn); filled circles: alkali basalt—trachyte suite (AkB-Tc); small circles: samples of the Sierra de los Cóndores and Los Molinos locality; *large circles* Almafuerte samples; *triangles* transitional basalt–latibasalt suite (TrB-Lb) in Sierra de Los Cóndores, Almafuerte and Despeñaderos localities; *square* ankaratrites from Los Molinos

Variation diagrams are consistent with fractionation of olivine, clinopyroxene and magnetite in both suites, as discussed in detail in Lagorio (2003, 2008). Within the alkaline suite, plagioclase and apatite removal is better supported from the late stages of the Almafuerte magmas, based on Sr and P_2O_5 lines of descent, respectively.

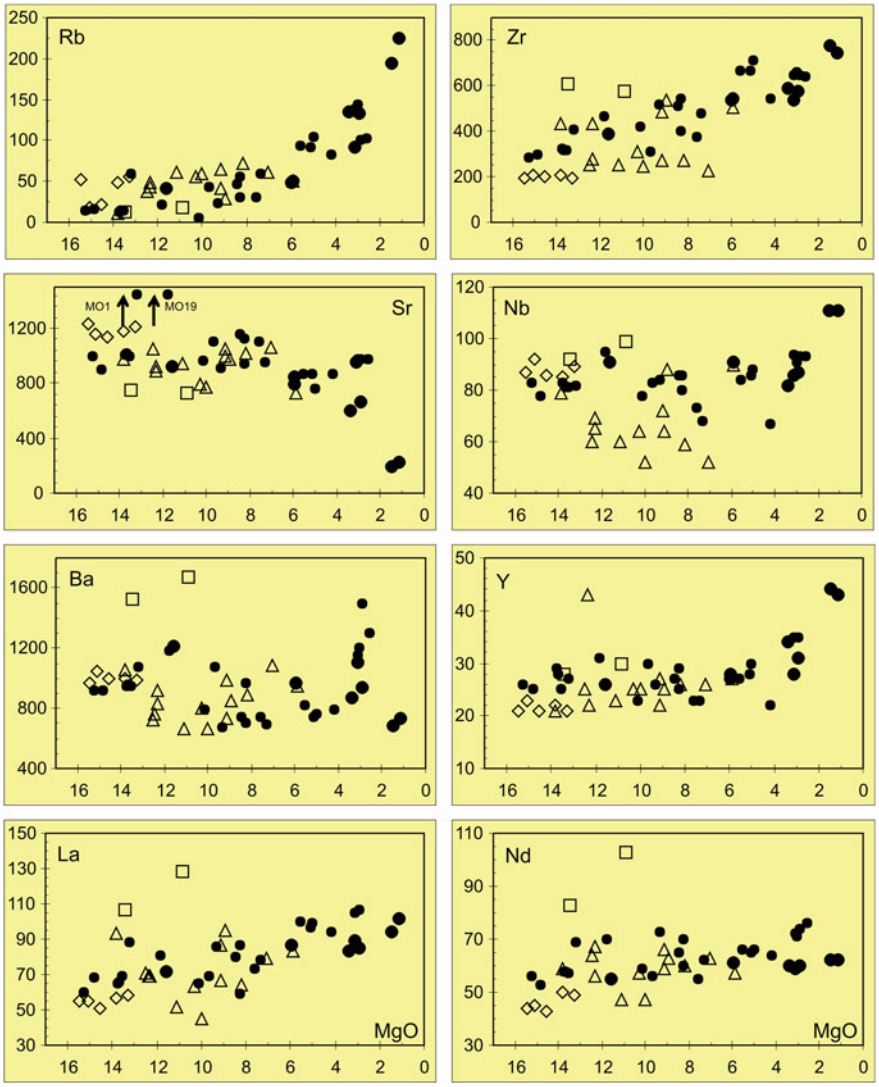

Fig. 2.14 Variation diagrams of trace elements (ppm) related to MgO (wt%). Adapted from Lagorio (2008) including also ankaratrites. Symbols as in Fig. 2.13

Relationship between incompatible elements (e.g. Zr vs. Th, Fig. 2.15a) both in alkaline and transitional suites shows no clear linear trends, suggesting that complete evolution must not be directly due only to simple crystal fractionation starting from primary magmas. The strong variation in the content of some incompatible elements (e.g. Zr) in the most primitive magmas is clearly visible in the

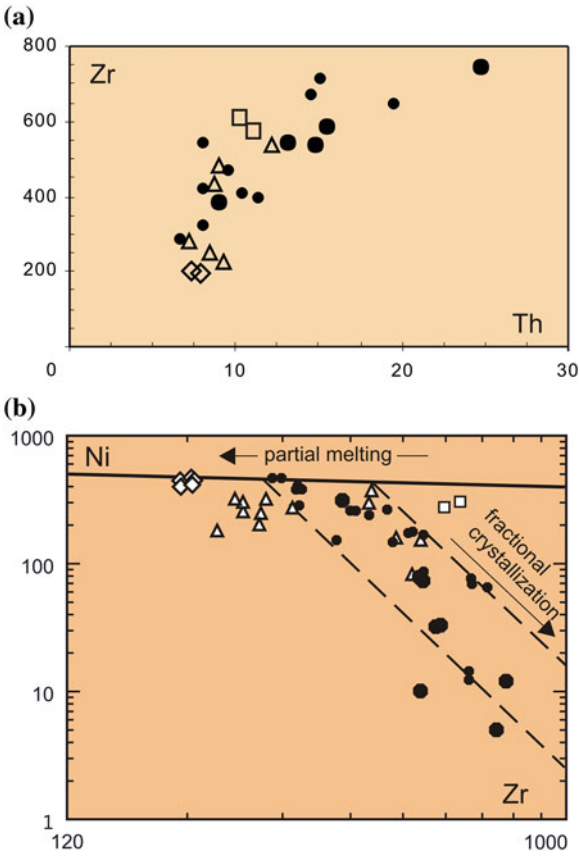

Fig. 2.15 Variation diagrams of trace elements for volcanic rocks of Sierra Chica, adapted by Lagorio (2008) including also ankaratrites. **a** Th versus Zr. **b** Zr versus Ni bilogarithmic diagram. Symbols as in Fig. 2.13

bilogarithmic Zr–Ni diagram (Fig. 2.15b), and the various negatively sloped linear trends that can be defined are compatible with evolution through various parental magmas, consistent with a heterogeneous mantle source. It is worthy to note that basanites show the lowest values of Zr (Fig. 2.15b), Hf, LREE and Sm, regarding the four distinguished groups, as well as the lowest La/Ta and La/Nb ratios (Fig. 2.16). On the other hand, alkaline and transitional basalts show variable contents of incompatible elements, particularly high for Zr (Fig. 2.15b), Hf and LREE in some transitional basalts; the latter are distinguished from the alkaline ones by their higher La/Ta, Th/Ta and La/Nb ratios (Fig. 2.16). Ankaratrites record the highest content of Zr (Fig. 2.15b), Ta, LREE, Sm, Hf, Ti and Tb, as well as high La/Ta ratio and the highest of La/Nb (Fig. 2.16).

In chondrite-normalized (cn; Boynton 1984) diagrams, the rocks of the alkaline suite have relationships $(La/Yb)_{cn}$ between 20 and 39 (Table 2.6; Lagorio 2008), showing patterns that diverge only for the trachyte of the Almafuerte locality (PM6; Fig. 2.17). The latter shows a steep LREE trend that tends to flatten out for HREE [$(Gd/Yb)_{cn}$ = 1.88] as well as a slight negative Eu anomaly (Eu/Eu* = 0.74),

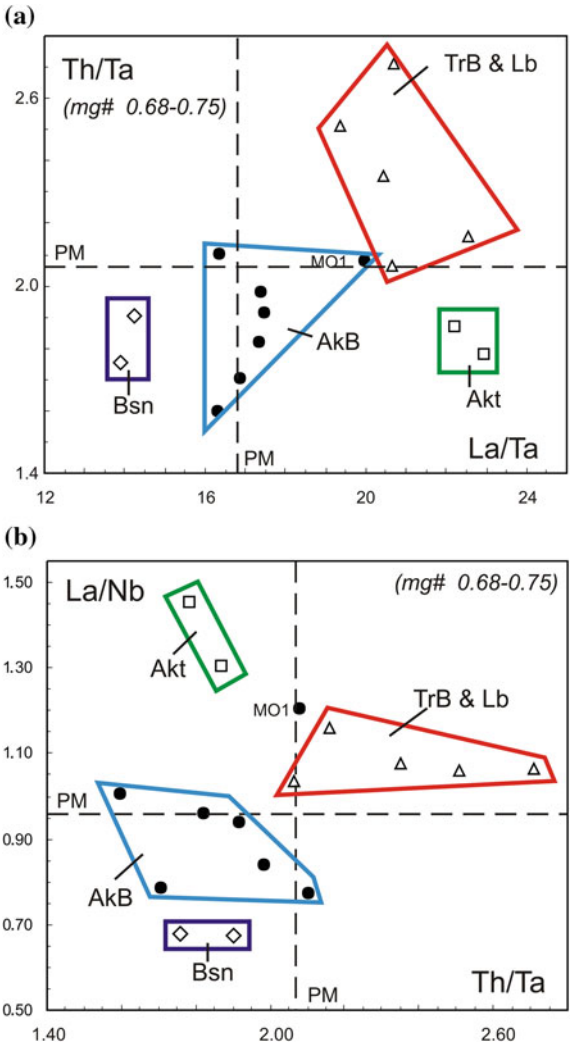

Fig. 2.16 **a** La/Ta versus Th/Ta and **b** Th/Ta versus La/Nb for the most primitive rocks of Sierra Chica (mg # 0.68–0.75) from the different groups of lithologies of Sierra Chica, adapted from Lagorio (2008) also including ankaratrites. *PM* primordial mantle according to Sun and McDonough (1989). Symbols as in Fig. 2.13

supporting fractionation of plagioclase. The transitional suite display $(La/Yb)_{cn}$ ratios between 25 and 41 (Table 2.6; Lagorio 2008), showing broadly similar patterns to those of the rocks of the alkaline suite, particularly rocks from Sierra de los Cóndores and Embalse Los Molinos (Fig. 2.17a). Basanites present a mean $(La/Yb)_{cn}$ of 28 (Table 2.6; Lagorio 2008) and also show patterns with no significant differences with respect to the latter ones (Fig. 2.17d). Ankaratrites display the highest $(La/Yb)_{cn}$ (average of 53, Table 2.6), with higher values for REE in comparison with the basanites, and the highest contents for LREE taken to account also the alkaline basalts (Fig. 2.17d).

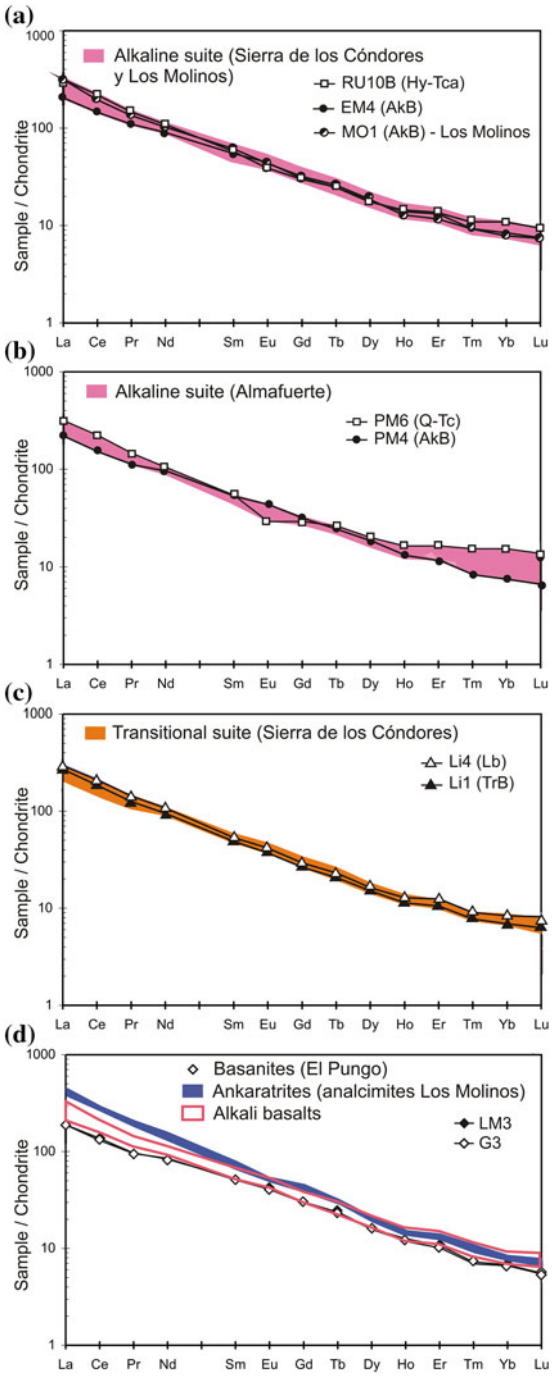
(a)
Alkaline suite (Sierra de los Cóndores y Los Molinos)
RU10B (Hy-Tca)
EM4 (AkB)
MO1 (AkB) - Los Molinos
Sample / Chondrite
1000
100
10
1
La Ce Pr Nd Sm Eu Gd Tb Dy Ho Er Tm Yb Lu
(b)
Alkaline suite (Almafuerte)
PM6 (Q-Tc)
PM4 (AkB)
Sample / Chondrite
1000
100
10
1
La Ce Pr Nd Sm Eu Gd Tb Dy Ho Er Tm Yb Lu
(c)
Transitional suite (Sierra de los Cóndores)
Li4 (Lb)
Li1 (TrB)
Sample / Chondrite
1000
100
10
1
La Ce Pr Nd Sm Eu Gd Tb Dy Ho Er Tm Yb Lu
(d)
Basanites (El Pungo)
Ankaratrites (analcimites Los Molinos)
Alkali basalts
LM3
G3
Sample / Chondrite
1000
100
10
1
La Ce Pr Nd Sm Eu Gd Tb Dy Ho Er Tm Yb Lu

◀ **Fig. 2.17** Chondrite-normalized (Boynton 1984) REE diagrams for rocks of Sierra Chica, adapted from Lagorio (2008) also including ankaratrites. **a** Alkaline suite from Sierra de los Cóndores and Los Molinos locality. **b** Alkaline suite from Almafuerte. **c** Transitional suite from Sierra de los Cóndores. **d** Basanites from El Pungo and ankaratrites from Los Molinos, compared with alkali basalts. *Coloured fields* all samples analysed in each group

In multi-element diagrams normalized to the primordial mantle (Sun and McDonough 1989), rocks of the alkaline suite show negative anomalies in Rb and K for the less evolved samples, showing a gradual increase in the contents of Rb, Th, K, Zr and Hf towards the Hy- and Q-normative trachyandesites and trachytes (Fig. 2.18a, b). Q-varieties are also characterized by negative Sr, P and Ti anomalies, more pronounced in trachytes (Fig. 2.18b). It should be noted that alkaline basalts of dykes from Los Molinos are distinguished by presenting a positive anomaly for Sr, in contrast to the clearly negative anomaly that characterizes all samples from Sierra de los Cóndores. Transitional suite shows similar patterns regarding the less evolved samples of the alkaline suite from Sierra de los Cóndores (Fig. 2.18c). However, a slightly negative spike of Ta is shown, particularly conferred by the most evolved latibasalt (Fig. 2.18c). Basanites patterns are similar to those of the most primitive rocks of both suites, though they clearly present the lowest contents of Zr and Hf as well as low tenors of REE (Fig. 2.18d). Ankaratrites record the highest values of Ta, LREE, P, Sm, Zr, Hf, Ti and Tb; they also display a clear negative anomaly for Sr, in contrast to what happens in relation to the other rocks (alkaline basalts) of the same locality (Los Molinos) (Fig. 2.18d).

2.1.1.7 Petrogenesis

Differentiation Processes

In order to test fractional crystallization quantitatively, mass balance calculations based on major elements (Stormer and Nicholls 1978) were carried out. Rayleigh's trace element contents were calculated using mass balance results and the partition coefficients employed by Lagorio (2003, 2008) and shown in Tables 2.7 and 2.8.

Some transitions appear compatible (sum of the squares of major element residua, $\Sigma res^2 < 1.0$) with simple fractional crystallization (Table 2.8), e.g. from EM3 (trachybasalt) to RU7 (trachyandesite), from PM1 (trachyandesite) to PM7 (trachyphonolite) and from Li1 (transitional basalt) to Li4 (latibasalt). The calculated/observed trace element ratios also are in general satisfactory (0.90–1.35; Table 2.8), except for Cr and Ni (0.28–2.10), and for Rb and Ba (0.57–1.77). Ni and Cr discrepancies may be partly due to uncertainties on partition coefficients, while those for Rb and Ba may probably reflect alteration. On the contrary, other transitions, e.g. from EM4 (alkali basalt) to EM3 (trachybasalt), similarly compatible with fractional crystallization in terms of major element results (though a higher Σres^2 is obtained, Table 2.8), reveal many trace element ratios quite different from

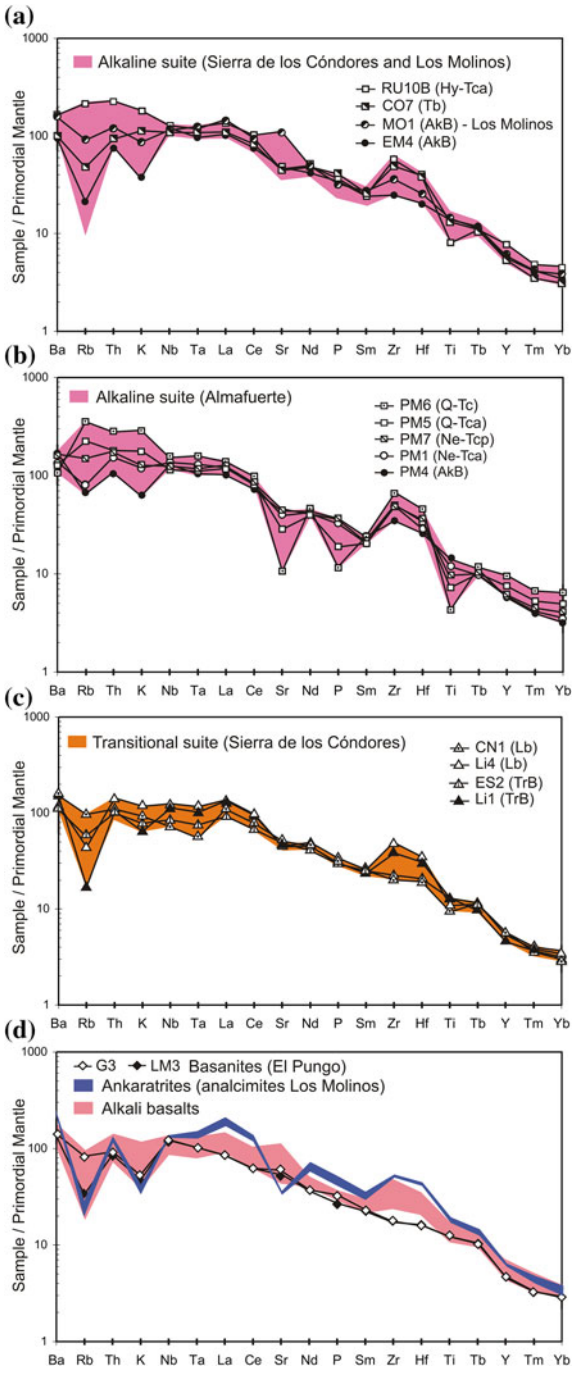
(a)
Alkaline suite (Sierra de los Cóndores and Los Molinos)
RU10B (Hy-Tca)
CO7 (Tb)
MO1 (AkB) - Los Molinos
EM4 (AkB)
Sample / Primordial Mantle
1000
100
10
1
Ba Rb Th K Nb Ta La Ce Sr Nd P Sm Zr Hf Ti Tb Y Tm Yb
(b)
Alkaline suite (Almafuerte)
PM6 (Q-Tc)
PM5 (Q-Tca)
PM7 (Ne-Tcp)
PM1 (Ne-Tca)
PM4 (AkB)
Sample / Primordial Mantle
1000
100
10
1
Ba Rb Th K Nb Ta La Ce Sr Nd P Sm Zr Hf Ti Tb Y Tm Yb
(c)
Transitional suite (Sierra de los Cóndores)
CN1 (Lb)
Li4 (Lb)
ES2 (TrB)
Li1 (TrB)
Sample / Primordial Mantle
1000
100
10
1
Ba Rb Th K Nb Ta La Ce Sr Nd P Sm Zr Hf Ti Tb Y Tm Yb
(d)
G3
LM3 Basanites (El Pungo)
Ankaratrites (analcimites Los Molinos)
Alkali basalts
Sample / Primordial Mantle
1000
100
10
1
Ba Rb Th K Nb Ta La Ce Sr Nd P Sm Zr Hf Ti Tb Y Tm Yb

◀ **Fig. 2.18** Primordial mantle (Sun and McDonough 1989) normalized multi-elemental plots for rocks of the Sierra Chica, adapted from Lagorio (2008) also including ankaratrites. **a** Alkaline suite in Sierra de los Cóndores and Los Molinos. **b** Alkaline suite from Almafuerte. **c** Transitional suite in Sierra de los Cóndores. **d** Basanites of El Pungo and ankaratrites of Los Molinos dam, compared with alkali basalts. *Coloured fields* all samples analysed in each group

1.0 (up to 1.96). It should be also noted that the transitional basalt to latibasalt transition is only supported starting from basalts with low normative hypersthene (<2 %, e.g. Li1, CN14).

Quantitative evidence therefore also indicates that simple fractional crystallization does not completely account for the SCC magmatic differentiation, suggesting therefore distinct parental magmas and/or evolution in an open-system magma chamber.

Actually, this is congruent with trace element variation diagrams. The remarkable variation in some IE contents (e.g. Zr) of the most primitive rocks is clearly seen in a Zr–Ni log–log diagram (Fig. 2.15b), and the diverse linear trends with negative slope (that can be defined) are more compatible with an evolution through different parental magmas.

Although there is some petrographic evidence of upper crustal contamination in some rocks (particularly in dykes from Los Molinos and in a few lavas of Sierra de los Cóndores, as previously stated by Gordillo and Lencinas 1967a, 1969), the lack of a significant Ta–Nb negative depletion in the multi-elemental diagrams may indicate that crustal contamination was not a relevant a process (Fig. 2.18, only latibasalt CN1 displays a slight anomaly). In a $(La/Nb)_{PM}$ versus K_2O plot (Fig. 2.19a), this sample also appears close to the lower crust ratio of Rudnick and Gao (2003); considering

Table 2.7 Mineral/liquid partition coefficients used for fractional crystallization modelling

	Ol		Cpx		Pl		Mt		Ap	
	P	E	P	E	P	E	P	E	P	E
Cr	2.78	2.78	5.69	5.69	0.03	0.03	4.21	7.70	0.01	0.01
Ni	15.5	15.5	2	2	0.03	0.03	2.39	6.54	0.01	0.01
Ba	0.09	0.09	0.07	0.01	0.63	3.90	0.14	0.14	0.95	0.95
Rb	0.08	0.08	0.1	0.01	0.03	0.20	0.08	0.08	0.01	0.01
Sr	0.01	0.01	0.33	0.1	2.5	4.41	0.16	0.16	1.67	1.67
La	0.01	0.01	0.22	0.1	0.12	0.46	0.53	0.53	5.16	5.16
Ce	0.01	0.01	0.34	0.20	0.14	0.36	0.56	0.56	6.34	6.34
Nd	0.01	0.01	0.68	0.35	0.07	0.31	0.55	0.55	6.6	6.6
Zr	0.05	0.01	0.24	0.24	0.01	0.01	0.35	0.35	0.01	0.01
Y	0.01	0.01	0.77	0.77	0.05	0.24	0.55	0.55	5.08	5.08
Nb	0.17	0.01	0.12	0.12	0.01	0.01	3.86	3.86	0.01	0.01
Th	0.04	0.04	0.13	0.13	0.02	0.16	0.18	0.11	0.95	0.95

Ol olivine, *Cpx* clinopyroxene, *Pl* plagioclase, *Mt* magnetite, *Ap* apatite. Data from Caroff et al. (1993), De Min (1993) and Comin-Chiaramonti et al. (1997). *P* and *E* primitive and evolved magmas, respectively

Table 2.8 Representative mass balance calculations for major elements (Stormer and Nicholls 1978) and trace elements (Rayleigh equation) for fractional crystallization within AkB-Tc and TrB-Lb suites, according to Lagorio (2008)

	EM4	EM3	Ol(90)	Cpx	Mt	Ap	EM3		EM4	EM3	EM3	Calc./obs.	EM3	Calc./obs.
	AkB	Tcb					calc.				FC		AFC	
SiO_2	46.82	51.08	41.02	48.53	0.04	0.00	51.15	Cr	653.00	282.00	119.00	0.42	95.00	0.34
TiO_2	2.90	2.32	0.00	2.6	22.67	0.00	2.50	Ni	464.00	152.00	17.00	0.11	12.00	0.08
Al_2O_3	9.71	14.21	0.02	4.86	2.57	0.00	14.38	Rb	14.00	30.00	22.00	0.73	29.00	0.97
FeO_t	10.61	8.78	9.45	6.11	72.88	0.00	8.79	Ba	918.00	745.00	1462.00	1.96	1478.00	1.98
MnO	0.16	0.14	0.15	0.11	1.12	0.07	0.13	Sr	994.00	1100.00	1495.00	1.36	1495.00	1.36
MgO	15.30	7.61	49.31	13.71	0.61	0.00	7.65	Nb	83.00	73.00	109.00	1.49	107.00	1.46
CaO	9.89	8.05	0.05	23.61	0.1	57.01	8.03	Zr	287.00	376.00	441.00	1.17	445.00	1.18
Na_2O	2.73	4.06	0.00	0.48	0.00	0.00	4.27	Y	26.00	23.00	33.00	1.43	34.00	1.46
K_2O	1.13	3.24	0.00	0.00	0.00	0.00	2.44	La	65.30	71.90	96.30	1.34	96.40	1.34
P_2O_5	0.75	0.52	0.00	0.00	0.00	42.92	0.66	Ce	121.00	135.10	171.00	1.27	170.90	1.26
Mineral (wt%)			40.06	49.29	8.92	1.73		Nd	56.10	53.90	72.60	1.35	71.80	1.33
F (%)	59.64			$\sum res^2 = 0.78$				Th	6.60	9.03	10.44	1.16	10.52	1.17

	EM3	RU7	Ol(86)	Cpx	Pl(46)	Mt	Ap	RU7		EM3	RU7	RU7	Calc./obs.
	Tcb	Tca						Calc.				FC	
SiO_2	51.08	56.07	40.19	51.78	56.86	0.27	0.00	55.84	Cr	282.00	88.00	136.00	1.55
TiO_2	2.32	2.15	0.00	1.16	0.2	21.14	0.00	2.09	Ni	152.00	70.00	45.00	0.64
Al_2O_3	14.21	14.97	0.00	2.36	26.88	1.69	0.00	14.84	Rb	30.00	92.00	52.00	0.57
FeO_t	8.78	6.74	12.88	5.4	0.46	75.28	0.00	6.60	Ba	745.00	738.00	1079.00	1.46
MnO	0.14	0.13	0.17	0.09	0.00	1.03	0.07	0.13	Sr	1100.00	863.00	903.00	1.05
MgO	7.61	5.13	46.51	15.94	0.00	0.17	0.00	5.11	Nb	73.00	86.00	99.00	1.15
CaO	8.05	5.31	0.25	22.88	8.91	0.42	57.01	5.35	Zr	376.00	670.00	637.00	0.95

(continued)

Table 2.8 (continued)

	EM3	RU7	Ol(86)	Cpx	Pl(46)	Mt	Ap	RU7		EM3	RU7	RU7	Calc./obs.
	Tcb	Tca						Calc.				FC	
Na_2O	4.06	3.77	0.00	0.39	6.15	0.00	0.00	4.39	Y	23.00	28.00	33.00	1.18
K_2O	3.24	5.11	0.00	0.00	0.54	0.00	0.00	5.40	La	71.90	84.00	107.90	1.28
P_2O_5	0.52	0.61	0.00	0.00	0.00	0.00	42.92	0.26	Ce	135.10	161.00	194.00	1.20
Mineral (wt%)			14.92	23.73	47.64	10.91	2.79		Nd	53.90	60.30	75.00	1.24
F (%)	55.41		$\sum res^2 = 0.70$						Th	9.03	14.50	15.43	1.06
	PM1	PM7	Ol(82)	Cpx	Pl(51)	Mt	Ap	PM7		PM1	PM7	PM7	Calc./obs.
	Tca	Tcp						calc.				FC	
SiO_2	52.36	55.29	39.52	50.36	56.16	0.11	0.00	55.25	Cr	81.00	20.00	42.00	2.10
TiO_2	2.59	2.05	0.04	1.73	0.14	29.87	0.00	2.14	Ni	73.00	10.00	25.00	2.50
Al_2O_3	15.47	17.59	0.05	3.54	27.21	1.35	0.00	17.66	Rb	51.00	92.00	63.00	0.68
FeO_t	8.30	6.49	16.50	8.57	0.46	66.38	0.00	6.42	Ba	972.00	1109.00	1029.00	0.93
MnO	0.11	0.10	0.21	0.18	0.00	2.17	0.07	0.05	Sr	846.00	949.00	852.00	0.90
MgO	5.95	3.12	43.39	13.76	0.00	0.03	0.00	3.13	Nb	91.00	86.00	102.00	1.19
CaO	6.20	4.76	0.23	21.18	9.36	0.09	57.01	4.76	Zr	543.00	539.00	660.00	1.22
Na_2O	4.70	6.13	0.04	0.68	5.33	0.00	0.00	5.68	Y	27.00	28.00	30.00	1.07
K_2O	3.59	3.85	0.02	0.00	1.35	0.00	0.00	4.32	La	80.60	89.40	93.30	1.04
P_2O_5	0.72	0.62	0.00	0.00	0.00	0.00	42.92	0.58	Ce	144.70	158.00	165.30	1.05
Mineral (wt%)			26.93	38.7	19.39	11.89	3.09		Nd	56.30	61.30	63.50	1.04
F (%)	79.70			$\sum res^2 = 0.44$					Th	13.20	14.80	16.06	1.09
	Li1	Li4	Ol(90)	Cpx	Mt	Ap	Li4		Li1	Li4	Li4	Calc./obs.	
	TrB	Lb					Calc.				FC		
SiO_2	48.55	52.70	41.02	50.70	0.28	0.00	52.50	Cr	492.00	270.00	125.00	0.46	

(continued)

Table 2.8 (continued)

	Li1	Li4	Ol(90)	Cpx	Mt	Ap	Li4		Li1	Li4	Li4	Calc./obs.
	TrB	Lb					Calc.				FC	
TiO_2	2.77	2.31	0.00	0.64	30.52	0.00	2.35	Ni	366.00	151.00	42.00	0.28
Al_2O_3	10.37	13.45	0.02	4.53	0.73	0.00	13.97	Rb	11.00	28.00	16.00	0.57
FeO_t	9.85	7.91	9.45	7.32	66.04	0.00	7.84	Ba	1057.00	852.00	1509.00	1.77
MnO	0.15	0.14	0.15	0.27	0.69	0.07	0.11	Sr	974.00	978.00	1316.00	1.35
MgO	13.87	8.98	49.31	13.40	1.38	0.00	9.10	Nb	79.00	88.00	95.00	1.08
CaO	9.60	7.25	0.05	22.58	0.36	57.01	7.41	Zr	436.00	538.00	605.00	1.12
Na_2O	2.22	2.91	0.00	0.55	0.00	0.00	3.08	Y	21.00	25.00	24.00	0.96
K_2O	1.96	3.61	0.00	0.00	0.00	0.00	3.15	La	91.60	93.40	119.80	1.28
P_2O_5	0.65	0.75	0.00	0.00	0.00	42.92	0.48	Ce	165.00	174.00	207.00	1.19
Mineral (wt%)			32.64	53.83	10.57	2.95		Nd	62.60	66.00	72.80	1.10
F (%)	67.03			$\sum res^2 = 0.67$				Th	8.76	12.10	12.41	1.03

AFC modelling (De Paolo 1981) for AkB-Tcb transition, with $r = 0.1$ and mean composition of Córdoba basement (Rapela et al. 1998) as the contaminant *It can be stop instead of full stop, so this paragraph could be immidiately after the other.AkB* alkali basalt, *Tcb* trachybasalt, *Tca* trachyandesite, *Tcp* trachyphonolite. Mineral phases, with their respective compositions, subtracted from the parent liquid: *Ol* olivine, *Cpx* clinopyroxene, *Mt* magnetite, *Pl* plagioclase, *Ap* apatite. In parentheses: forsterite and anorthite contents of olivine and plagioclase, respectively; *calc.* calculated composition, *obs.* observed composition. *Mineral (wt%)* amount of the subtracted minerals, *F (%)* weight fraction of residual liquid, $\sum res^2$ sum of squares of major element residuals. *FC* fractional crystallization; *AFC* assimilation and fractional crystallization. EM4 is similar to EM5 and comes from the same level (picritic basalts of Gordillo and Lencinas), so that mineral phases employed in the modelling are those measured in EM5

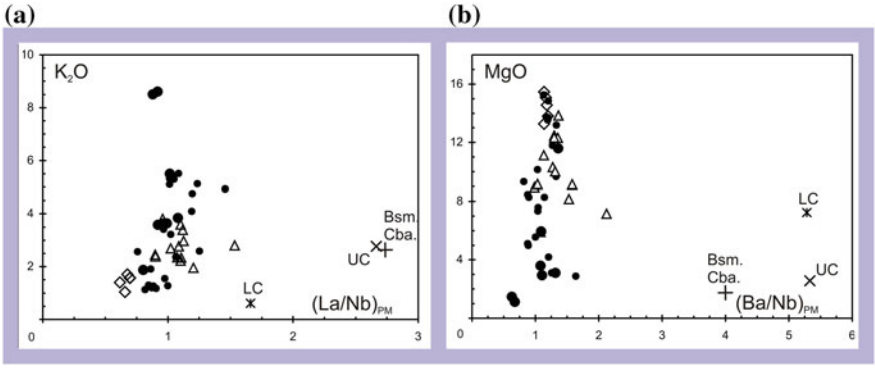

Fig. 2.19 **a** $(La/Nb)_{PM}$ ratios versus K_2O (wt%). **b** $(Ba/Nb)_{PM}$ ratio versus MgO (wt%) for the volcanic rocks of SCC, based on Lagorio (2008). *PM* primordial mantle normalization (Sun and McDonough 1989); Bsm. *Cba* Córdoba basement (Rapela et al. 1988); *UC* and *LC* upper and lower crust, respectively, from Rudnick and Gao (2003)

other ratios such as $(Ba/Nb)_{PM}$ (all samples display ratios < 2; Fig. 2.19b), and La/Ta (mean value = 19), crustal interaction does not appear as remarkable.

It should also be noted that no significant discrepancies in calculated/observed Th contents (typical upper crustal immobile element) appear in the Rayleigh crystal fractionation model (Table 2.8), despite some controversy in the partition coefficients. Anyway, AFC modelling (assimilation and fractional crystallization; De Paolo 1981) was also performed for the EM4–EM3 transition, considering the mean composition of the Córdoba crystalline basement (Rapela et al. 1998) as the contaminant. Calculations show in this case that this model does not give a satisfactory quantitative solution either (Table 2.8).

From six Sr–Nd isotopic data from Sierra de los Cóndores provided by Lucassen et al. (2002), five have ℇSr (125 Ma) from 15.1 to 24.1 and ℇNd (125 Ma) between −3.5 and −6.1; only one sample indicates significant crustal contamination (ℇSr = 50.8 and ℇNd = −5.1). Nevertheless, Pb isotopes also obtained by the latter authors point out <10 % contamination with lower crust, not detectable through Sr–Nd isotopes.

Textural evidence of solid–liquid disequilibrium from some plagioclase and clinopyroxene macro- and phenocrysts, consistent with frequent slight core to rim Ca and Mg increments, and particularly with the common Mg increase from clinopyroxene micro- and phenocryst rims towards groundmass cpx-microlites, suggests interaction with less evolved magma batches (e.g. Shimizu and Le Roex 1986; O'Brien et al. 1988), as in the RTF model of O'Hara and Mathews (1981). Therefore, the ocellar textures of some alkali basalts and trachybasalts reflecting local liquid immiscibility (e.g. Philpotts 1976; Shelley 1993) are also in accordance with mechanical interaction between magmas. This type of process is also reflected by the pegmatoid alkaline gabbroid segregations that occur in some basanitic rocks of southern Sierra de los Cóndores, as described by Escayola et al. (1998), bearing analogies with those reported in younger volcanic rocks of the Chaján locality by Galliski et al. (1996, 2004).

In summary, the available data suggest that the SCC magma evolution must have taken place at crustal level(s) from distinct parental melts, mainly through fractional crystallization in an open-system magma chamber, particularly involving local magma mixing with more primitive batches, besides some amount of crustal contamination.

Mantle Source

Some of the more magnesium-rich rocks of SCC can be considered primary magmas due to their high mg# values (>0.68) and Ni contents (>200 ppm), as it is shown in Table 2.6. Representative samples are the basanite G3 (mg# 0.74, Ni = 443 ppm), the alkali basalts such as EM4, MO1 and PM4 (mg# 0.75, 0.74 and 0.69; Ni = 464, 249 and 311 ppm, respectively) and the transitional basalts such as Li1 and CN14 (mg# 0.74 and 0.73, Ni = 366 and 314 ppm, respectively), as described by Lagorio (2003, 2008). The latter reveal primary magmas, in equilibrium with olivine from the mantle ($Fo_{89\text{-}90}$), also consistent with the presence of dunitic and/or spinel lherzolite xenoliths. $(La/Yb)_{cn}$ values are high (24–41), strongly supporting garnet in the peridotite residua, as stated by Kay and Ramos (1996) for magmas from Los Molinos and Almafuerte localities. These latter authors pointed out that some IE ratios (e.g. La/Ta, La/Ba) of rocks from those localities were characteristic of OIB magmas, also supported by the isotopic data. Therefore, they characterized a garnet-bearing OIB-like mantle source for magmas from Sierra Chica de Córdoba. Such a mantle source was after also outlined for magmas of Sierra de los Cóndores by Sánchez and Bermúdez (1997). Garnet in the mantle source was confirmed by the presence of garnet-bearing xenoliths in basanites from southern Sierra de los Cóndores pointed out by Escayola et al. (1998).

Lagorio (2003, 2008), considering geochemical data from the entire Sierra Chica, pointed out that low Al_2O_3 content (<15 %) together with high olivine (20–26 %) and variable nepheline (3–15 %) or low orthopyroxene (≤1) CIPW values suggest high depths of melting (Green 1970), notionally towards the garnet–spinel transition (about 26 kbar, near 100 km depth; Takahashi and Kushiro 1983).

On the other hand, thermobarometric studies in the garnet-bearing lherzolite xenoliths hosted in basanitic lavas from southern Sierra de los Cóndores allowed Escayola et al. (1998, 1999) to estimate depths of up to 160 km in the mantle for the generation of such magmas.

Furthermore, negative anomalies for K and Rb in multi-element diagrams (Fig. 2.18) are consistent with the presence of residual phlogopite in the source.

The melting degrees for the primary magma genesis were calculated by mass balance (Stormer and Nicholls 1978) using the major element compositions of an enriched peridotite. Calculations were carried out for both dry and hydrous (phlogopite) garnet peridotites (P1 and P2, respectively, Table 2.9).

Results indicate that similar degrees of melting are necessary to match the magma compositions of the basanite, the alkali and transitional basalts. Melting

Table 2.9 Anhydrous and hydrous peridotite mineral assemblages calculated (Stormer and Nicholls 1978) from chemical compositions of Ringwood (1966; P1 and P2) and calculated mineral assemblages of mantle residua after extraction of G3, EM4, MO1, PM4, Li1, and CN14 primary magmas

	P1	G3	EM4	MO1	PM4	Li1	CN14
	Initial	Resid.	Resid.	Resid.	Resid.	Resid.	Resid.
OL[a] (wt%)	54.88	58.40	59.52	60.51	59.54	61.25	62.04
OPX[b]	18.83	20.64	19.78	19.14	19.03	18.82	17.59
CPX[c]	11.14	8.64	8.66	8.63	9.38	8.51	9.25
GT[b]	15.14	12.32	12.05	11.72	12.05	11.42	11.12
$\sum res^2$	0.53	0.41	0.38	0.35	0.38	0.36	0.34
F (%)		6.38	7.19	7.39	5.84	8.20	7.91
	P2	G3	EM4	MO1	PM4	Li1	CN14
	Initial	Resid.	Resid.	Resid.	Resid.	Resid.	Resid.
OL[a] (wt%)	54.49	57.51	58.66	59.00	58.48	59.63	60.26
OPX[b]	18.12	19.71	19.00	18.59	18.37	18.28	17.36
CPX[c]	11.37	9.23	9.13	9.34	9.84	9.23	9.80
GT[b]	13.16	10.92	10.50	11.13	10.80	10.68	10.60
PHL[d]	2.86	2.64	2.70	1.94	2.50	2.19	1.97
$\sum res^b$	0.40	0.31	0.28	0.30	0.30	0.30	0.29
F (%)		5.48	6.47	5.84	4.99	6.61	6.35

Mantle mineral compositions: *OL* olivine, *OPX* orthopyroxene, *CPX* clinopyroxene, *GT* garnet, *PHL* phlogopite, according to: [a]De Min (1993), [b]MacGregor (1974), [c]Bristow (1984), [d]Wilkinson and Le Maitre (1987). $\sum res^2$ sum of squares of major element residuals; *F* melting degree; *resid.* residua

degrees are between 6–8 % and 5–7 % for dry and hydrous sources, respectively (Table 2.9). It is clear that if the modelling is performed from a peridotite less enriched in incompatible elements, percentages of melting do not exceed 2 %. In fact, it should be noted that, previously, Kay and Ramos (1996) obtained degrees of melting <2 % from the magmas represented by the analcimites of Los Molinos.

Incompatible trace elements (IE) in the peridotitic sources were calculated, assuming batch melting (Hanson 1978) from pyrolite composition, considering the partition coefficients used by Comin-Chiaramonti et al. (1997) and the calculated melting degrees and solid residua (Table 2.9). As K- and Rb-negative spikes of the primary magmas IE- patterns support phlogopite as a residual phase in the mantle (Fig. 2.20), a hydrous source was therefore preferred.

The IE contents in the initial sources were calculated from the primary basanite, alkali and transitional basalts and plotted in multi-elemental diagrams (Fig. 2.20). Their enrichment relative to the primitive mantle of Sun and McDonough (1989) may be up to 10–20 times (e.g. for Ba and K).

In summary, our calculations indicate that the slight compositional features and differences concerning basanite, alkaline and transitional suite primary melts mainly reflect heterogeneous lithospheric mantle sources.

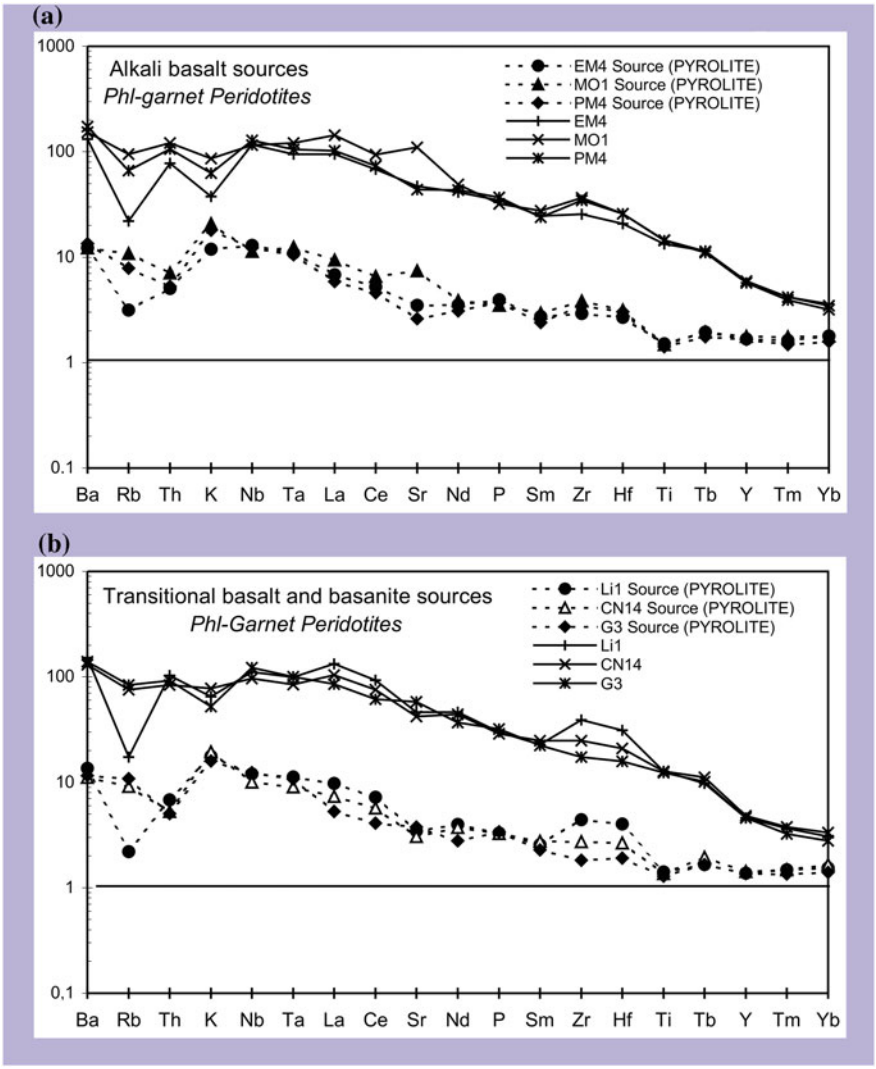

Fig. 2.20 Multi-elemental plots of calculated (batch melting; Hanson 1978) mantle sources, normalized to primordial mantle (PM) of Sun and McDonough (1989) for distinct primary magmas of Sierra Chica de Córdoba, starting from an enriched peridotite (pyrolite; Ringwood 1966), as shown in Lagorio (2008). **a** Garnet phlogopite mantle sources of primary alkali basalts and **b** garnet phlogopite mantle sources of primary transitional basalts and basanite. Each figure also includes multi-element plots for the respective primary magmas

2.1.1.8 Comparison with Alkaline Volcanism Around Paraná Basin

Distinction in high- and low-Ti types of Paraná (Bellieni et al. 1984) and Gondwana (Cox 1988) basalts was also adopted by Gibson et al. (1996) to discriminate the

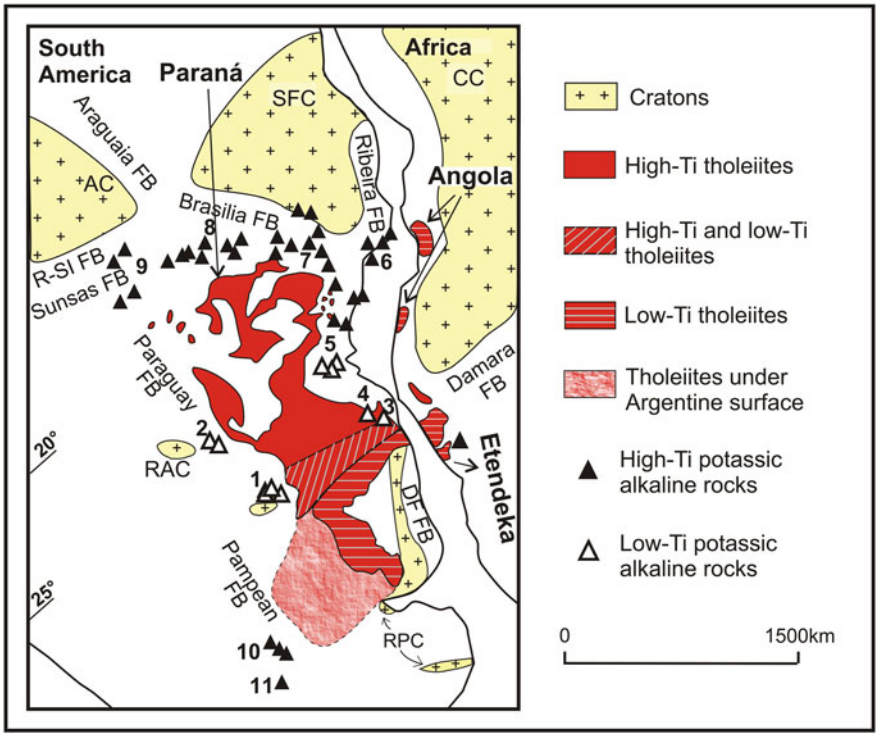

Fig. 2.21 Location of Sierra Chica of Córdoba (SCC) relative to other high-Ti and low-Ti mafic potassic rocks and continental flood basalts across western and central Gondwana, modified from Piccirillo and Melfi (1988), Gibson et al. (1996), Marzoli et al. (1999) and Lagorio (2008). *AC* Amazonian craton, *SFC* San Francisco craton, *CC* Congo craton, *RAC* Río Apa craton, *RPC* Río de La Plata craton; *FB* fold belt, *DF FB* Dom Feliciano fold belt, *R-SI FB* Rondonia-San Ignacio fold belt, *1* eastern Paraguay, *2* Amambay, *3* Anitápolis, *4* Lages, *5* Ponta Grossa, *6* Serra do Mar, *7* Alto Paranaíba Igneous Province, *8* Goiás Alkaline Province, *9* Poxoréu, *10* Sierra Chica of Córdoba, *11* Chaján

mafic potassic rocks related to Paraná basin (Figs. 2.21). Low-Ti potassic alkaline rocks outcrop along the western (e.g. eastern Paraguay, Amambay) and eastern (e.g. Lages, Anitápolis, Ponta Grossa) borders of the central sector of the Paraná basin (Fig. 2.21). Instead, the high-Ti types are located in the northern and eastern margins of the northern part of the basin (e.g. Alto Paranaíba, Goiás, Serra do Mar; Fig. 2.21). The potassic rocks of Sierra Chica of Córdoba (SCC) are of high Ti and are located in the south-western edge of the Paraná basin (in fact, the Chaco-Paraná basin; Figs. 1.1a, b and 2.21), as pointed out by Lagorio (2008). Similarly, Late Cretaceous rocks from the locality of Chaján (southern Córdoba) are also potassic as well as high Ti and have a peripheral location with respect to the tholeiitic volcanic flows of Paraná, though they are slightly more distant, about 150 km south-west of the Sierra Chica (Figs. 1.1a and 2.21).

As it is well-known from the literature, low- and high-Ti potassic rocks around the Paraná basin greatly differ in terms of K, Nb, Ta and La relationships, as pointed out by several authors. The low-Ti rocks have IE patterns with negative spikes (e.g. eastern Paraguay; La/Nb_{PM} higher than 1.6, e.g. Comin-Chiaramonti et al. 1997, 2013), whereas the high-Ti ones do not reveal any distinct Nb-Ta anomaly, or may even show a slight positive spike (e.g. Alto Paranaíba; Gibson et al. 1995).

Comparison of the most primitive magmas of Sierra Chica of Córdoba (SCC) shows similar patterns to those from the Alto Paranaíba igneous province (APIP) and Goias alkaline province (GAP), as well as the ones from the locality of Chaján (Fig. 2.22a). However, rocks from APIP have higher contents of LIL and LRE elements, and also La/Yb ratios (normalized relations up to 155), according to the ultrapotassic nature that characterizes that province (Gibson et al. 1995, Carlson et al. 1996, 2007). By contrast, low-Ti rocks (e.g. eastern Paraguay, Anitápolis) have patterns distinctively characterized by a negative anomaly for Nb–Ta (Fig. 2.22b). According to Comin-Chiaramonti et al. (1997, 2013), these compositional differences might reflect different IE enrichments, therefore metasomatic events, that have occurred in Early–Middle Proterozoic (low Ti: 2.0 to 1.5 Ga) and Late Proterozoic (high-Ti: 1.0 to 0.5 Ga), respectively, from Nd model ages presented by diverse authors. Gibson et al. (1996) also pointed out that the low-Ti magmas are associated with the cratonic regions, while the high-Ti ones are located in Proterozoic mobile belts.

On the other hand, the initial isotopic ratios of Sr and Nd samples from the Sierra Chica of Córdoba presented by Kay and Ramos (1996) and Lucassen et al. (2002) are plotted next to the composition of enriched mantle I (EMI), as well as the high-Ti alkaline localities APIP and GAP (Fig. 2.23). The same is observed for the Chaján rocks, as shown in the figure, from data presented by Lucassen et al. (2002). These authors, on the basis of Pb isotopes characterized an enriched mantle, similar to the ancient mantle located beneath the Brazilian shield, but with distinguishing characteristics between Sierra de los Cóndores (southern Sierra Chica) and Chaján, as the high $^{208}Pb/^{204}Pb$ ratios of rocks from the former are clearly more similar to those of the alkaline provinces of Paraná. Lucassen et al. (2002) also pointed out the significant isotopic difference between the source of the magmas of Córdoba and that of the Salta Group (northern Argentina; Fig. 2.22a). The latter volcanism is mainly sodic and of Late Cretaceous age; its source is clearly depleted, as it has been previously reported by Kay and Ramos (1996) from Sr and Nd isotopic data. Morover, Lucassen et al. (2007) reinforced this evidence, also for most of the Cretaceous alkaline mafic intra-plate rocks along the back arc of the Central Andes, as they were derived from a depleted lithospheric mantle according to a complete isotopic study.

The new $^{40}Ar/^{39}Ar$ dating of SCC of 129.6 ± 1.0 Ma is in agreement with geochronological data obtained so far (see Table 2.1), indicating that this volcanism is Early Cretaceous in age and slightly posthumous to the large tholeiitic event of PMP.

In relation to the age of other potassic localities around the Paraná basin, as central–eastern Paraguay and Anitápolis (Brazil), a comparison must be performed

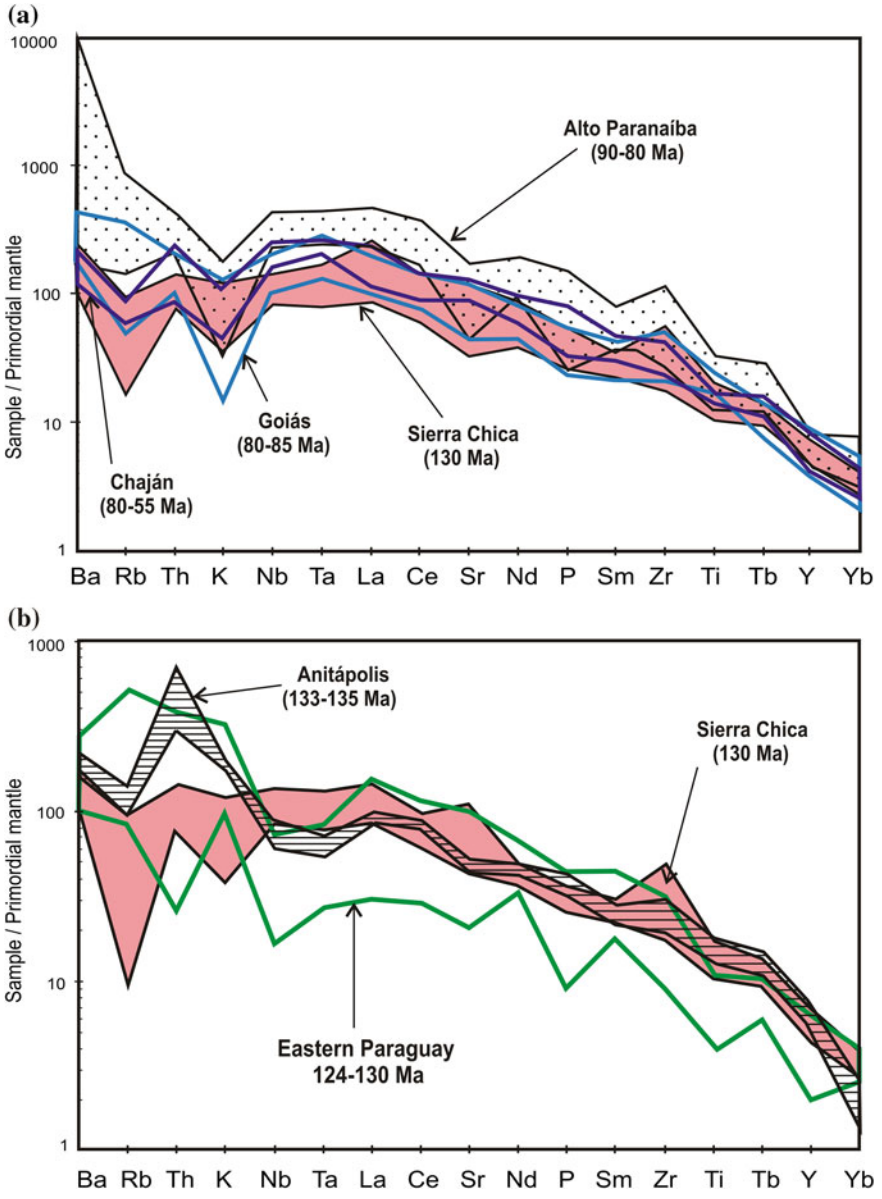

Fig. 2.22 Primordial mantle (Sun and McDonough 1989) normalized multi-element plots for the most primitive rocks (mg# 0.68–0.75) of Sierra Chica of Córdoba in comparison with: **a** high-Ti mafic potassic rocks of Alto Paranaíba and Goiás Provinces from Brazil (Gibson et al. 1995, 2006; Carlson et al. 1996, 2007) and Chaján locality (Córdoba, Argentina; Viramonte et al. 1994; Galliski et al. 1996; Quenardelle and Montenegro 1998) and **b** low-Ti less evolved potassic rocks of eastern Paraguay (Comin-Chiaramonti et al. 1997, 2007, 2013) and Anitápolis (Brazil; Comin-Chiaramonti et al. 1999). Modified from Lagorio (2008) and Lagorio et al. (2014)

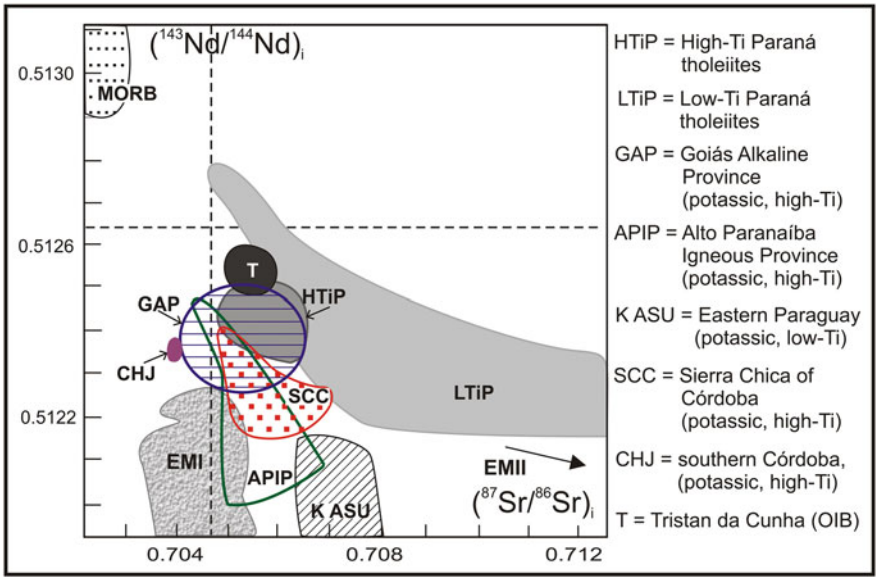

Fig. 2.23 Initial $^{87}Sr/^{86}Sr$ versus $^{143}Nd/^{144}Nd$ of the alkaline volcanic rocks of Sierra Chica of Córdoba (SCC; data: Kay and Ramos 1996; Lucassen et al. 2002) compared to other alkaline potassic localities, as Chaján (CHJ; data: Lucassen et al. 2002) and others peripheral to the Paraná Magmatic Province (PMP), as the Alto Paranaíba Igneous Province (APIP; Gibson et al. 1995; Carlson et al. 1996, 2007), Goiás Alkaline Province (GAP; Carlson et al. 1996, 2007) and eastern Paraguay (K ASU; Comin-Chiaramonti et al. 1997, 2007), together with those of high-Ti and low-Ti tholeiites from Paraná Magmatic Province (PMP; data: Piccirillo and Melfi 1988; Peate and Hawkesworth 1996; Peate 1997), Tristan da Cunha (TC; data: le Roex et al. 1990), MORB, EMI and EMII of Zindler and Hart (1986). Based on Lagorio et al. (2014)

taking into account the latest data given by diverse authors. For eastern Paraguay, weighted mean, $^{40}Ar/^{39}Ar$ dating on phlogopite is 127.56 ± 0.45 Ma, from samples that gave the best spectra according to Gibson et al. (2006); using the new age standard of Kuiper et al. (2008) the date is 128.39 Ma. Otherwise, $^{40}Ar/^{39}Ar$ dating performed by other authors span from 129.0 ± 2 Ma to 123.6 ± 0.5 Ma (Comin-Chiaramonti et al. 2007), and after applying the above-mentioned standard, they range between 129.8 and 124.4 Ma. On the other hand, Anitápolis yielded an age between 135 and 132 Ma, according to Gibson et al. (2006) with Kuiper´s recalculation of (2008). Therefore, SCC volcanic event is partially coeval with respect to eastern Paraguay one and younger than that of Anitápolis, beyond that all of them are Early Cretaceous in age.

By contrast, SCC volcanism is older than high-Ti potassic localities in Brazil (e.g. Alto Paranaíba, Goiás and Serra do Mar), as the latter are of Late Cretaceous/Palaeogene age according to diverse authors (e.g. Gibson et al. 1995, Carlson et al. 2007). Likewise, rocks from Chaján and Estancia Guasta (Figs. 1.1a and 2.21, Córdoba Province, Argentina) were formed contemporaneously with

those of the Brazilian localities, taken into account ages provided by other authors (e.g. Valencio et al. 1980; Gordillo et al. 1983), and all of them are clearly posthumous with respect to the Paraná Magmatic Province.

SCC volcanism, as other alkaline localities from SE Brazil, is located over a mobile belt; in this case, the Pampean belt, coeval with Brazilian orogens (e.g. Paraguay and Araguaia fold belts), considered as Late Proterozoic–Early Cambrian (e.g. Escayola et al. 2007) or Early–Mid-Cambrian in age (e.g. Rapela et al. 2007, 2011, Thover et al. 2010; Casquet et al. 2012), whereas the APIP and GAP volcanism are placed on the Brasilia mobile belt. It should be noted that subduction-related granitoids outcrop north of the Sierra Chica (in Sierra Norte of Córdoba; Lira et al. 2014), with ages of 537 ± 4 Ma and 530 ± 4 Ma (Iannizzotto et al. 2013); they are associated with Cambrian to Ordovician volcanic and subvolcanic bodies of calc-alkaline nature (O´Leary et al. 2014). Nevertheless, the volcanic rocks of SCC do not reveal chemical parameters that can be easily related to slab-derived mantle metasomatism, as the lack of a negative Nb-Ta anomaly, low La/Nb (0.6–1.2) and Ba/Nb (9–13) ratios, La/Ta < 25 and Ba/La < 20, as in rocks from high-Ti localities of Brazil. Therefore, this ancient subduction must have not contaminated the source of the magmas of SCC; precisely Nd model ages obtained by Lucassen et al. (2002) vary between 1.22 and 0.96 Ga, suggesting a reactivation of lithospheric mantle modified during Mesoproterozoic times. While the age of metasomatism in the lithospheric mantle of APIP and GAP is not exactly defined, isotopic data allowed to infer that it must have taken place during the configuration of the Brasilia mobile belt in the Middle to Late Proterozoic (Carlson et al. 2007). Therefore, the metasomatic events affecting the mantle sources of SCC, GAP and APIP seem to have been at least partially coeval.

Geochemical features reflect small-scale heterogeneity of SCC lithospheric mantle source (Lagorio 2008). This might be more related to metasomatic events involving volatile-rich small-volume melts from the asthenosphere, as indicated by the occurrence of trapped primary CO_2 inclusions and bleb-like glass in olivines from spinel peridotite nodules sampled by SCC alkali basalts (Lagorio and Montenegro 2004). Also, the study of garnet-bearing mantle xenoliths from southern Sierra de los Cóndores let Escayola et al. (1998, 1999) describe metasomatic processes in the lithospheric mantle, which is in agreement with most of the reports from the peripheral localities around Paraná basin (e.g. Gibson et al. 1995, 2006; Comin-Chiaramonti et al. 1997, 2007, 2013).

2.1.2 Early Cretaceous in the Levalle Basin of Córdoba Province

In southern Córdoba Province, there are other Lower Cretaceous rift deposits that belong to the Levalle basin (Fig. 2.2a), though they are presently buried. This basin

is probably composed of three megasequences according to geophysical information and a well that was drilled to test its petroleum potential (Webster et al. 2004; Chebli et al. 2005). In its lower sequence, no lavas are interbedded with sedimentary deposits, and it is covered by a series of basalt flows and sills over 800 m thick with some thin beds of reddish-brown sandstone and claystone interbedded that constitute the intermediate sequence. The basalts have the typical characteristics of alkali–olivine basalts, commonly found in rift basins. Cuttings were dated by the K–Ar method and yielded 110 ± 6 Ma, indicating that the basalts were emplaced during Aptian times. Their composition closely resembles the rift-related basalts of Sierra Chica rather than those of the Paraná Magmatic Province (Webster et al. 2004; Chebli et al. 2005). In the sedimentary, lower section at least ten sills were drilled. These black intrusive rocks are mostly of basaltic nature, and their absolute K–Ar dating is widely divergent (Denison 1996 in Chebli et al. 2005) with an average of 103.3 Ma. Nevertheless, a dating obtained in a microdioritic sill was 147 ± 7 Ma (Oxfordian/Kimmeridgian times). It should be noted that this is significantly older than the K/Ar age of 110 Ma of the basalts overlying this lower sequence, and it is also difficult to reconcile with reliable biostratigraphic data recovered from this part of the column (Calegari et al. 2014). The most logical explanation is that an excess of radiogenic argon must have caused such an old age. It is worthy to note that perhaps the Levalle basin is buried because it is further south-east to Nazca flat slab (see Fig. 1 of Giménez et al. 2011) and, therefore, it was not seriously affected by Tertiary tectonics. As a consequence, rocks of the diverse sequences were not eroded. Despite having only one well that was drilled, it was possible to evaluate the huge thickness of about 800 m of volcanic rocks that form the intermediate sequence filling this basin.

2.2 Early Cretaceous in San Luis Province

To the west, in Sierra de las Quijadas and Cerrillada de las Cabras (Figs. 2.1 and 2.2a), Province of San Luis, Cretaceous basaltic rocks are recognized as lava flows and dykes interbedded with a sedimentary sequence that belong to the Las Salinas depocenter of the Western System Rift (Fig. 2.2a), and are comparable to those outcropping in Sierra Chica de Córdoba (Gordillo 1972; Costa et al. 2001). Available K–Ar dating indicates that ages range between 165 ± 3 Ma and 101 ± Ma (González 1971; Yrigoyen 1975; INGEIS 1977; Linares and González 1990). Their geochemical features are similar to those of the basalts of Córdoba, particularly to those of El Pungo locality (Martínez et al. 2012). Anyway, comparison between samples of Sierra Chica and those presented by Martínez et al. (2012) reveals lower contents in all the REE for the latter, particularly in the rock from Sierra de las Quijadas (Fig. 2.24a). In the same way, the multi-elemental diagram shows lower contents of Th, Nb, Ta and P, also specially in that sample (Fig. 2.24b), that lets infer differences in their respective mantle sources.

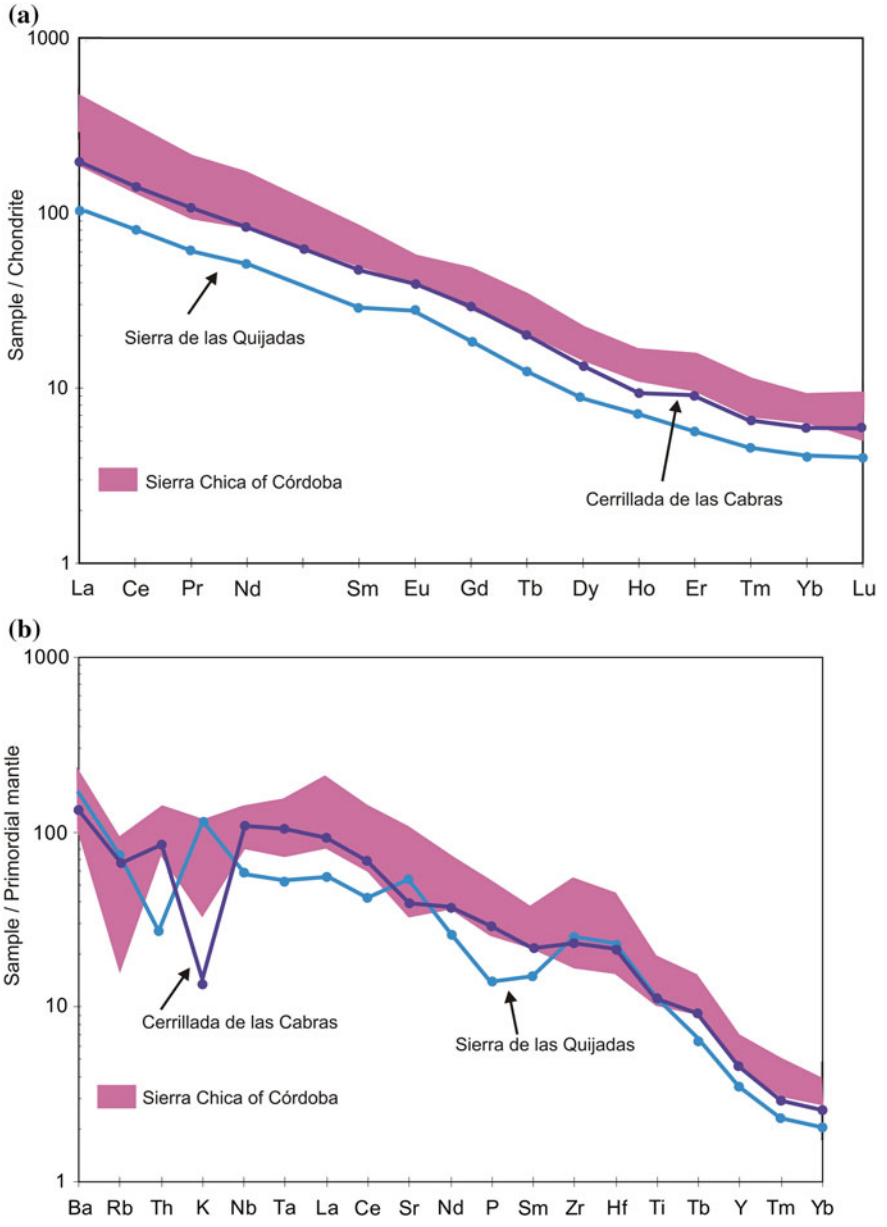

Fig. 2.24 **a** Chondrite-normalized (Boynton 1984) REE diagram for rocks of Sierra Chica of Córdoba (Lagorio 2008) in comparison with samples of Sierra de las Quijadas and Cerrillada de las Cabras from San Luis Province (Martínez et al. 2012). **b** Primordial mantle (Sun and McDonouth 1989) normalized multi-elemental plots for both groups of rocks, according those authors respectively

2.3 Probable Early Cretaceous Rocks in La Pampa and Buenos Aires Provinces

Further south, between the basins of Macachín–Quehué (Fig. 2.2a) and Colorado (La Pampa and Buenos Aires provinces; Fig. 2.2a), few and small outcrops of basalts were recognized by Silva Nieto et al. (2014). Their petrographic features seem to be more consistent with a subalkaline nature, instead of the alkaline one that characterizes volcanism in rifts of both Central and Western Systems. Nevertheless, geochemical data and radiometric ages are necessary for a better understanding of these volcanic rocks.

In the same way, basaltic levels have been reported (e.g. Raggio et al. 2012) in the subsurface of the aulacogenic Salado basin (Fig. 1.1b). Both geochemical and geochronological data are needed to characterize these rocks in the context of Gondwana break-up and the opening of the South Atlantic Ocean.

References

Ancheta MD, Sánchez ML, Marclé R (2002) Petrografía y geoquímica de las volcanitas de la Formación El Saucecito (Cretácico Inferior), Córdoba, Argentina. 15° Congreso Geológico Argentino, Actas, El Calafate, vol 2, pp 158–163

Astini RA, del Valle Oviedo N (2014) Cubierta sedimentaria mesozoica. In: Martino RD, Guereschi AB (eds) Geología y Recursos Naturales de la Provincia de Córdoba, Relatorio del 19º Congreso Geológico Argentino. Asociación Geológica Argentina, Córdoba, pp 435–472

Astini RA, Pezzi LI, Massei GA (1993) Paleogeografía y paleoambientes del Cretácico de la sierra de Pajarillo-Copacabana-Masa, noroeste de Córdoba. 12° Congreso Geológico Argentino, Actas, Mendoza, vol 1, pp 107–176

Bain Larrahona HG (1940) Estudios geológicos en la provincia de Córdoba. Boletín de Informaciones Petroleras. YPF, 192 p

Bellieni G, Piccirillo EM, Zanettin B (1981) Classification and nomenclature of basalts. IUGS, Subcommission of the Systematics of Igneous Rocks, Circular 34. Contrib Miner Petrol 87:1–19

Bellieni G, Comin-Chiaramonti P, Marques LS, Melfi AJ, Piccirillo EM, Nardy AJ, Roisemberg A (1984) High- and low-TiO_2 flood basalts from the Paraná plateau (Brasil): petrology and geochemical aspects bearing on their mantle origin. Neues Jahrb Mineral Abh 150:273–306

Bodenbender G (1907) Contribución al conocimiento geológico de la República Argentina. Anales del Ministerio de Agricultura y Secretaría de Geología, Mineralogía y Minería, Buenos Aires, vol 2(3), pp 1–35

Bodenbender G (1929) Triásico y Terciario de la falda oriental de las Sierras de Córdoba. Bol Acad Nac Cienc Córdoba 31:73–139

Boynton WV (1984) Cosmochemistry of the rare earth elements: meteorite studies. In: Henderson P (ed) Rare Earth element geochemistry. Elsevier, Amsterdam, pp 63–114

Bristow, JK (1984) Picritic rocks of the North Lebombo and South-East Zimbabwe. Geological Society of South-Africa Special Publication 13:105–123

Busby-Spera CJ, White JDL (1987) Variation in peperite textures associated with differing host-sediment properties. Bull Volc 49:765–775

Calegari RJ, Chebli G, Manoni RS, Lázzari V (2014) Las cuencas cretácicas de la región central del país: General Levalle. In: Martino RD, Guereschi AB (eds) Geología y Recursos Naturales

de la Provincia de Córdoba, Relatorio del 19º Congreso Geológico Argentino. Asociación Geológica Argentina, Córdoba, 913–938

Caminos R, González P (1996) Mapa Geológico de la República Argentina. Escala 1:5.000.000. Dirección Nacional del Servicio Geológico. Secretaría de Minería de la Nación. Buenos Aires

Carlson RW, Esperança S, Svisero DP (1996) Chemical and Os isotopic study of Cretaceous potassic rocks from Southern Brazil. Contrib Miner Petrol 125:393–405

Carlson RW, Araujo ALN, Junqueira-Brod TC, Gasparf JC, Brod JA, Petrinovic IA, Hollanda MH, Pimentel MM, Sichel S (2007) Chemical and Isotopic relationships between peridotite xenoliths and magic-ultrapotassic rocks from Southern Brazil. Chem Geol 242:415–434

Carmichael ISE (1967) The iron-titanium oxides of salic volcanic rocks and their associated ferromagnesian silicates. Contrib Miner Petrol 14:36–63

Caroff M, Maury RC, Leterrier J, Joron JL, Cotten J, Guille G (1993) Trace element behaviour in the alkali basalt-comenditic trachyte series from Mururoa Atoll, French Polynesia. Lithos 30:1–22

Casquet C, Rapela CW, Pankhurst RJ, Baldo EG, Galindo C, Fanning CM, Dahlquist JA, Saavedra J (2012) A history of Proterozoic s in southern South America: from Rodinia to Gondwana. Geosci Front 3(2):137–145

Cejudo Ruiz R, Goguitchaivili A, Geuna SE, Alva-Valdivia L, Solé J, Morales J (2006) Early Cretaceous absolute geomagnetic paleointensities from Córdoba province (Argentina). Earth Planets Space 58(10):1333–1339

Chebli GA, Spalletti LA, Rivarola D, de Elorriaga E, Webster R (2005) Cuencas Cretácicas de la Región Central de la Argentina. Frontera Exploratoria de la Argentina. In: Chebli GA, Coriñas JS, Spalletti LA, Legarreta L, Vallejo EL (eds) 6º Congreso de Exploración y Desarrollo de Hidrocarburos, IAPG, Buenos Aires, pp 193–215

Comin-Chiaramonti P, Cundari A, Piccirillo EM, Gomes CB, Castorina F, Censi P, De Min A, Marzoli A, Speziale S, Velázquez VF (1997) Potassic and sodic igneous rocks from Eastern Paraguay: their origin from the lithospheric mantle and genetic relationships with the associated Paraná flood tholeiites. J Petrol 38:495–528

Comin-Chiaramonti P, Cundari A, DeGraff JM, Gomes CB and Piccirillo EM (1999) Early Cretaceous-Tertiary magmatism in Eastern Paraguay (western Paraná basin): geological, geophysical and geochemical relationships. J Geodyn 28:375–391

Comin-Chiaramonti P, Marzoli A, Gomes CB, Milan A, Riccomini C, Velásquez VF, Mantovani MSM, Renne P, Tassinari CCG, Vasconcelos PM (2007) Origin of Post-Paleozoic magmatism in Eastern Paraguay. In: Foulguer GR, Jurdy DM (eds) Plates, plumes, and planetary processes. Geological Society of America Special Papers, Boulder, Colorado, vol 430, pp 603–633

Comin-Chiaramonti P, De Min A, Cundari A, Girardi VAV, Ernesto M, Gomes CB, Riccomini C (2013) Magmatism in the Asunción-Sapucai-Villarrica Graben (Eastern Paraguay) Revisited: petrological, geophysical, geochemical and geodynamic inferences. Hindawi Publishing Corporation. J Geol Res 2013, Article ID 590835, 22 pp. 10.1155/2013/590835

Cortelezzi CR, Traversa L, Paulicevic PE (1981) Estudio petrológico y ensayos físicos de las rocas alcalinas del sur de las provincias de Córdoba y San Luis. 8° Congreso Geológico Argentino, Actas, San Luis, vol 4, pp 885–901

Costa CH, Gardini CE, Chiesa JO, Ortiz Suárez AE, Ojeda GE, Rivarola DL, Tognelli GC, Strasser EN, Carugno Durán AO, Morla PN, Guerstein PG, Sales DA, Vinciguerra HM (2001) Hoja Geológica 3366-III, San Luis. Provincias de San Luis y Mendoza, vol 293. Instituto de Geología y Recursos Minerales, Servicio Geológico Minero Argentino, Boletín, Buenos Aires, 67 p

Cox KG (1988) The Karoo province. In: MacDougall JD (ed) Continental flood basalts. Kluwer Academic, Dordrecht, pp 239–271

Cundari A, Ferguson AK (1982) Significance of the pyroxene chemistry from leucite bearing and related assemblages. Tschermaks Mineralogische und Petrographische Mitteilungen 30:189–204

Cundari A, Comin-Chiaramonti P (1996) Mineral chemistry of alkaline rocks from the Asunción–Sapukai graben (central-eastern Paraguay). In: Comin-Chiaramonti P, Gomes CB (eds.) Alkaline magmatism in central-eastern Paraguay. Relationships with coeval magmatism in Brazil. Edusp/Fapesp, São Paulo, pp 181–194

De la Roche H, Leterrier P, Grandclaude P, Marchal M (1980) A classification of volcanic and plutonic rocks using R1-R2 diagram and major element analysis. Its relationships with current nomenclature. Chem Geol 29:183–210

De Min A (1993) Il magmatismo mesozoico K-alcalino del Paraguay Oriental: aspetti petrogenetici ed implicanze geodinamiche. Unpublished doctoral thesis, Universitá di Trieste, Trieste, 242 p

De Paolo DJ (1981) Trace elements and isotopic effects of combined wallrock assimilation and fractional crystallization. Earth Planet Sci Lett 43:201–211

Deer WA, Howie RA, Zussman J (1992) An introduction to the rock-forming minerals. Longman Scientific and Technical, Essex, 696 p

Delpino D, Sánchez ML, Bermúdez A, Marclé R, Ancheta D (1999) Los depósitos hidroclásticos y estrombolianos del Grupo El Pungo, Córdoba. 14° Congreso Geológico Argentino, Actas, Salta, vol 2, pp 197–199

Escayola MP, Viramonte JG, Becchio R, Franz G, Arnosio M, Popridkin MC (1998) Xenolitos en volcanitas alcalinas cretácicas del sector sur de la Sierra de Los Cóndores, Sierras Pampeanas de Córdoba, Argentina. 10º Congreso Latinoamericano de Geología y 6° Congreso Nacional de Geología Económica, Actas, Buenos Aires, vol 2, pp 354–358

Escayola MP, Franz G, Becchio R, Viramonte JG, Lucassen F (1999) Naturaleza y evolución de la litósfera subcontinental durante el rifting Cretácico en las Sierras Pampeanas de Córdoba, Argentina. 14° Congreso Geológico Argentino, Actas, Salta, vol 2, pp 200–203

Escayola MP, Pimentel MM, Armstrong R (2007) Neoproterozoic backarc basin: Sensitive high-resolution ion microprobe U-Pb and Sm-Nd isotopic evidence from the Eastern Pampean Ranges, Argentina. Geology 35(6):495–498

Ferreira Pittau ML, Escayola MP, Garrido A, (2008) Ciclos eruptivos del Grupo Sierra de los Cóndores (Sierra Chica de Córdoba): Nuevas características petrológicas y evolutivas. 17º Congreso Geológico Argentino, Actas, vol 3, pp 1347–1348

Ferreira L, Escayola MP, Viramonte JG, Franz G (1999) Secuencias volcano-sedimentarias del complejo volcánico Los Cóndores, Córdoba: litoestratigrafía y mecanismos eruptivos. 14° Congreso Geológico Argentino, Actas, Salta, vol 2, pp 204–206

Galliski MA, Dorais M, Lira R (1996) Las pegmatitas ijolíticas de La Madera, provincia de Córdoba: Quimismo de sus minerales y model genético. 13º Congreso Geológico Argentino y 3º Congreso de Exploración de Hidrocarburos, Actas, vol 3, pp 207–225.

Galliski MA, Lira R, Dorais MJ (2004) Low-pressure differentiation of melanephelinitic magma and the origin of ijolite pegmatites at La Madera, Córdoba, Argentina. The Canadian Mineralogist 42(6):1799–1823

Geuna S (1997) Geología y paleomagnetismo de unidades cretácicas de la provincia de Córdoba. Unpublished doctoral thesis, Universidad Nacional de Córdoba, Córdoba, 263 p

Geuna SE (1998) Paleomagnetismo del Grupo Sierra de Los Cóndores (Cretácico Inferior de Córdoba): correlación magnetoestratigráfica local, y sus consecuencias en la interpretación geológica. Rev Asoc Geol Argentina 53(1):69–82

Geuna SE, Vizán H (1998) New Early Cretaceous palaeomagnetic pole from Córdoba Province (Argentina): revision of previous studies and implications for the South American database. Geophys J Int 135:1085–1100

Geuna SE, Escosteguy LD, Miró R, Candiani JC, Gaido MF (2008) La susceptibilidad magnética del Batolito de Achala (Devónico, Sierra Grande de Córdoba) y sus diferencias con otros granitos achalianos. Rev Asoc Geol Argentina 63(3):380–394

Geuna SE, Lagorio SL, Vizan H (2015) Oxidation processes and their effects on the magnetic remanence of Early Cretaceous subaerial basalts from Sierra Chica de Córdoba, Argentina. In: Ort MH, Porreca M, Geissman JW (eds) The use of palaeomagnetism and rock magnetism to

understand volcanic processes, vol 396. Geological Society Special Publication, London, pp 239–263
Gibson SA, Thompson RN, Leonardos OH, Dickin AP, Mitchell JG (1995) The late cretaceous impact of the Trinidade mantle plume: evidence from large-volume, mafic, potassic magmatism in SE Brasil. J Petrol 36:189–229
Gibson SA, Thompson RN, Dickin AP, Leonardos OH (1996) Erratum to "High-Ti and low-Ti mafic potassic magmas: key to plume-litosphere interactions and continental flood-basalt genesis". Earth Planet Sci Lett 141:325–341
Gibson SA, Thompson RN, Day JA (2006) Timescales and mechanism of plume lithosphere interactions: $^{40}Ar/^{39}Ar$ geochronology and geochemistry of alkaline igneous rocks from the Paraná-Etendeka large igneous province. Earth Planet Sci Lett 251:1–17
Giménez ME, Dávila F, Astini R, Martínez P (2011) Interpretación gravimétrica y estructura cortical en la Cuenca de General Levalle, Provincia de Córdoba, Argentina. Rev Mex Cienc Geol 28(1):105–117
González RR (1971) Edades radimétricas de algunos cuerpos eruptivos de la República Argentina. Rev Asoc Geol Argentina 26(3):411–412
González RR, Kawashita K (1972) Edades potasio-argón de rocas básicas de la provincia de Córdoba. Rev Asoc Geol Argentina 27:259–260
Gordillo CE (1972) Petrografía y composición química de los basaltos de la sierra de Las Quijadas – San Luis – y sus relaciones con los basaltos cretácicos de Córdoba, vol 1(3–4). Boletín de la Asociación Geológica de Córdoba, Córdoba, pp 127–129
Gordillo CE, Lencinas A (1967a) Geología y petrología del extremo norte de la Sierra de Los Cóndores, Córdoba, vol 46(1). Boletín Academia Nacional de Ciencias, Córdoba, pp 73–108
Gordillo CE, Lencinas A (1967b) El basalto nefelínico de El Pungo, Córdoba, vol 46(1). Boletín Academia Nacional de Ciencias, Córdoba, pp 109–115
Gordillo CE, Lencinas A (1969) Perfil geológico de la sierra Chica de Córdoba en la zona del río Los Molinos, con especial referencia a los diques traquibasálticos que la atraviesan, vol 47. Boletín Academia Nacional de Ciencias, Córdoba, pp 27–50
Gordillo CE, Lencinas A (1980) Sierras Pampeanas de Córdoba y San Luis. In: Turner JCM (ed) 2º Simposio de Geologia Regional Argentina 1, Academia Nacional de Ciencias, Córdoba, pp 577–650
Gordillo CE, Linares E, Daziano C (1983) Nuevo afloramiento de nefelinita olivínica: Estancia Guasta, Sierras de Córdoba. Rev Asoc Geol Argentina 28 (3–4): 485–489
Green DH (1970) A review of experimental evidence on the origin of basaltic and nephelinitic magmas. Phys Earth Planet Inter 3:221–235
Hanson GN (1978) The application of trace elements to the petrogenesis of igneous rocks of granitic composition. Earth Planet Sci Lett 38:26–43
Iannizzotto NF, Rapela CW, Baldo EGA, Galindo C, Fanning CM, Pankhurst RJ (2013) The Sierra Norte-Ambargasta batholiths: late Ediacaran-Early Cambrian magmatism associated with Pampean transpressional tectonics. J S Am Earth Sci 42:127–143
INGEIS (1977) Nuevas constantes a utilizar en los métodos de datación radimétrica. Rev Asoc Geol Argentina 32:239–240
Kay SM, Ramos VA (1996) El magmatismo cretácico de las sierras de Córdoba y sus implicancias tectónicas. 13° Congreso Geológico Argentino y 3° Congreso de Exploración de Hidrocarburos, Actas, Buenos Aires, vol 3, pp 453–464
Kraemer PE, Escayola MP, Martino RD (1995) Hipótesis sobre la evolución tectónica neoproterozoica de las Sierras Pampeanas de Córdoba (30° 40′–32° 40′), Argentina. Rev Asoc Geol Argentina 50(1–4):47–59
Kuiper KF, Deino A, Hilgen FJ, Krijgsman W, Renne PR, Wijbrans JB (2008) Synchronizing rock clocks of Earth history. Science 320:500–504
Kull V, Methol E (1979) Descripción geológica de la Hoja 21i, Alta Gracia. Dirección Nacional de Geología y Minería. Boletín, Buenos Aires, vol 55, p 72

Lagorio SL (1998) Geoquímica y petrogénesis de volcanitas cretácicas de la sierra Chica de Córdoba (Argentina). 10° Congreso Latinoamericano de Geología y 6° Congreso Nacional de Geología Económica, Actas, Buenos Aires, vol 2, pp 314–320

Lagorio SL (2003) El volcanismo cretácico alcalino de la sierra Chica de Córdoba: geoquímica, petrogénesis e implicancias geodinámicas. Unpublished doctoral thesis, Universidad Nacional de Buenos Aires, Buenos Aires, 400 p

Lagorio SL (2008) Early Cretaceous alkaline volcanism of the Sierra Chica de Córdoba (Argentina): mineralogy, geochemistry and petrogenesis. J S Am Earth Sci 26:152–171

Lagorio SL, Montenegro TF (2004) Nódulos lherzolíticos espinélicos en basaltos alcalinos del norte de la sierra de los Cóndores (Córdoba). In: Brodtkorb M, Koukharsky M, Quenardelle S, Montenegro T (eds) Avances en Mineralogía, Metalogenia y Petrología 2004. Universidad de Buenos Aires y Universidad Nacional de Río Cuarto, pp 343–348

Lagorio SL, Geuna SE, Iacumin M, Vizán H (1997) Características geoquímicas del volcanismo cretácico del sector norte de la Sierra de Los Cóndores (Córdoba, Argentina). 8° Congreso Geológico Chileno, Actas, Antofagasta, vol 2, 1334–1338

Lagorio SL, Vizán H, Geuna SE (2014) El volcanismo alcalino cretácico. In: Martino RD, Guereschi AB (eds) Geología y Recursos Naturales de la Provincia de Córdoba, Relatorio del 19º Congreso Geológico Argentino. Asociación Geológica Argentina, Córdoba, pp 473–511

Le Bas MJ, Le Maitre RW, Strekeisen A, Zanetin B (1986) A chemical classification of volcanic rock based on the total alkali-silica diagram. J Petrol 27:745–750

le Roex AP (1985) Geochemistry, mineralogy and magmatic evolution of the basaltic and trachytic lavas form Gough Island, South Atlantic. J Petrol 26:149–186

le Roex A, Cliff RA, Adair BJL (1990) Trsitan da Cunha, South Atlantic: geochemistry and petrogeneis of a basanite-phonolite lavas series. J Petrol 31:779–812

Lencinas AN (1971) Geología del valle de Punilla entre Bialet Masse y La Cumbre, provincia de Córdoba, vol 1(2). Boletín Asociación Geológica de Córdoba, Córdoba, pp 61–70

Linares E, González R (1990) Catálogo de edades radimétricas de la República Argentina 1957–1987. Publicaciones especiales de la Asociación Geológica Argentina, Serie B, Didáctica y Complementaria, vol 19. Ascociación Geológica Argentina, Buenos Aires, 628 p

Linares E, Valencio DA (1974) Edades Potasio-Argón y paleomagnetismo de los diques traquibasálticos del río de Los Molinos, Córdoba, República Argentina. Rev Asoc Geol Argentina 29(3):341–348

Lira R, Sfragulla J (2014) El magmatismo devónico-carbonífero: El batolito de Achala y los plutones menores al norte del cerro Champaquí. In: Martino RD, Guereschi AB (eds) Geología y Recursos Naturales de la Provincia de Córdoba, Relatorio del 19º Congreso Geológico Argentino. Asociación Geológica Argentina, Córdoba, pp 293–347

Lira R, Poklepovic MF, O´Leary MS (2014) El magmatismo cámbrico en el batolito de Sierra Norte-Ambargasta. In: Martino RD, Guereschi AB (eds) Geología y Recursos Naturales de la Provinica de Córdoba, Relatorio del 19º Congreso Geológico Argentino. Asociación Geológica Argentina, Córdoba, pp 183–215

Lucassen F, Escayola MP, Romer RL, Viramonte JG, Koch K, Franz G (2002) Isotopic composition of Late Mesozoic basic and ultrabasic rocks from the Andes (23–32° S)—implications for the Andean mantle. Contrib Miner Petrol 143:336–349

Lucassen F, Franz G, Romer RL, Schultz F, Dulski P, Wemmer K (2007) Pre-Cenozoic intra-plate magmatism along the Central Andes (17–34ºS): Composition of the mantle at an active margin. Lithos 99: 312–338

Lucero Michaut NH, Gamkosian A, Jarsun B, Zamora E, Sigismondi M, Miró R, Caminos R (1995) Mapa Geológico de la Provincia de Córdoba. Secretaría de Minería, Dirección Nacional del Servicio Geológico

Martino R, Kraemer P, Escayola MP, Giambastiani M, Arnosio M (1995) Transecta de las Sierras Pampeanas de Córdoba a los 32° S. Rev Asoc Geol Argentina 50(1–4):60–77

Martino RD, Guereschi AB, Carignano CA, Calegari R, Manoni R (2014) La estructura de las cuencas extensionales cretácicas de las Sierras de Córdoba. In: Martino RD, Guereschi AB

(eds) Geología y Recursos Naturales de la Provincia de Córdoba, Relatorio del 19º Congreso Geológico Argentino. Asociación Geológica Argentina, Córdoba, pp 513–538

Marzoli A, Melluso L, Morra V, Renne PR, Sgrosso I, D'Antonio M, Duarte Morais L, Morais EAA, Ricci G (1999) Geochronology and petrology of Cretaceous basaltic magmatism in the Kwanza basin (western Angola), and relationships with the Paraná-Etendeka continental flood basalt province. J Geodyn 28:341–356

MacGregor ID (1974) The system $MgO–Al_2O_3–SiO_2$: solubility of Al2O3 in enstatite for spinel and garnet peridotite compositions. American Mineralogist 59:110–119

Mendía JE (1978) Paleomagnetic study of alkaline vulcanites from Almafuerte, province of Córdoba, Argentina. Geophys J Roy Astron Soc 54:539–546

Minudri CA, Sánchez ML (1994) Paleoambientes de sedimentación de la sección superior del Grupo Sierra de Los Cóndores (Cretácico Inferior), Córdoba, Argentina. 5° Reunión Argentina de Sedimentología, Actas, pp 29–34

Morimoto K, Fabries J, Ferguson AK, Ginzburg IV, Ross M, Seifert FA, Zussman J, Aoki K, Gottardi G (1988) Nomenclature of pyroxenes. Mineral Petrol 39:55–76

Nimis P (1995) A clinopyroxene geobarometer for basaltic systems based on crystal-structure modeling. Contrib Miner Petrol 121:115–125

Nimis P, Ulmer P (1998) Clinopyroxene geobarometry of magmatic rocks. Part 1: an expanded structural geobarometer for anhydrous and hydrous, basic and ultrabasic systems. Contrib Miner Petrol 133:122–135

O'Brien HE, Irving AI, McCallum IS (1988) Complex zoning and resorption of phenocrysts in mixed potassic mafic magmas of the Highwood Mountains, Montana. Am Mineral 73:1007–1024

O'Hara MJ, Mathews RE (1981) Geochemical evolution in an advancing, periodically replenished, periodically tapped, continuously fractionated magma chamber. J Geol Soc London 138:237–277

O´Leary MS, Lira R, Poklepovic MF (2014) Volcanismo y subvolcanismo del sector centro-oeste del batolito Sierra Norte-Ambargasta. In: Martino RD, Guereschi AB (eds) Geología y Recursos Naturales de la Provincia de Córdoba, Relatorio 19º Congreso Geológico Argentino. Asociación Geológica Argentina, Córdoba, pp 217-232

Oviedo N, Astini RA (2014) Depósitos volcanosedimentarios del Cretácico en Las Cumbres y vertiente oriental de la Sierra Chica, Córdoba, y redefinición de la Formación El Pungo. Rev Asoc Geol Argentina 71(4):472–483

Papike JJ, Cameron K, Baldwin K (1974) Amphiboles and pyroxenes: characterization of other than quadrilateral components and estimates of ferric iron from microprobe data. Bull Geol Soc Am 6:1053–1054

Pastore F (1930) Notas sobre Triasico y Terciario de la falda oriental de las Sierras de Cordoba. Relaciones morfológico-tectónicas. Rocas volcánicas del doctor Bodenbender. Anales de la Sociedad Cientifica Argentina 110:399–407

Peate DW (1997) The Paraná-Etendeka Province. In: Mahoney JJ, Coffin MF (eds) Large igneous provinces: continental oceanic and planetary flood volcanism, vol 100. Geophysical Monograph American Geophysical Union, Boulder, Colorado, pp 215–245

Peate DW, Hawkesworth CJ (1996) Lithospheric to asthenospheric transition in low-Ti flood basalts from Southern Paraná, Brazil. Chem Geol 127:1–24

Pensa M (1957) Contribución al conocimiento de los meláfiros en las sierras de Córdoba. Representación cartográfica y perfiles. Relaciones morfológicas, tectónicas y correlación con las diversas efusiones en el país. Revista Universidad Nacional de Córdoba, Facultad de Ciencias Exactas, Físicas y Naturales, vol 19(3–4), pp 471–500

Philpotts AR (1976) Silicate liquid immiscibility: its probable extent and petrogenetic significance. Am J Sci 276:1147–1177

Piccirillo EM, Melfi AJ (1988) The Mesozoic Flood Volcanism from the Paraná Basin (Brazil): petrogenetic and geophysical aspects. Universidad de São Paulo, San Pablo, 600 p

Piovano EL (1994) Facies de mantos de crecida y cauces efímeros en la Formación Saldán, Cretácico Inferior, sierra Chica de Córdoba. 5° Reunión Argentina de Sedimentología, Actas, pp 35–40

Piovano EL (1996) Correlación de la Formación Saldán (Cretácico temprano) con otras secuencias de las Sierras Pampeanas y de las cuencas Chacoparanense y de Paraná. Rev Asoc Geol Argentina 51(1):29–36

Piovano EL, Astini RA (1990) Facies de abanico aluvial semiárido en la Formación Saldán, quebrada del río Suquía, Sierra Chica de Córdoba. 3° Reunión Argentina de Sedimentología, Actas, San Juan, pp 217–222

Poiré D, Sánchez ML, Villegas M (1989) Facies sedimentarias de la sección inferior del Grupo Sierra de Los Cóndores, Embalse Río Tercero, Provincia de Córdoba, República Argentina. Contribuciones de los Simposios sobre Cretácico de América Latina. Parte A: Eventos y Registro Sedimentario, pp 121–132

Quenardelle S, Montenegro TF (1998) Las rocas fóidicas de Córdoba (Chaján) y San Luis (Las Chacras), Argentina. Petrología y Geoquímica. 10º Congreso Latinoamericano de Geología y 6º Congreso Nacional de Geología Económica, Actas, Buenos Aires, vol 2, pp 300–305

Ramos VA (1999) Evolución tectónica de la Argentina. Geología Argentina. Anales del Instituto de Geología y Recursos Minerales 29(24):715–784

Ramos VA, Escayola MP, Mutti DI, Vujovich GI (2000) Proterozoic-early Paleozoic ophioltes of the Andean basement of southern South America. In: Dilek Y, Moores EM, Elthon D, Nicholas A (eds) Ophiolites and Oceanic Crust: new insights from field studies and the Ocean Drilling Program, Geological Society of America Special Paper, Boulder, Colorado, vol 349, 331–349

Raggio F, Gerster R, Welsink H (2012) Cuencas del Salado y Punta del Este. Petrotecnia, diciembre 2012

Rapela CW, Pankhurst RJ, Casquet C, Baldo E, Saavedra J, Galindo C, Fanning CM (1998) The Pampean Orogeny of the southern proto-Andes: cambrian continental collision in the Sierras de Córdoba. In: Pankhurst RJ, Rapela CW (eds) The Proto-Andean Margin of Gondwana, vol 142. Geological Society London Special Publications, pp 181–217

Rapela CW, Pankhurst RJ, Casquet C, Fanning CM, Baldo EG, González-Casado JM, Galindo C, Dahlquist J (2007) The Río de la Plata craton and the assembly of SW Gondwana. Earth-Sci Rev 83:49–82

Rapela CW, Fanning CM, Casquet C, Pankhurst RJ, Spalletti L, Poiré D, Baldo EG (2011) The Río de la Plata craton and the adjoining Pan-African/brasiliano shield: their origins and incorporation into south-west Gondwana. Gondwana Res 20(4):673–690

Ringwood AE (1966) The chemical composition and origin of the Earth. In: Hurley PM (ed) Advances in earth sciences: contribution to the international conference on the earth sciences. Cambridge MIT Press, pp 287–356

Rossello E, Mozetic ME (1999) Caracterización estructural y significado geotectónico de los depocentros cretácicos continentales del centro–oeste argentino. Boletim do 5º Simpósio sobre o Cretáceo do Brasil, UNESP–Campus de Rio Claro/SP:107–113

Rudnick RL, Gao S (2003) Composition of the continental crust. In: Rudnick RL (ed) Tretease on geochemistry, vol 3. The Crust. Elsevier, Amsterdam, p 1–64

Sánchez ML (2001a) Sedimentología de la Formación El Rosario (Cretácico), La Cumbre, provincia de Córdoba, Argentina. 11° Congreso Latinoamericano de Geología y 3° Congreso Uruguayo de Geología, versión CD-ROM, Montevideo

Sánchez ML (2001b) Sedimentología de la Formación Peñón Blanco (Cretácico), en la zona de La Cumbre, provincia de Córdoba, Argentina. 11° Congreso Latinoamericano de Geología y 3° Congreso Uruguayo de Geología, CD-ROM, Montevideo

Sánchez ML, Bermúdez A (1997) Caracterización geoquímica del volcanismo cretácico de la Sierra de los Cóndores, Córdoba. Argentina. 8º Congreso Geológico Chileno, Actas, Antofagasta, vol 2, pp 1522–1527

Sánchez ML, Villegas MB, Poiré DG (1990) Paleogeografía del Cretácico Inferior en el área de la sierra de Los Cóndores, provincia de Córdoba. 3° Reunión Argentina de Sedimentología, Actas, San Juan, pp 235–246

Sánchez ML, Pérez Posio C, Sisto F (1995) Modelo cinemático de la cuenca de Los Cóndores (Cretácico Inferior) en la provincia de Córdoba. 5° Jornadas Pampeanas de Ciencias Naturales, Actas, Santa Rosa, 1993, vol 2, pp 75–81

Sánchez ML, Toro E, Delpino D, Bermúdez A (1999) Geología y estratigrafía de las rocas cretácicas de La Cumbre - Estancia El Rosario, Córdoba. 14° Congreso Geológico Argentino, Actas, Salta, vol 1, pp 445–448

Sánchez ML, Ancheta MD, Marclé R (2001) Las volcanitas de la Formación El Saucecito, Grupo El Pungo (Cretácico Inferior), Córdoba, Argentina. 11° Congreso Latinoamericano de Geología y 3° Congreso Uruguayo de Geología, CD-ROM, Montevideo

Sánchez ML, Ancheta MD, Marcle R (2002) Rocas volcánicas cretácicas de la cuenca de El Pungo, Córdoba. 15° Congreso Geológico Argentino, Actas CD-ROM, El Calafate

Schmidt CJ, Astini RA, Costa CH, Gardini CE, Kraemer PE (1995) Cretaceous rifting, alluvial fan sedimentation and Neogene inversion, southern Sierras Pampeanas, Argentina. In: Tankard AJ, Suárez Soruco R, Welsink HJ (eds) Petroleum basins of South America, vol 62. American Association of Petroleum Geologists, Memoir, Tulsa, pp 341–357

Schröder C (1967) Estudio geológico y geotécnico referente al aprovechamiento hidroeléctrico y para riego del río Tercero en "Piedras Moras". Prov. de Córdoba. Trabajo Final de Licenciatura, Universidad de Buenos Aires (unpublished), Buenos Aires 47 p

Shelley D (1993) Igneous and Metamorphic rocks under the microscope. Chapman and Hall, London, 445 p

Shimizu N, Le Roex AP (1986) The chemical zoning of augite phenocrysts in alkaline basalts from Gough Island, South Atlantic. J Volcanol Geoth Res 29:159–188

Silva Nieto DG, Espejo PM, Lagorio SL (2014) Hallazgo de basaltos de probable edad cretácica en el centro este de La Pampa. 19º Congreso Geológico Argentino, Actas CD-Rom, Córdoba

Sisto FA, Cortés JM (1992) Tectónica cretácico-cenozoica del tramo sur de la Sierra de Los Cóndores, Sierras Pampeanas de Córdoba. 7° Reunión de Microtectónica, Actas, pp 63–69

Sisto F, Sánchez ML, Perez Posio C (1993) Dinámica y cinemática cenozoica del frente de fracturación Puesto Viejo - La Cantera, sierra de los Cóndores, provincia de Córdoba, República Argentina. 9° Reunión de Microtectónica, Actas, Mendoza, pp 7–8

Sisto F, Sánchez ML, Perez Posio C, (1995) Dinámica y cinemática cenozoica de las principales estructuras de la Sierra de los Cóndores, provincia de Córdoba, República Argentina. 5° Jornadas Pampeanas de Ciencias Naturales, Actas, Santa Rosa, 1993, vol 2, pp 82–88

Spencer KJ, Lindsley DH (1981) A solution model for coexisting iron-titanium oxides. Am Mineral 66:1189–1201

Stipanicic PN, Linares E (1969) Edades radimétricas determinadas para la República Argentina y su significado geológico, vol 47(1). Boletín de la Academia Nacional de Ciencias, Córdoba, pp 51–96

Stormer JC, Nicholls J (1978) XLFRAC: A program for the interactive testing of magmatic testing of magmatic differentiation models. Comput Geosci 4:143–159

Sun SS, McDonough WF (1989) Chemical and isotopic systematics of oceanic basalts: Implications for mantle composition and processes. In: Saunders AD, Norry MJ (eds) Magmatism in the ocean basins, vol 42. Special Publication Geological Society of London, London, pp 313–345

Takahashi E, Kushiro I (1983) Melting of a dry peridotite at high pressure and basalt magma genesis. Am Mineral 68:859–879

Tankard AJ, Uliana MA, Welsnik HJ, Ramos VA, Turic M, França AB, Milani EJB, de Brito Neves B, Eyles N, Skarmeta J, Santa Ana H, Wiens F, Cirbián M, López Paulsen O, Germs GJB, De Wit MJ, Machacha T, McG. Miller R (1995) Structural and tectonic controls of basin evolution in Southwestern Gondwana during the Phanerozoic. In: Tankard AJ, Suárez Soruco R, Welsink HJ (eds) Petroleum basins of South America, vol 62. American Association of Petroleum Geologists, Memoir, Tulsa, pp 5–52

Thover E, Trindade RIF, Solum JG, Hall CM, Riccomini C, Nogueira AC (2010) Closing the Clymene ocean and bending a Brasiliano belt: evidence for the Cambrian formation of Gondwana, southeast Amazon craton. Geology 38(3):267–270

Uliana MA, Biddle KT, Cerdan J (1990) Mesozoic extension and the formation of Argentine sedimentary basins. In: Tankard AJ, Balkwill HR (eds) Extensional tectonics and stratigraphy of the North Atlantic margins, vol 46. American Association of Petroleum Geologists, Memoir, Tulsa, 599–614

Valencio DA (1972) Palaeomagnetism of the lower Cretaceous Vulcanitas Cerro Colorado Formation of the Sierra de los Cóndores Group, province of Córdoba, Argentina. Earth Planet Sci Lett 16:370–378

Valencio DA, Vilas JF (1972) Sequence of the continental movements occurred prior to and after the formation of the South Atlantic. Anais de la Academia Brasileira de Ciencias 48:377–386

Valencio DA, López MG, Solá P, Villani C (1980) El significado geológico de los resultados del estudio paleomagnético de vulcanitas alcalinas de las provincias de San Luis y Córdoba. Rev Asoc Geol Argentina 25(3):340–347

Viramonte J, Deruelle B, Moorbath S, Mazzuoli R, Omarini R (1994) El volanismo alcalino de Chaján–Las Chacras, Córdoba–San Luis, Argentina. 7º Congreso Geológico Chileno, Actas, Concepción, vol 2, 1273–1277

Webster RE, Chebli GA, Fischer FJ (2004) General Levalle basin, Argentina: a frontier Lower Cretaceous rift basin. Am Assoc Petrol Geol Bull 88(5): 627–652

Wilkinson JFG, Le Maitre RW (1987) Upper mantle amphiboles and micas and TiO_2, K_2O and P_2O_5 abundance and 100 Mg/(Mg + Fe^{2+}) ratios of common basalts and andesites: implications for modal mantle metasomatism and undepleted mantle compositions. Journal of Petrology 28:37–73

Yrigoyen MR (1975). La edad cretácica del Grupo Gigante (San Luis) y su relación con cuencas circunvecinas. 1º Congreso Argentino de Paleontología y Bioestratigrafía, Actas, Tucumán, vol 2, pp 29–56

Zindler A, Hart S (1986) Chemical geodynamics. Ann Earth Planet Sci 14:493–571

http://www.springer.com/978-3-319-29591-6

Early Cretaceous Volcanism in Central and Eastern Argentina During Gondwana Break-Up

Lagorio, S.L.; Vizán, H.; Geuna, S.E.

2016, X, 141 p. 39 illus. in color., Softcover
ISBN: 978-3-319-29591-6